García-Fernández, A.; Aznar, E.; Martínez-Máñez, R.; Sancenón Galarza, F. (23-0). New Advances in In Vivo Applications of Gated Mesoporous Silica as Drug Delivery Nanocarriers. Small. 16(3):1-62. https://doi.org/10.1002/smll.201902242

New advances in *in vivo* applications of gated mesoporous silica as drug delivery nanocarriers

Alba García-Fernández, Elena Aznar, Ramón Martínez-Máñez, and Félix Sancenón*

A. García-Fernández, Dr. E. Aznar, Prof. R. Martínez-Máñez, Dr. F. Sancenón
Instituto Interuniversitario de Investigación de Reconocimiento Molecular y Desarrollo Tecnológico (IDM), Universitat Politècnica de València, Universitat de València. Universitat Politècnica de València, Camino de Vera s/n, 46022, Valencia, Spain.

A. García-Fernández, Dr. E. Aznar, Prof. R. Martínez-Máñez, Dr. F. Sancenón
CIBER de Bioingeniería, Biomateriales y Nanomedicina (CIBER-BBN).

A. García-Fernández, Dr. E. Aznar, Prof. R. Martínez-Máñez, Dr. F. Sancenón
Unidad Mixta UPV-CIPF de Investigación en Mecanismos de Enfermedades y Nanomedicina, Valencia, Universitat Politècnica de València, Centro de Investigación Príncipe Felipe, València, Spain.

Dr. E. Aznar, Prof. R. Martínez-Máñez, Dr. F. Sancenón
Unidad Mixta de Investigación en Nanomedicina y Sensores. Universitat Politècnica de València, IIS La Fe, Valencia, Spain.

E-mail: rmaez@qim.upv.es

Keywords: gated materials, mesoporous silica nanoparticles, controlled release, *in vivo*, gating mechanisms

Abstract: One appealing concept in the field of hybrid materials is related to the design of gated materials. These materials are prepared in such a way that the release of chemical or biochemical species from voids of porous supports to a solution is triggered upon the application of external stimuli. Such gated materials are mainly composed of two subunits: (i) a porous inorganic scaffold in which a cargo is stored and (ii) certain molecular or supramolecular entities, grafted onto the external surface, which can control mass transport from the inner of pores. On the basis of this concept, a large number of examples have been developed in the past ten years. The present review aims to be a comprehensive overview of gated materials used in drug delivery applications in *in vivo* models from 2016 to date.

1. Introduction

In last years, nanomedicine and nanotherapy are gaining an increasing attention as alternative to conventional treatments in main pathologies which requires a selective and controlled drug administration.[1] Numerous nanocarriers with different characteristics have been designed and applied in drug delivery protocols, such as liposomes, micelles, polymers, dendrimers, quantum dots (QDs), gold (AuNPs) or metal oxide nanoparticles, silica-based materials, etc.[2] All these systems are able to store drugs and deliver them passively or in a controlled way. Passive systems include nanocarriers in which the drug is released by simply diffusion or by degradation of the material.[3] This type of passive systems are characteristic of organic nanoparticles such as liposomes, micelles or polymers and the timing of release is fundamental to reach the target site and achieve the desired drug effect. In contrast, a more sophisticated delivery strategy is based on on-command drug delivery, in which nanocarriers are tailored to deliver their cargo in the presence of certain stimuli. An attractive approach in this context is related with the design of "gated materials".[4]

Gated materials are predesigned to deliver molecules from a porous support in response to selected stimuli.[5] Among possible porous systems, mesoporous silica nanoparticles (MSNs) are perhaps the most widely used. MSNs present unique characteristics as high loading capacity, biocompatibility, chemical inertness and high surface area which can be easily functionalised using the well-known alkoysilane chemistry.[6] Therefore, these gated materials are composed by two subunits: (i) an inorganic porous scaffold in which a cargo (ca. drugs, dyes, fluorophores, small biomolecules) is loaded and (ii) (bio)molecules or supramolecular ensembles attached onto the external surface acting as gatekeepers.[7] The role of gatekeepers is to confine the cargo in the inner of the porous support. In the presence of external stimulus the gatekeeper changes its size/shape/conformation or is simply displaced

allowing cargo release in a controlled fashion. Moreover, gated nanoparticles can be designed to target selected cells or tissues by adding biological ligands onto their external surface.

While organic-based nanoparticles are used today in several realistic biomedical applications, most of the studies with gated MSNs have been focused in the design of new gated systems. However, the number of more realistic *in vivo* studies regarding gated mesoporous silica has increased dramatically in last years.[8] In fact gated nanomaterials showing a controlled drug release in the presence of selected stimuli hold an enormous potential as tools for drug delivery for the development of new therapies to improve efficacy and safety of drug administration.[9] Given the relevance of gated materials in the last years, the present review aims to be a comprehensive overview of gated materials used in drug delivery applications in *in vivo* models from 2016 to date (see Table 1 for the different cell types and Table 2 for the *in vivo* models used). Porous systems in which the drug is delivered by simple diffusion are not included in this review. The present review is divided taking into account the stimuli used to trigger payload release from gated materials.

Table 1. Cell Lines used in studies with gated materials

Cell line	Description	References
4T1	stage IV human breast cancer	54,83,107,111,117
A549	human lung adenocarcinoma cells	19,31,34,47,62,90,100,116
A549/MDR	multidrug-resistant human lung adenocarcinoma cells	47
BCEC	primary brain capillary endothelial cells	50
Beas2B	human bronchial epithelial cells	71
bEnd.3	mouse brain endothelial cell	36
BT-474	human breast cancer cells	33
C26	mouse colon cancer cells	23
C6	Rat malignant glioma	50,51,101
CD133+ Hep2	CD133+ human carcinoma	113
CD-44-positive HeLa	CD-44-positive human cervix carcinoma cells	26
CHO	Chinese hamster ovary cells	28
DL	Dalton's lymphoma	93
DLD-1	human colorectal cells	32
Dox-resistant DL	mouse highly methastatic lymphoma cells	52

HCT-116	human colorectal cells	32,81
HCT-8	human ileocecal colorectal adenocarcinoma	112
HEK293	human embryonic kidney cells	101,102
HeLa	human cervix carcinoma cells	10,14, 17, 46, 73,87,100,105,106,108,112,116,118,119
Hep3B	Cancer stem cells from human hepatocellular carcinoma	66
HepG2	human liver cancer cells	11,22,28,30,38,64,77,87,102,104,112
HepG2/ADR	dox-resistant human liver cancer cells	38,56
HL-60	human promyelocytic leukemia cells	90
HT-1080	human fibrosarcoma	79
HT29	human colon cancer cells	82
Huh7	human hepatocarcinoma	92
HUVEC	human umbilical vein endothelial cells	112
K-562	human myelogenous leukemia cells	93
KB	human mouth epidermal carcinoma cells	21
MC-38	mouse colon carcinoma cells	81
MC3T3-E1	mouse preosteoblast	95
MCF-10	human non-tumorigenic epithelial breast cell line	94
MCF-7	human breast cancer cells	13,23,24,40,42,48, 60,65,72,76,90,93,103
MCF-7/ADR	multidrug-resistant breast cancer cells	13,85
MDA-MB-231	human breast carcinoma cells	24,27,37,39,40, 41, 48,54,55,58,59,69,70,84,86,94
MiaPaca2	human pancreatic cancer cell	29, 109
NCI-H226	human lung squamous cell carcinoma	92
Neuro-2a cells	mouse neuroblastoma cell line	75
Panc-1	human pancreatic cancer cells	75, 109
PC9	human lung adenocarcinoma	71
QGY-7703	mouse hepatocellular carcinoma cells	12
RAW264.7	mouse macrophages	68, 95
S2VP10	human pancreatic ductal adenocarcinoma	29
SAOS-2	human primary osteogenic sarcoma	92
SCC7	Mouse squamous cell carcinoma	33
SGC7901/ADR	drug-resistant human gastric cancer cells	20
SH-SY5Y	Head and neck squamous cell carcinoma	33
SK-MEL-103	human melanoma cells	92
SMMC-7721	human hepatocarcinoma cell line	15,18,25
SMMC-7721	human hepatocarcinoma cell line	110
SW480	human colorectal cancer cells	45,49,63
TC-83 virus positive HeLa	TC-83 virus-positive human cervix carcinoma cells	57
THP-1	human leukemic monocytes cells	80
U-2-OS	human osteosarcoma	93
U87MG	human primary glioblastoma cells	36,53
UT-SCC-42B	human head and neck squamous cell carcinoma	92
VEGF-negative L929	VEGF-negative mouse fibroblast cells	18
VEGF-positive HeLa	VEGF-positive human cervix carcinoma cells	16
WSU-HN6	human oral squamous caercinoma cells	43
	primary murine microglia cells	67

Table 2. Animal models used in studies with gated materials

Organism	Description	References
Bacteria	*E.coli* CFT 073	120
Bacteria	*E.coli* DH5α	120
Bacteria	*S. marescens* 21639	120
Chicken	Chick chorioallantoic membrane	118
Chicken	MDA-MB-231 inoculated 10-days old embryos	59
Mice	4T1 tumor-bearing mice	54,59,83,107,108,111,117
Mice	A549 xenograft	19,62,90
Mice	A549/MDR xenograft	47
Mice	air pouch model	80
Mice	B16-OVA melanoma tumor-bearing	68
Mice	bleomycin-induced pulmonary fibrosis mouse model	92
Mice	C26 xenograft	23
Mice	C3H/HeN murine model	57
Mice	C6 xenograft	50,51, 101
Mice	CD133+ Hep2 tumor-bearing mice	113
Mice	Chronic constriction injury of sciatic nerve	67
Mice	DLD-1 xenograft	32
Mice	DL-tumor bearing mice	52, 93
Mice	EL4 tumor-bearing	115
Mice	EMT-6 tumor-bering mice	112
Mice	H22-tumor bearing mice	10,12,18,25,30, 104, 116
Mice	H29 xenograft	82
Mice	HeLa tumor-bearing mice	14, 16,21,26,46,73,100,105,106
Mice	Hep3B cancer stem cells-tumor bearing	66
Mice	HepG2 xenograft	11, 22,28,38,64,77, 102
Mice	HepG2/ADR xenograft	56
Mice	HT-1080 tumor-bearing mice	79
Mice	LLC xenograft	30
Mice	MCF-7 xenograft	42,48, 60,65,72
Mice	MCF-7/ADR-tumor bearing severe combined immunodeficient mice	13,85
Mice	MDA-MB-231 tumor-bearing mice	24,27, 37,39,40,41, 55,58,70,76,84,86,91,94,103
Mice	MDA-MB-231/NQO1 tumor-bearing mice	91
Mice	MiaPaca 2 xenograft	34
Mice	NCI-H226 tumor-bearing mice	92
Mice	non tumoral BALB/c	81
Mice	non tumoral C57BL/6 mice	68
Mice	non tumoral Kunming mice	117
Mice	Panc-1 xenograft	109
Mice	PC9-DR tumor-bearing mice	71
Mice	S180 sarcoma-bearing nude mice	69
Mice	SCC7 xenograft	33

Mice	SCID mice with orthotopic S2013 tumor	29
Mice	SCID mice with orthotopic S2VP10 tumor	29
Mice	SGC7901/ADR tumor-bearing mice	20
Mice	SK-MEL-103 tumor-bearing mice	92
Mice	SMMC-7721 tumor-bearing nude mice	15, 17, 110
Mice	streptozotocin-induced type I diabetic mice	119
Mice	SW480 xenograft	45,49, 63
Mice	U87MG tumor-bearing mice	53
Mice	WSU-HN6 tumor-bearing nude mice	43
Rat	Sprague-Dawley	36,43
Rat	Wistar	96,97
Zebrafish	heart failure sqKR15 model	74

2. pH-responsive drug delivery systems

Among different stimuli used to trigger cargo release in gated materials, pH is, perhaps, the most commonly employed. pH-triggered gated materials are a promising tool to prepared nanodevices for drug delivery applications taking into account the pH differences between the extracellular environment (neutral pH) and that of endosomes/lysosomes (slightly acidic pH), which allow drug release inside cells minimizing undesired drug delivery in the extracellular media. Besides, the acidic microenvironment found in certain tumours, due to the overproduction of lactic acid, can also be used for the targeted drug release. Several approaches have been used for the preparation of pH-triggered gated supports. One common approach is the inclusion of pH-hydrolysable linkages (such as imine, hydrazone, acetals, ketals, amides and esters) on the capping ensemble. The hydrolysis of such bonds induces the detachment of the cap with subsequent pore opening and payload delivery. Another approach consists of coating the nanoparticles with different ionisable polymers or biomolecules which use electrostatic interactions as main assembly forces. For these systems, protonation/deprotonation of the coating components induce disruption of the electrostatic interactions, detachment of the polymers from the mesoporous surface and cargo delivery. Moreover, some few examples takes advantage of protonation-induced conformation changes in the gating ensemble to induce payload release. Besides, the use of lipid bilayers,

resembling those founds in living cells, as gating ensembles has also been extensively explored. For this purpose several simple or complex (functionalised with polymers or targeting biomolecules) phospholipids have been be used for the preparation of bilayers which coated the external surface of the loaded nanoparticles inhibiting cargo release. These lipid bilayers facilitate the cellular uptake of nanoparticles and subsequent cargo delivery upon cell membrane fusion and disruption of the coating in the acidic environment in the lysosomes.

2.1. Hydrolysis of chemical bonds

One of the most commonly used strategy to prepare pH-sensitive caps is the incorporation of pH-hydrolysable linkages onto bulky (bio)molecules. The anchoring of these bulky (bio)molecules in the external surface of the loaded mesoporous supports inhibit cargo delivery. However, hydrolysis of pH-sensitive linkages in the cap at acidic pH results in detachment of the capping ensemble and cargo delivery. The most common pH-sensitive linkages used are imine, hydrazone, acetals, ketals, amides and esters. For instance, Jiang and co-workers prepared MSNs loaded with doxorubicin (Dox) and capped with dextrin, which were able to release the entrapped drug in acidic environments (Figure 1).[10] The prepared MSNs were functionalised with aminopropyl moieties and then dextrin was covalently anchored through the reaction of its anomeric carbon with the amine groups on the external surface. Vicinal diols in the dextrin units were further oxidized to dialdehydes using KIO_4. Finally, the pores of the nanoparticles were loaded with Dox and capped upon addition of tetraethylenepentamine which acted as crosslinking agent forming imine bonds with the aldehyde moieties in the oxidised dextrin. Phosphate buffered saline (PBS) suspensions of the nanoparticles at pH 7.4 showed a moderate Dox release (28% after 24 h). However at pH 6.0 a marked drug release was observed (94% after 24 h) due to imine hydrolysis and subsequent pore opening. Confocal laser scanning microscopy (CLSM) studies showed that nanoparticles were efficiently endocytosed by HeLa cells. Besides, it was found that at pH 6.0 nanoparticles

(at 2.5 mg/L) were able to kill 90% of HeLa cells whereas at pH 7.4 ca. 70% of cells remained alive as a marked contrast with free Dox administration which induced significant reductions in cell viability at pH 7.4. Finally, nanoparticles were intravenously injected in H22-bearing mouse and *in vivo* tissue distribution of the nanoparticles was studied. Nanoparticles were preferentially accumulated in tumour (via enhanced permeability and retention (EPR) effect) whereas negligible amounts were detected in heart, spleen, lung and kidney.

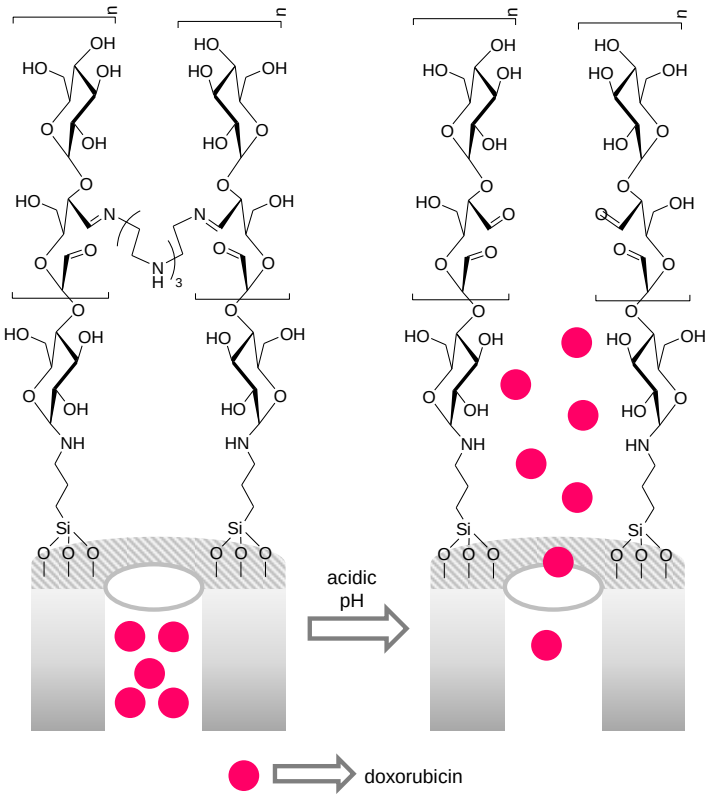

Figure 1. MSNs loaded with Dox and capped with a dextrin derivative. Cargo release is observed upon acidic hydrolysis of imine bonds.

Hollow MSNs were used by Cai and co-workers as inorganic scaffold for the preparation of pH-sensitive nanodevices for tumour therapy.[11] Hollow MSNs were functionalized with aminopropyl moieties. The amino groups were reacted with 4-carboxyphenylboronic acid using 1-ethyl-3-(3-dimethylaminopropyl)carbodiimide (EDC)/*N*-hydroxysuccinimide (NHS)

and the pores loaded with Dox. Afterward, phenylboronic acid moieties were reacted with a catechol functionalised with β-cyclodextrin (β-CD). Finally, the pores were capped upon addition of an adamantane-derivatised poly(ethylene glycol) (PEG), which also contained a pH-sensitive benzylimine moiety, by the formation of supramolecular inclusion complexes (Figure 2). Controlled cargo release of the nanoparticles at pH 7.4, 6.8 and 5.0, mimicking physiological pH, tumour microenvironment and intracellular endosome, were carried out. After 24 h, only 20 and 34% of the entrapped Dox was released at pH 7.4 and 6.8. As clear contrast, a marked release (ca. 80% after 24 h) was observed at pH 5.0 which was ascribed to the hydrolysis of the imine bonds and the boronic esters in the capping ensemble. Transmission electron microscopy (TEM) and CLSM studies showed that the prepared nanoparticles were efficiently internalized by HepG2 cells and were located in the cytoplasm. Treatment of HepG2 cells with the capped nanoparticles induced a remarkable reduction in HepG2 viability due to Dox release and apoptosis by fracturing nuclear deoxyribonucleic acid (DNA) structure. *In vivo* experiments, carried out with HepG2 xenograft nude mice treated with the nanodevice, showed a marked tumour growth inhibition, compared to free drug, ascribed to controlled Dox release from nanoparticles. Besides, biodistribution studies showed accumulation of nanoparticles in tumour, liver, spleen and lungs while small amounts were observed at heart and kidneys.

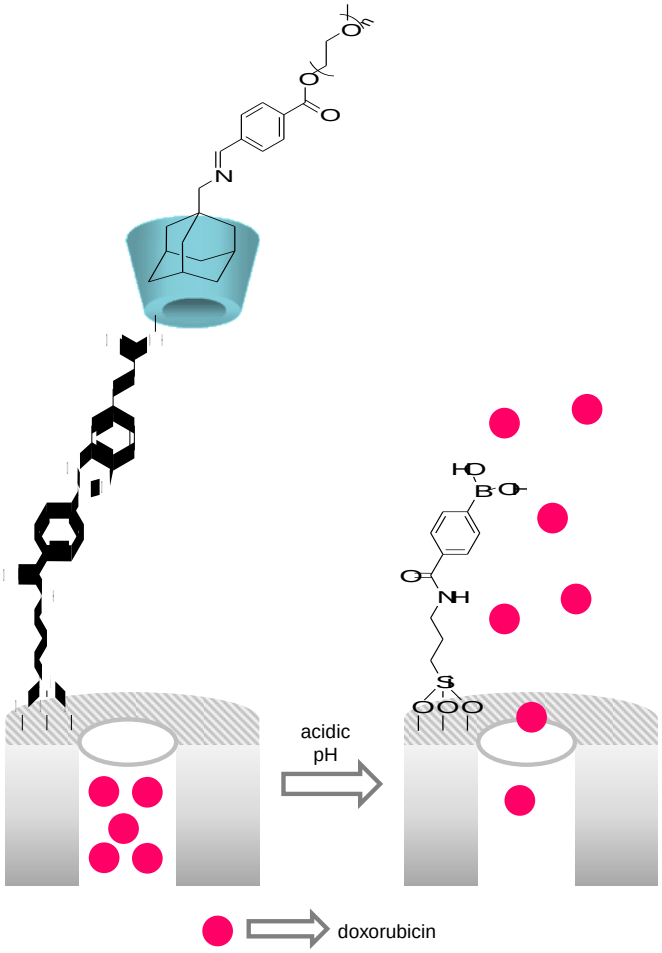

Figure 2. MSNs loaded with Dox, functionalised with a β-CD derivative and capped by the formation of a supramolecular complex inclusion with an adamantane-derivatised PEG Cargo release is observed upon acidic hydrolysis of the imine and the boronic esters bonds.

Dendritic MSNs with pore diameter of 9.3 nm were prepared by Tang et al. and used for the co-delivery of drugs and plasmids.[12] The authors decorated the external and internal surface of the inorganic scaffold with aminopropyl groups which were reacted with 4-imidazolecarboxaldehyde yielding nanoparticles derivatised with imidazole heterocycles linked through acidic pH-labile imine bonds. Then, pores were loaded with Dox and with survivin short hairpin (shRNA)-expressing plasmid (iSur-pDNA) (Figure 3). PBS suspensions of the nanoparticles at pH 7.4 showed moderate release of both Dox (ca. 30% after 120 h) and plasmid whereas an enhanced delivery of both cargos (80% of drug after 120 h) was observed

at acidic (5.0) pH. The observed release at acidic pH was ascribed to the hydrolysis of imine bonds that detached imidazole heterocycles from the nanoparticles. The prepared nanoparticles were efficiently endocytosed through a clathrin-mediated process by QGY-7703 cells. The acidic pH in the endosomes protonated the imidazole rings and induced imine bond hydrolysis, provoking osmotic swelling, rupture and endosomal escape of the drug and plasmid. Once in the nucleus, the shRNA mediated the inhibition of surviving expression increasing the sensitization of QGY-7703 cells to Dox. As a consequence a marked reduction in cell viability was observed. Besides, intravenously administration of nanoparticles to mice bearing H-22 cells induced a marked reduction in tumour volume due to accumulation of nanodevices, though EPR effect, and controlled co-delivery of Dox and plasmid. As a clear contrast, when mice bearing H-22 were treated with free Dox tumour volume remained nearly unaltered.

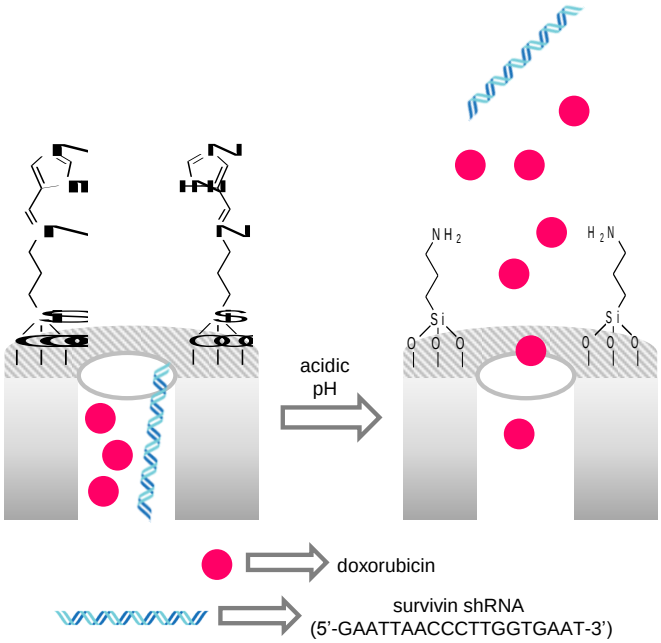

Figure 3. Dendritic MSNs loaded with Dox and survivin shRNA-expressing plasmid (iSur-pDNA) and functionalized with imidazole heterocycles. The observed release at acidic pH was ascribed to the hydrolysis of imine bonds.

Nanodevices able to deliver, in a simultaneous fashion, a drug and small interfering RNA (siRNA) fragments for cancer therapy were also developed by Zeng and co-workers (Figure 4).[13] The authors functionalised MSNs with aminopropyl groups and the amines on the surface were reacted with 4-formylbenzoic acid using EDC/NHS as coupling agents. The obtained aldehyde-functionalised MSNs were loaded with glycoprotein P (P-gp) siRNA and the pores were capped upon reaction of the aldehyde moieties with Dox and with a folic acid (FA) derivative containing an amine terminated PEG, through the formation of acid-labile imine bond. In the final nanoparticles FA was used to active cancer targeting. Controlled release experiments showed a moderate Dox (18.6% after 48 h) and siRNA delivery when nanoparticles were suspended in PBS at pH 7.4. However, when pH was lowered to 5.0, a marked Dox (53.7% over the same time period) and siRNA was observed. In the acidic environment the imine bonds, which linked Dox onto the external surface of the nanodevice, are hydrolysed with subsequent pore opening and drug and siRNA delivery. CLSM studies carried out with MCF-7 and MCF-7/ADR showed that nanodevices were efficiently internalized by both cell lines. Besides, Western blot analysis carried out with MCF-7/ADR cells and the nanodevices showed a moderate knockdown of P-gp protein due to the controlled delivery of encapsulated siRNA. On the other hand, 3-(4,5-dimethylthiazol-2-yl)-2,5-diphenyltetrazolium bromide (MTT) assays showed a dose-dependent reduction in MCF-7 cell viability due to the release of both siRNA and Dox. However, for Dox resistant MCF-7/ADR cells only a moderate reduction in viability after 48 h due to the siRNA-induced knockdown of P-gp protein and the release of the grafted drug was observed. Finally, female severe combined immunodeficient mice with MCF-7/ADR tumour were administered with the prepared nanodevice via tail vein injection. Nanoparticles accumulated in tumours due to EPR effect and to the presence of FA as targeting ligand. The subsequent simultaneous release of Dox and siRNA in the tumour acidic environment induced a marked reduction in tumour size. As clear contrast, when mice were treated with a combination of Dox and P-gp

siRNA, inhibition of tumour growth was also observed but not as marked as when treated with the nanodevice. Finally, histological analysis of the major organs (heart, liver, spleen, lung and kidney) showed no obvious morphological changes pointing out the biocompatibility of the prepared nanodevice. Besides, histological analysis revealed apoptotic and necrotic regions in tumour tissues from mice treated with the nanodevice.

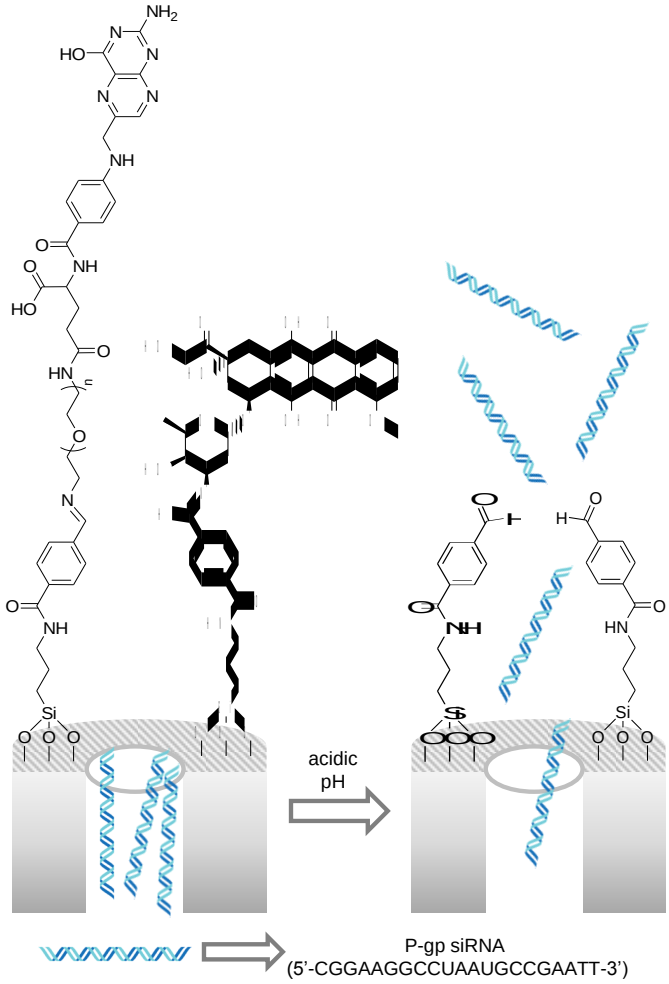

Figure 4. MSNs loaded with P-gp siRNA and capped with a FA derivative containing a PEG and with Dox. P-gp siRNA and Dox were released upon hydrolysis of the acid-labile imine bonds.

Pan and co-workers prepared anti-tumour nanodevices also based on MSNs loaded and gated with Dox (Figure 5).[14] In this case, MSNs were functionalised with aminopropyl moieties and the amino groups reacted with *p*-carboxy benzaldehyde. In a second step, the pores of the

aldehyde-functionalised mesoporous nanoparticles were loaded with Dox and then capped with the same drug through the formation of acid-labile imine bonds. A second set of nanoparticles loaded with Dox and capped with the drug and with amino terminated poly(ethylene glycol) moieties were also prepared. *In vitro* studies showed that Dox release at neutral pH for both nanoparticles was negligible (ca. 11% after 24 h) whereas a marked drug release was observed at pH 5.4 (ca. 86% after 24 h). This marked increase in drug release was ascribed to the hydrolysis of imine bonds at acidic pH which detached Dox and PEG molecules from the nanoparticles' surface. CLSM studies showed that both nanoparticles were effectively internalized by HeLa cells. Besides, MTT assays carried out with both nanoparticles and HeLa cells showed a dose-dependent reduction in viability. Finally, the anti-tumour efficacy of both nanoparticles was assessed in nude mice with HeLa cell xenograft tumour model, for this purpose intravenous administration by tail vein injection of the nanoparticles was compared to free drug administration. The results showed that nanoparticles clearly accumulated in tumours, through EPR effect, and induced a marked inhibition in tumour size and volume. This tumour size inhibition was higher than that obtained for mice treated only with free Dox. Besides, histological analysis revealed apoptotic and necrotic regions in tumour tissues from mice treated with the nanoparticles.

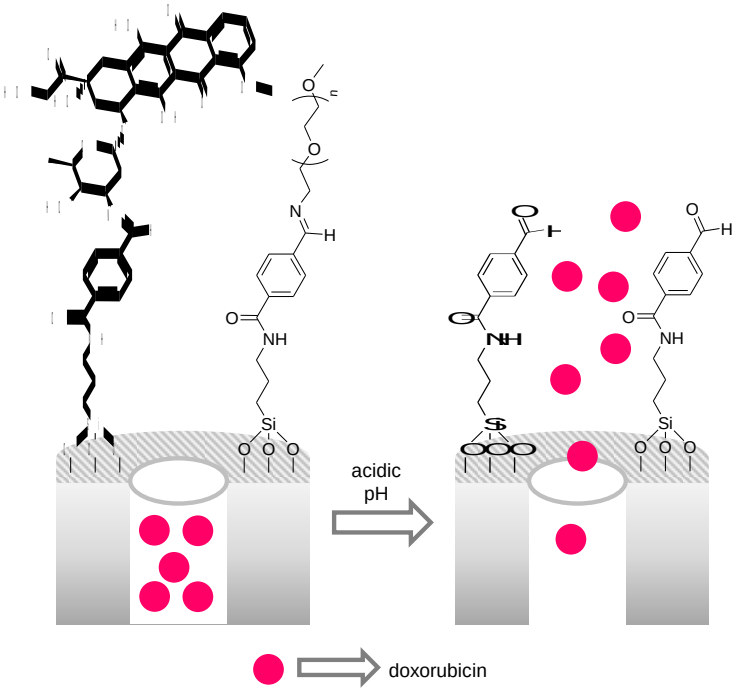

Figure 5. MSNs loaded with Dox and capped with Dox and with an amino terminated poly(ethylene glycol). Drug release was ascribed to the hydrolysis of imine bonds at acidic pH.

Xu and co-workers prepared MSNs loaded with anti-tumour drug paclitaxel (PTX) and modified with amino groups. On the other hand, FA (FA) was conjugated to NH_2-PEG-COOH through the formation of amide bonds. Finally FA-PEG was coupled to the amine containing MSNs yielding the final nanoparticles (Figure 6).[15] Drug release assays were performed with the loaded nanoparticles in an acidic environment and release of PTX was assessed. Drug release in in human liver cancer SMMC-7721 cells was also confirmed. Delivery in cells was attributed to FA recognition by the FA-receptor, which mediated endocytosis of the nanoparticles with the subsequent drug release in endocytic cell compartments due to the hydrolysis of the amide bonds. The biodistribution and anti-tumour efficacy of the solid was evaluated in SMMC-7721 tumour-bearing nude-mice as liver cancer model by intravenously tail injection of the nanoparticles. The nanoparticles presented a high tumour accumulation and the tumour growth was greatly inhibited when compared to free PTX.

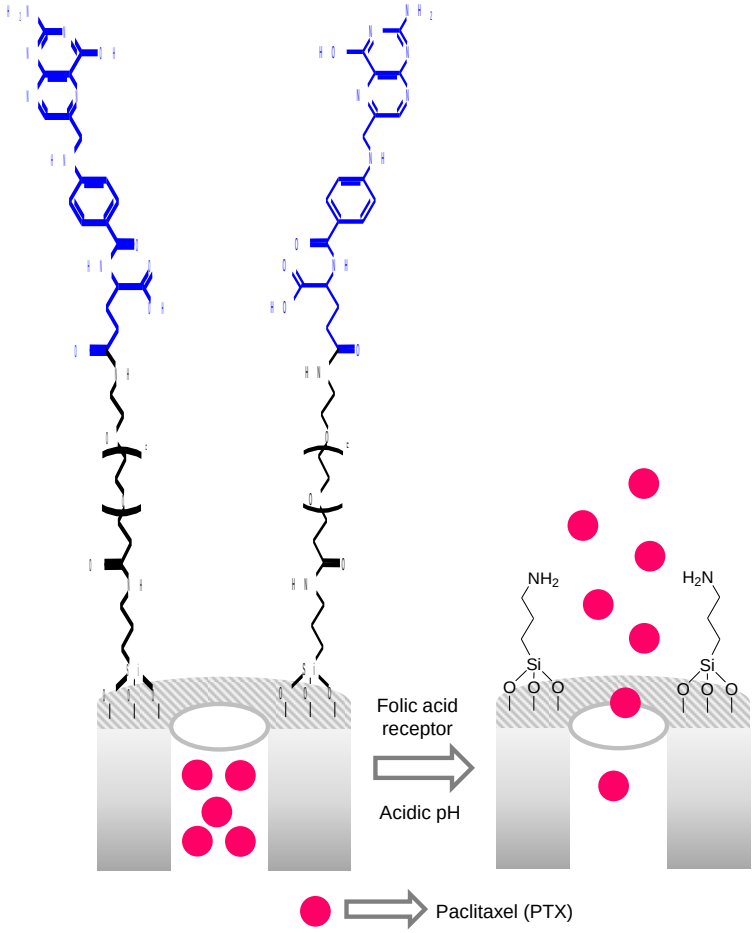

Figure 6. MSNs loaded with PTX and capped with PEG derivatised with FA. Cargo release at acidic pH is due to the hydrolysis of the amide bonds.

Yang and co-workers reported CdTe QDs integrated into hollow MSNs loaded with Dox and capped with the vascular endothelial growth factor (VEGF) antibody for cancer detection and treatment (Figure 7).[16] The nanoparticles were functionalised with amino groups and then reacted with succinimidyl-PEG_{5k}-maleimide to include PEG_{5000}-maleimide moieties onto the external surface of the nanoparticles through amide linkages. Finally a thiol-modified VEGF antibody was attached onto the nanoparticles through a Michael addition reaction. Drug release was confirmed by the authors at 37° in simulated physiological conditions at pH 6.5 and 5.0, whereas at pH 7.4 a non-significant drug delivery was observed. CLSM *in vitro* studies (measuring the fluorescence of the CdTe QDs) carried out with VEGF-positive HeLa

cells and VEGF-negative L929 fibroblast cells showed preferential internalization of the nanodevice in the VEGF-positive cells. *In vivo* studies were carried out with HeLa cells tumours in female nude mice. Intravenously administration of the prepared material showed the preferentially accumulation of the nanoparticles in tumours attributed to the EPR effect.

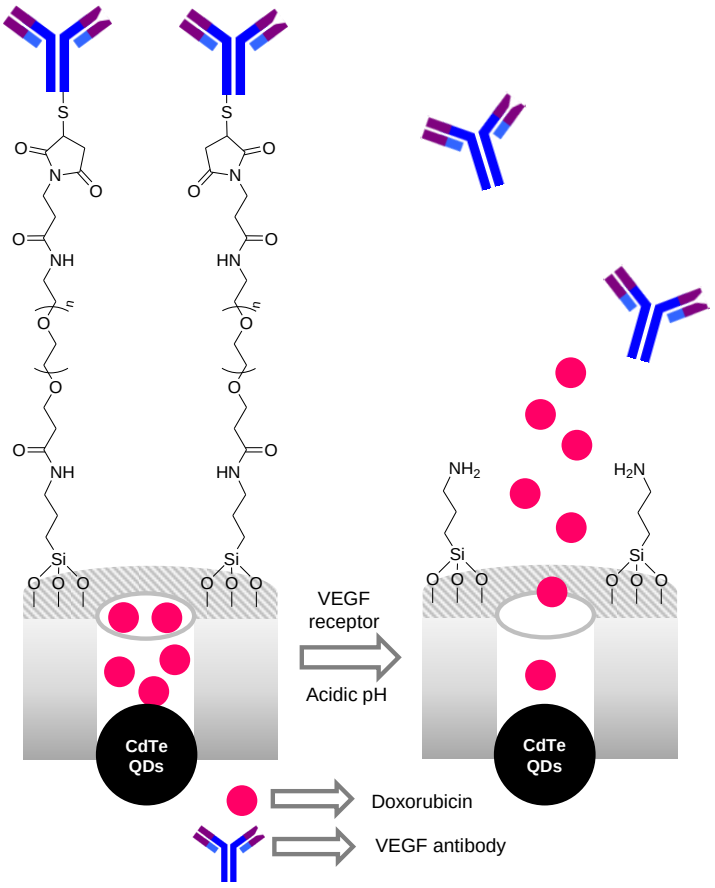

Figure 7. CdTe QDs integrated into hollow MSNs loaded with Dox and capped with PEG functionalized with VEGF antibody. Drug release is due to the hydrolysis of the amide bonds.

A pH-responsive nanodevice for mitochondrial targeting was prepared by Huang and co-workers (Figure 8).[17] In a first step, *N*-(2-hydroxypropyl)methacrylamide based-polymer was functionalised with 2,3-dimethylmaleic anhydride. In addition, MSNs functionalized with amino groups were prepared using a co-condensation protocol and the pores were loaded with docetaxel. The final nanodevice was obtained by coating the docetaxel-loaded MSNs with the negatively charged polymer through electrostatic interactions with the positively charged

nanoparticle surface. Aqueous suspensions of the nanodevice at pH 7.4 showed a moderate docetaxel release (ca. 20% after 10 h) that was increase at acidic pH (ca. 50 and 60% at pH 6.5 and 5.0 respectively). The observed release at acidic pH was ascribed to the hydrolysis of amide moieties onto the polymeric shell. This hydrolysis induced the detachment of 2,3-dimethylmaleate moieties from the capping polymer with subsequent disruption of electrostatic interactions. CLSM studies showed internalization of the nanodevice in HeLa cells. After 1 h of internalization the nanoparticles were entrapped in the lysosomes and, after polymer hydrolysis and detachment, positively-charged nanoparticles escaped from the lysosomes and accumulated in the mitochondria. MTT assays carried out with HeLa cells showed a dose-dependent reduction in cell viability due to docetaxel release. Tumour growth inhibition (72.6%) was observed for HeLa tumour-bearing nude mice upon treatment with the nanoparticles by tail vein injection. A major therapeutic effect was achieved with the nanoformulation compared to the free drug.

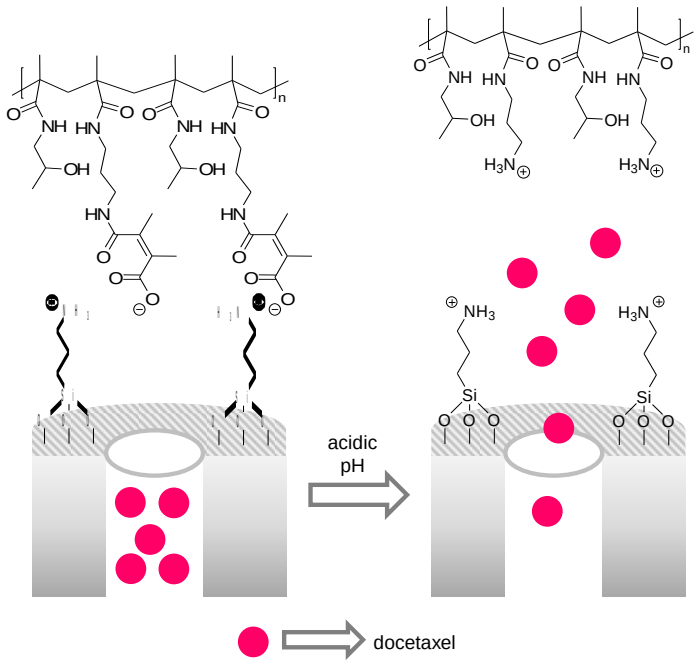

Figure 8. MSNs loaded with docetaxel and electrostatically capped with the modified *N*-(2-hydroxypropyl)methacrylamide based-polymer.

Nanodevices, based on MSNs, for the pH-triggered controlled release of ursolic acid and sorafenib were prepared and characterized by Shao and co-workers.[18] MSNs were reacted with (3-aminopropyl)triehoxysilane (APTES) and the amino groups were further treated with succinic anhydride. Then, the pores were loaded with ursolic acid or with sorafenib and capped with chitosan (CS) (pH-sensitive gate) through an amidation reaction using EDC/NHS. CS was additionally conjugated with lactobionic acid (LA) which is used as targeting ligands to ASGPR receptor overexpressed in hepatocellular carcinoma cells (Figure 9). Both nanoparticles presented a moderate cargo release at pH 7.4 (ca. 25% of the entrapped drug after 96 h) whereas a marked enhancement in delivery was observed at pH 5.5 (ca. 65% of the payload). Confocal microscopy studies showed internalization of the nanoparticles, in this case functionalized with fluorescein isothiocyanate (FITC), by SMMC-7721 cells, which overexpressed ASGPR receptor. Besides, MTT experiments showed a dose-dependent reduction in SMMC-7721 cells viability when treated with a mixture of both nanoparticles as a consequence of its internalization and subsequent drug co-release. *In vivo* controlled release of a mixture of both nanoparticles was tested into Kunming mice with H22 cells subcutaneously injected into its right hind leg. Administration of a mixture of both nanoparticles induced a marked reduction in tumour volume (ca. 40% related to the control group without any treatment) ascribed to solids accumulation in tumour due to EPR effect and to an efficient co-release of both drugs. Besides, *in vivo* antiproliferation studies of tumour sections of mice treated with the nanoparticles mixture showed a marked reduction in the expression of the epidermal growth factor (EGFR) protein. Finally, both nanoparticles were also able to supress metastasis of H22 cells to the lungs.

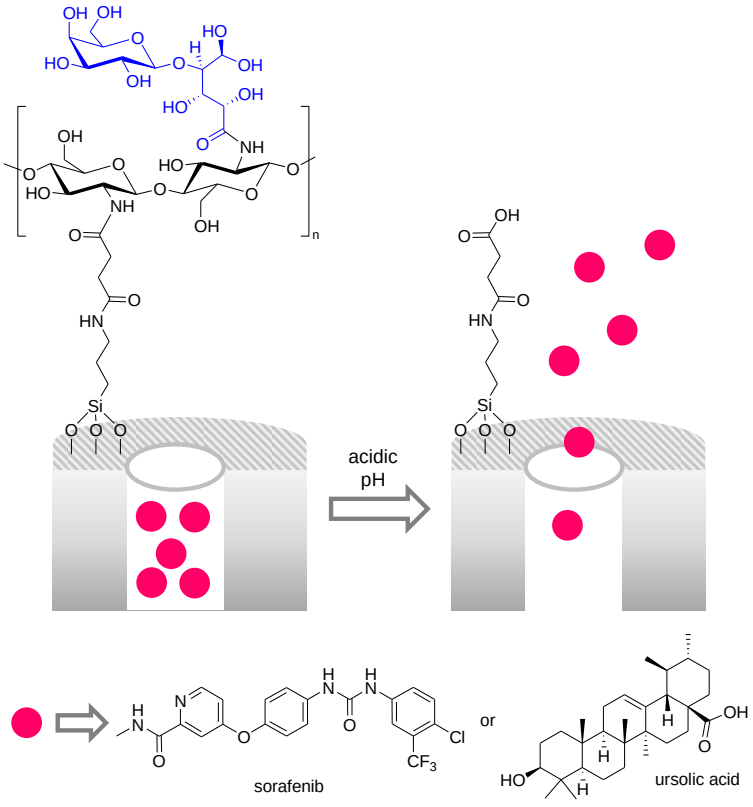

Figure 9. MSNs loaded with ursolic acid or sorafenib and capped with CS polymer functionalised with LA. Hydrolysis of amide bond at acidic pH induced drug release.

Cai et al. functionalised hollow MSNs with 3-triethoxysilylpropyl succinic anhydride and then the anhydride moieties were hydrolysed to yield carboxylic acid groups onto the external surface of the inorganic support.[19] In a second step, CS was anchored onto the external surface of the hollow MSNs through an amidation reaction using EDC/NHS for carboxylic acid activation. Afterward, the amine moieties of the grafted CS were reacted with dimethylmaleic anhydride yielding hollow MSNs with a negatively charged coating onto the external surface. On the other hand, cisplatin was transformed to oxoplatin and this complex functionalized with succinic anhydride. Then, the obtained complex was grafted onto polyamidoamine (PAMAM) dendrimers using EDC/NHS as coupling agents. For the preparation of the final nanodevice the pores of the functionalised hollow MSNs were loaded with gemcitabine and capped, through electrostatic interactions, with the Pt complex-

containing PAMAM dendrimers (Figure 10). *In vitro* studies carried out with the prepared nanodevice at pH 7.4 showed negligible dendrimer and gemcitabine release. However, a marked release of both components was observed at pH 6.8 due to the hydrolysis of the amide groups in the CS cap. This hydrolysis induced the appearance of positive charges in the grafted CS with subsequent dendrimer detachment due to electrostatic repulsions. Besides, if ascorbic acid was present in the environment at pH 6.8, cisplatin was also released from the dendrimers. CLSM studies carried out with A549 cells incubated with the nanodevice, in which PAMAM was labelled with FITC, at pH 6.8 showed a strong fluorescence in the cytoplasm due to nanoparticles internalization and escape from the lysosomes due to the proton sponge effect. The *in vitro* anti-tumour efficacy of the prepared solid was tested in multicellular spheroids of A549 cells. Treatment of spheroids with the nanodevice at pH 6.8 induced a marked inhibition in its growth ascribed to apoptosis. Besides, administration by tail vein injection of nanodevices or free drugs to A549 tumour-xenografted mice model showed a remarked inhibition of tumour growth. This therapeutic benefit was ascribed to gemcitabine and cisplatin release in the acidic tumour environment.

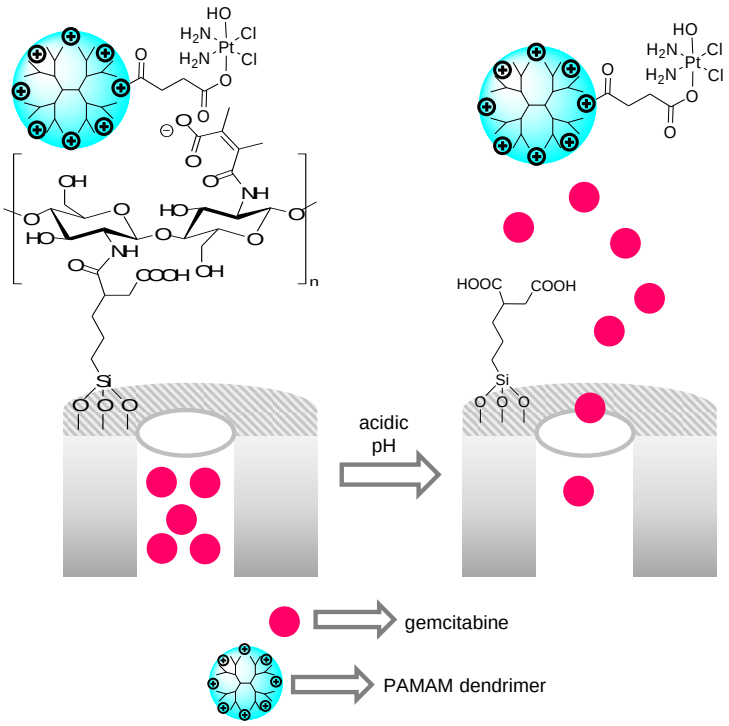

Figure 10. MSNs loaded with gemcitabine and capped with Pt complex-containing PAMAM dendrimers.

Fang and co-workers prepared MSNs loaded simultaneously with Dox and quercetin and decorated with hyaluronic acid (HA) for gastric carcinoma treatment (Figure 11).[20] MSNs were functionalised with aminopropyl moieties, the pores were loaded with both Dox and quercetin and finally the system was capped upon *N*,*N*'-dicyclohexylcarbodiimide (DCC)/NHS-mediated amidation with HA. Aqueous suspensions of the prepared nanoparticles showed a moderate drug release at pH 7.4 (30% after 24 h) that was enhanced to 80% at pH 5.0 after 24 h, probably due to the hydrolysis of amide bond which linked HA onto the external surface of the nanoparticles. *In vitro* studies carried out with gastric carcinoma SGC7901/ADR cells, indicated uptake of the nanoparticles due to HA interaction with CD44 receptor overexpressed by this cell line, and a marked reduction in viability. Besides, treatment of SGC7901/ADR tumour bearing nude mice with the prepared nanoparticles showed a marked reduction in tumour volume compared to the free drug.

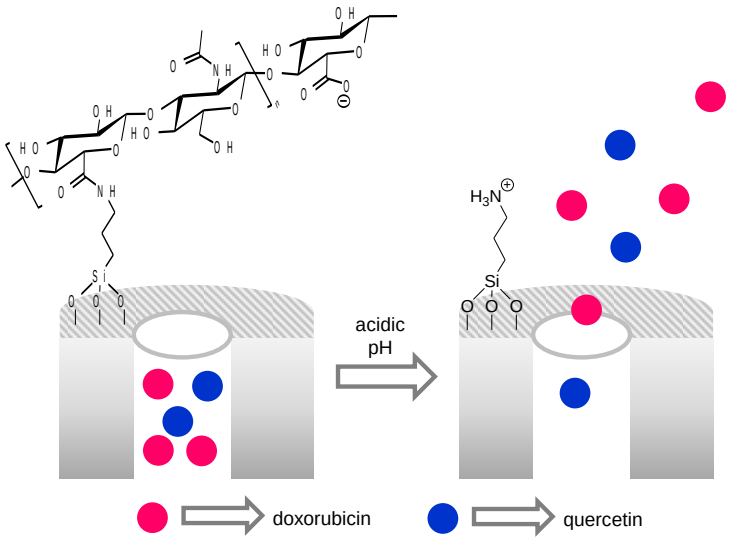

Figure 11. MSNs loaded with Dox and quercetin and coated with HA. Hydrolysis of amide bonds at acidic pH induced drug delivery.

Lu and co-workers used hollow MSNs as carriers for *in vivo* cancer therapy (Figure 12).[21] (3-aminopropyl)triehoxysilane was reacted with FITC or with rhodamine B isothiocyanate and the obtained trialkoxysilane-derivatised fluorophores were grafted onto the external surface of the hollow MSNs. The external surface of the fluorescent nanoparticles was further functionalised with octadecyltrimethoxysilane in order to obtain a hydrophobic outer surface. Finally, the pores were loaded with Dox and capped upon addition of an amphiphilic derivative which contained FA (as targeting ligand) and benzalacetal moieties (a pH-sensitive group). This compound formed a hydrophobic shell around the loaded nanoparticles via van der Waals non-covalent interactions with the grafted octadecyl chains. PBS suspensions of the nanoparticles at pH 7.4 showed a negligible Dox release (ca. 2% after 60 h) that was enhanced (ca. 60% after 60 h) at acidic pH. The marked release found at pH 5.0 was ascribed to the hydrolysis of de benzalacetal moiety in the amphiphilic capping compound with subsequent detachment of FA from the nanoparticle's surface and pore opening. Besides, the prepared nanoparticles showed a dose-dependent reduction in viability of KB cells (overexpressing FA receptors) due to their endocytosis and subsequent Dox release. CLSM (measuring the emission from the grafted fluorescein and the loaded Dox) and flow cytometry assays showed a marked larger uptake of the nanoparticles by KB cells than by human hepatoma 7402 cells (in which the FA receptor is not overexpressed). *In vivo* studies carried out with female athymic nude mice bearing HeLa cell tumours and treated with the prepared capped nanoparticles confirmed the preferentially accumulation of nanoparticles in tumours (by measuring rhodamine B emission). Besides, a marked inhibition in tumour growth and a reduction in their volume were also observed with the nanoformulation, evidencing the therapeutic benefit of the nanoparticles compared to free drug therapy.

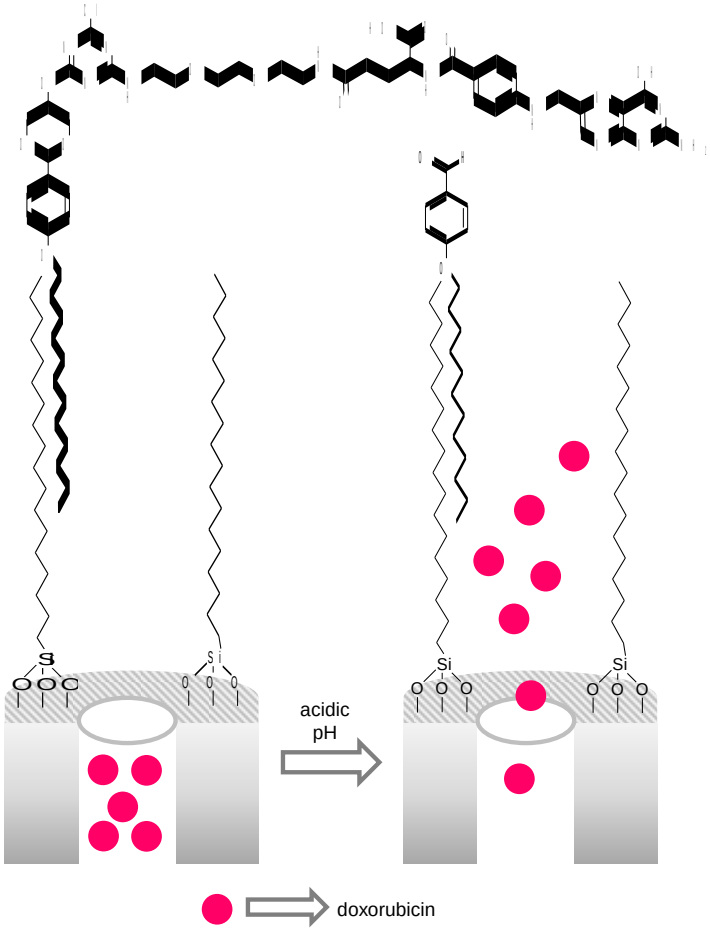

Figure 12. MSNs loaded with Dox, grafted with octadecyl chains and finally capped with an amphiphilic compound functionalised with FA and bearing a pH sensitive benzalacetal linkage. Additionally, fluorescein and rhodamine B were covalently attached to the nanoparticles (not shown). Hydrolysis of de benzalacetal moiety at acidic pH induced cargo delivery.

Hollow MSNs were used by Cai et al for the preparation of pH-sensitive nanodevices for targeted tumour therapy (Figure 13).[22] For this purpose, hollow MSNs were firstly functionalised with aminopropyl moieties. Then, in a second step, the amino groups were reacted with pyruvic acid using EDC/NHS as coupling agents. Afterward, the pores were loaded with FITC or with Dox and, finally, capped upon the formation of pH-sensible hydrazone bonds upon reaction with a HA derivative modified with hydrazine. PBS

suspensions at pH 7.4 of the FITC-loaded nanoparticles showed negligible dye release (9.6% after 60 h). However, as a clear contrast, a marked dye delivery was observed at pH 6.0 (49% after 60 h) and 5.0 (81% after 60 h) due to the hydrolysis of hydrazone bonds with the subsequent detachment of HA from the nanoparticles. Dox-loaded nanoparticles showed a dose dependent reduction in HepG2 cells viability due to the HA mediated endocytosis and drug release. CLSM carried out with HepG2 cells demonstrated an efficient uptake of the Dox-loaded nanoparticles. The intracellular acidic pH induced Dox release that diffused into cell nuclei resulting in apoptosis. Finally, *in vivo* studies were performed using male nude mice xenografts with HepG2 cells intravenously injected with the prepared solid. The nanoparticles induced a marked reduction of tumour size due to preferential HA-receptor mediated endocytosis and EPR effect. As a clear contrast, administration of free Dox induced a less marked reduction in tumour size. Biodistribution studies showed preferential accumulation of the nanoparticles in tumour and moderate amounts in liver, spleen and lungs.

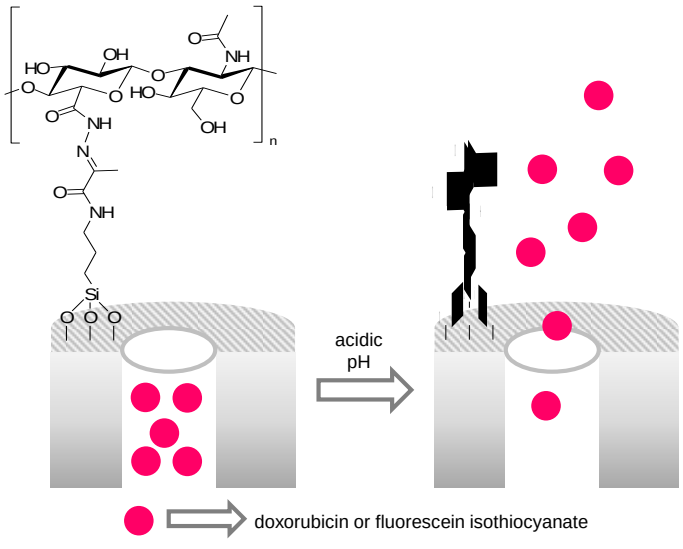

Figure 13. MSNs loaded with Dox and capped with HA modified with hydrazine. Hydrolysis of hydrazone bonds at acidic pH induced cargo release.

2.2. Protonation

Several pH-triggered reported nanodevices used bulky molecules or organic polymers as capping ensembles containing ionisable units. The underlying idea in these systems is to cover the external surface of loaded nanoparticles with these units usually trough electrostatic interactions. In the final capped particles protonation of ionisable units in the capping ensemble disrupts the electrostatic interactions with subsequent coating detachment and pore opening. This simple concept was used by Nejabat et al. that reported Dox-loaded hollow MSNs capped with the AS1411 aptamer to enhance the target delivery to colon adenocarcinoma (Figure 14).[23] The nanoparticles were loaded with Dox and modified with amino groups. Then, the external surface was coated, through electrostatic interactions, with acetylated carboxymethyl cellulose. Finally, the AS1411 aptamer was covalently attached to the carboxylic acid groups onto the external cellulose coating through the formation of amide bonds. When the nanomaterial reached the nucleolin receptor present in cancer cells the nanoparticles were endocytosed. After this process, the acidic pH in the lysosomes induced protonation of the carboxylates of the acetylated carboxymethyl cellulose coating. As a consequence the electrostatic interactions between the cellulose coating and the protonated amino groups (grafted onto the external surface of the support) were disrupted and the polymer detached from the surface with subsequent cargo release. The pH-dependent Dox delivery was corroborated in citrate buffer at pH 5.4. *In vitro* cytotoxicity studies were performed to evaluate the activity of the solid in MCF-7 breast cancer cells and C26 colon cancer cells and finally, the material was studied *in vivo* in a C26 xenograft tumour-bearing mouse model of colon carcinoma. The animals were divided in groups and different treatments administered intravenously by tail vein injection. A significant therapeutic effect to reduce tumour growth was observed with the AS1411 aptamer nanoformulation compared when using the non-targeted formulation and free Dox.

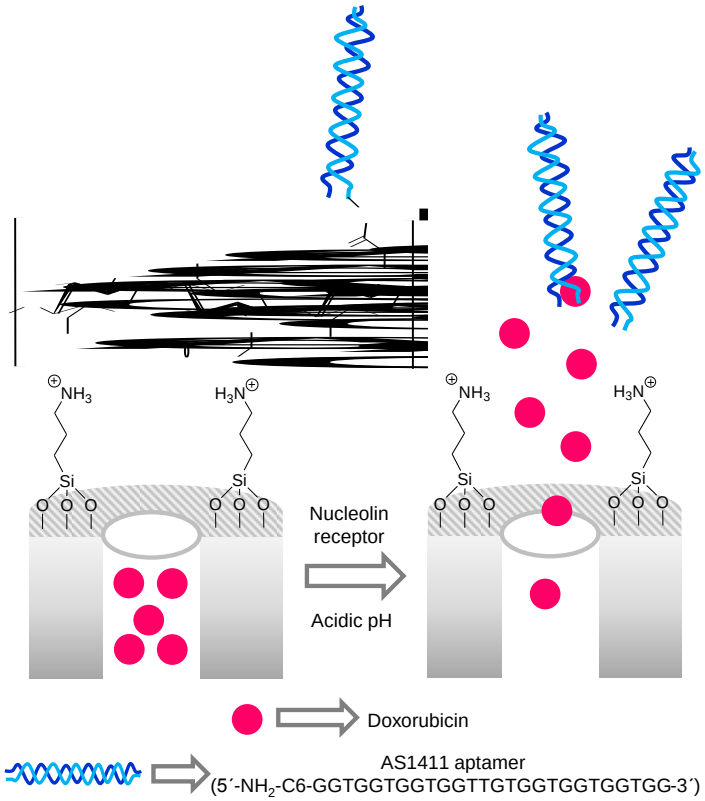

Figure 14. MSNs loaded with Dox, grafted with amino groups and capped electrostatically with acetylated carboxymethyl cellulose containing the modified AS1411 aptamer. Protonation of carboxylate groups induced cargo release.

Murugan and co-workers described a pH-responsive nanosystem based on polymer-coated MSNs loaded with the anti-tumour agent topotecan (TPT) and quercetin for dual drug delivery in breast cancer (Figure 15).[24] The MSNs were loaded with TPT and coated with a poly(acrylic acid)-CS layer. Moreover the drug quercetin was entrapped in the polymer matrix, and the arginine-glycine-aspartic acid (cRGD) peptide grafted, through the formation of amide linkages, onto the poly(acrylic acid)-CS layer to target cancer cells. The amide bonds in the polymeric coating, after the cellular uptake mediated by cRGD signal, were hydrolysed by the low pH in the lysosomal compartment yielding to cargo release as a consequence of polymer disruption. A significant drug release was observed at acidic pH whereas in physiological conditions (pH 7.4) negligible delivery was registered. The *in vitro* and *in vivo*

anti-tumour activity of the nanomaterial was evaluated in a breast cancer model. The nanocarrier exhibited a remarkable capability to target cancer cells and achieved a sustained dual drug release in the triple negative breast cancer and multidrug resistant (MDR) breast cancer models (MDA-MB-231 and MCF-7). Significant tumour growth suppression was achieved in MDA-MB-231 tumour-bearing mice after intravenously treatment with the nanoparticles. The nanoparticles also improved the specific accumulation of the drugs into tumour site, thus enhancing their anti-tumour activity showing a lower toxicity and adverse effects than the free drugs.

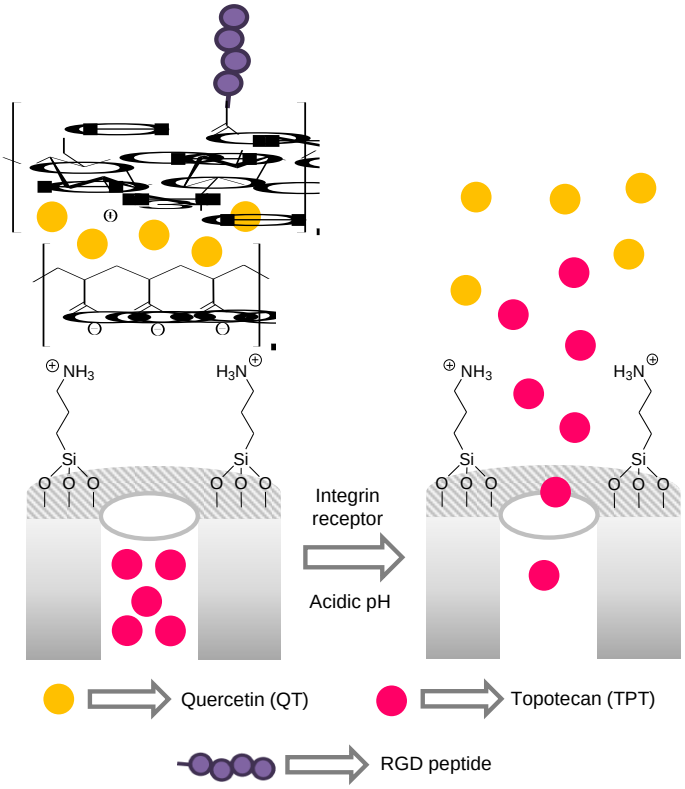

Figure 15. MSNs loaded with TPT, grafted with amino groups and capped electrostatically with a layer of a poly(acrylic acid)-CS.

Li and co-workers encapsulated arsenic trioxide (a drug for haematological diseases approved by the FDA) nanoparticles onto MSNs and the prepared nanodevice was used for *in vivo* tumour treatment (Figure 16).[25] The authors functionalised MSNs with aminopropyl groups using a co-condensation procedure. Then, the pores were loaded with arsenic trioxide

nanoparticles and finally capped upon addition of polyacrylic acid, which formed a polymeric coating around the loaded MSNs through electrostatic interactions. Aqueous suspensions of the final nanoparticles showed a moderate arsenic trioxide release at pH 7.4 (40.5% after 48 h) which was enhanced at acidic pH (76.1 and 59.8% at pH 5.0 and 6.0 respectively). The observed enhancement at acidic pH was ascribed to polyacrylic acid detachment from the nanoparticles surface after protonation. MTT assays showed a dose-dependent reduction in the viability of SMMC-7721 cells. Besides, flow cytometry analysis indicated that nanoparticles were able to arrest proliferation of SMMC-7721 cells at G0/G1 phase. *In vivo* experiments, carried out with Kunming mice xenograft with H22 cells showed a marked reduction in tumour volume and size, compared to free drug group, after intravenously treatment with the nanoparticles. These results were ascribed to the nanoparticle accumulation in tumour, through EPR effect, and to the release of arsenic trioxide.

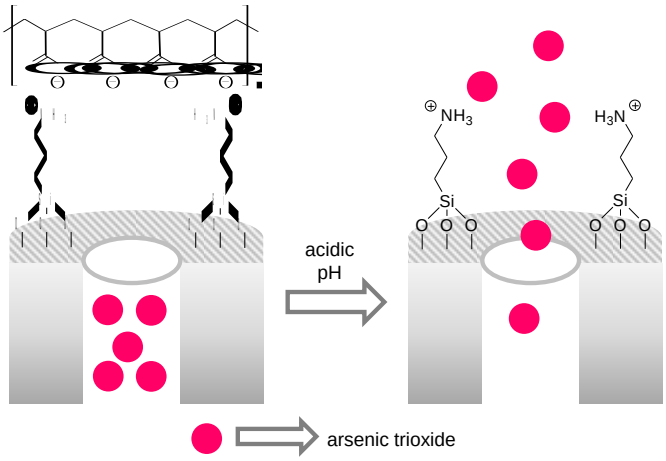

Figure 16. MSNs loaded with arsenic trioxide, functionalised with amino groups and capped with polyacrylic acid. Protonation of carboxylate groups induced cargo release.

Reduced graphene oxide has been also used as support to develop gated materials with *in vivo* application.[26] Wu and workers prepared a pH-driven system using reduced graphene oxide coated with mesoporous silica as support (Figure 17). In a first step, graphene oxide was reduced by the polymerization of dopamine on top of the support which formed a

polydopamine (PDA) layer to increase solubility and stability of the material. Then, mesoporous silica was grown by co-condensation of tetraethyl orthosilicate (TEOS) and APTES in the presence of cetyltrimethylammonium bromide (CTAB). The material was then loaded with Dox and finally capped with HA due to the electrostatic interaction of carboxylate moieties of the polysaccharide with amine groups in the support. Dox release in PBS at pH 7.4 was around 30% at 72 h. However, when pH was fixed at 5.4 Dox release increased until 65% for the same period of time. At acidic pH, the reduction of the electrostatic interaction between amines and HA resulted in polymer detachment which triggered Dox release. The nanocomposite also showed a photothermal release enhancing mechanism. When samples were irradiated with 808 nm laser light (1.5 W/cm^2, 5 min) Dox release was increased ca. 5% at both pH. *In vitro* experiments with CD-44-positive HeLa cells showed high biocompatibility of the unloaded nanomaterial and a dose-dependent cytotoxicity for Dox loaded system. Additionally, cells treated with the unloaded material and irradiated with near infrared (NIR) light showed significant viability decrease. Best results were obtained when cells were treated with Dox-loaded nanomaterial, using an equivalent Dox concentration of 5μM, and irradiated. In this case, a synergic effect was observed and cell viability was reduced until 15% in 24h. The authors also confirmed that cells pretreated with HA showed higher viability when treated with Dox-loaded systems. This effect could be correlated with certain nanocomposite uptake inhibition due to a HA-receptor mediated nanocomposite uptake. Finally, Cy5-loaded nanocomposite was injected intravenously in HeLa tumour-bearing mice. *In vivo* fluorescence images confirmed tumour accumulation and slight liver and spleen signals due to renal clearance. Finally, treatment with Dox-loaded nanomaterial leads to some tumour suppression growth. In contrast, dual treatment with the nanocomposite and NIR light induced practically complete tumour regression within 12 days.

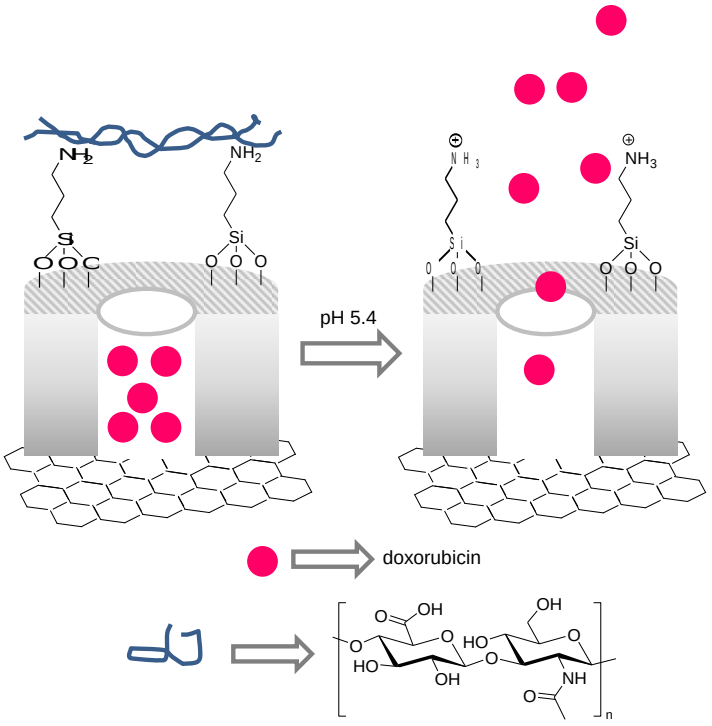

Figure 17. Silica mesoporous-coated reduced graphene oxide loaded with Dox and capped with HA. At acidic pH electrostatic interaction between amine groups and carboxylates of HA is reduced and Dox is released.

Dual targeted (cytosol and nucleus) MSNs able to release two different drugs were prepared by Kannan and co-workers (Figure 18).[27] The synthesis started with the functionalisation of the external surface of MSNs with aminopropyl moieties and pore loading with TPT. Then the amino groups were reacted with a fluorescein-transactivator of transcription (TAT) peptide, which has the ability to transport nanoparticles inside nucleus via the coordination with importin receptors, using EDC/NHS as coupling agents. The final nanodevice was prepared by adsorbing though electrostatic interactions onto the external surface of the nanoparticles poly(acrylic acid) functionalized with the RGD peptide, able to interact with integrin receptors overexpressed in tumour cells, and citraconic acid containing metformin. Aqueous suspensions of the nanoparticles at pH 7.4 showed negligible cargo release after 48 h (13.1 and 17.3 % of TPT and metformin respectively). However, at pH 4.8, a marked delivery of

both drugs was observed (88.8 and 93.3% of TPT and metformin, respectively) after the same period of time. At acidic pH, the carboxylate moieties of poly(acrylic acid)-RGB and citraconic acid-metformin were protonated and both coatings detached from the nanoparticles surface with subsequent TPT release. The cytotoxicity of the prepared nanoparticles in MDA-MB-231 cells (overexpressed integrin receptors) was tested using MTT assays. These tests indicated that nanoparticles induced a marked reduction in the viability of MDA-MB-231 cells due to its receptor-mediated endocytosis and subsequent release of metformin in the cytoplasm and TPT in the nucleus via internalization of the uncapped nanoparticles mediated by the TAT peptide. CLSM and bio-TEM studies confirmed the selective release of metformin in the cytoplasm, the TAT-mediated nuclear internalisation of the uncapped nanoparticles and the metformin delivery in the nucleus. Release of both drugs induced cell apoptosis. Athymic nude female mice xenograft with MDA-MB-231 cells were treated with the prepared nanoparticles and compared to free drug administration by tail vein injection. A marked reduction in tumour volume was observed with the nanoparticles, enhancing the therapeutic effect of the drugs. Besides, histopathology studies revealed minimal damage in heart, lung and kidneys.

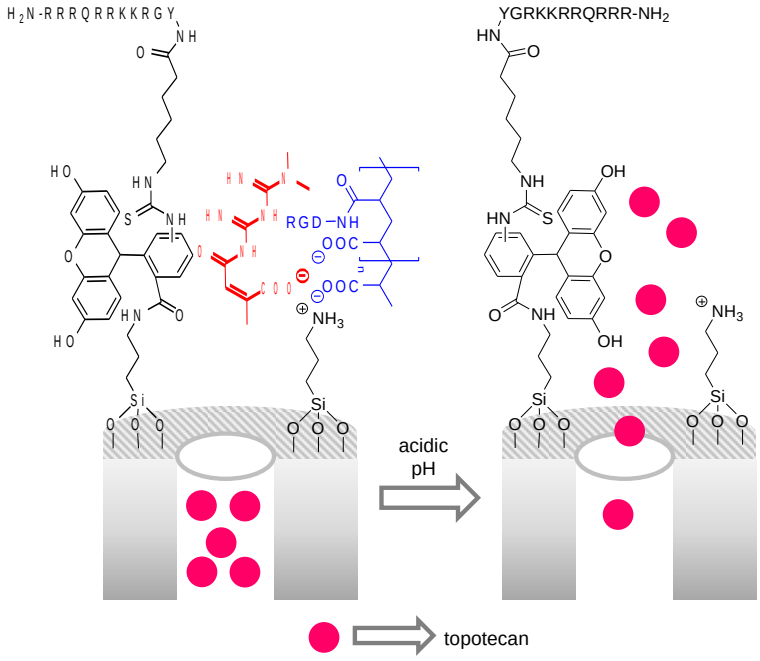

Figure 18. MSNs loaded with TPT, grafted with a fluorescein-TAT peptide and capped with poly(acrylic acid) functionalized with RGD peptide (in blue) and citraconic acid containing metformin (in red). Cargo delivery is triggered by protonation of the carboxylate groups.

Alibolandi and co-workers prepared a theranostic system based on MSNs and Au nanoparticles for computed tomography (CT) detection and controlled drug release.[28] MSNs functionalised with aminopropyl moieties were prepared using a co-condensation procedure and the pores were loaded with 5-fluorouracil or with rhodamine 6G. Afterward, the external surface of the loaded support was decorated with Au nanoparticles coated with citrate through electrostatic interactions. In the next step, the external surface of the Au nanoparticles was functionalised with a PEG polymer bearing thiol and carboxylate moieties on its ends. Finally, the carboxylate end of the grafted PEG was functionalised with the EpCAM aptamer using EDC/NHS as coupling agents, to target a trans-membrane glycosylated protein overexpressed in various adenocarcinomas and with low levels of expression in healthy tissues (Figure 19). Aqueous suspensions of the prepared nanoparticles showed negligible release at pH 7.4 (ca. 3% after 96 h) whereas a moderate enhancement in delivery (30% after 96 h) was observed at pH 5.5. Cargo release was ascribed to citrate protonation and detachment of Au nanoparticles. Confocal microscopy and flow cytometry measurements, carried out with rhodamine 6G-loaded nanoparticles, showed a marked internalization in HepG2 cells (overexpressing EpCAM protein) through receptor-mediated endocytosis whereas negligible uptake was observed for EpCAM negative CHO cells. MTT assays showed a marked reduction of HepG2 cells viability when treated with 5-fluorouracil-loaded capped nanoparticles due to receptor-mediated uptake and subsequent drug release. *In vivo* IVIS imaging studies, carried out with C57BL/6 nude mice xenograft with HepG2 cells treated with rhodamine 6G-loaded nanoparticles showed a marked accumulation of the nanodevice in the tumours after 6 h post-

injection due to EPR effect and active targeting. Besides, CT measurements also showed the nanodevice accumulation in tumours.

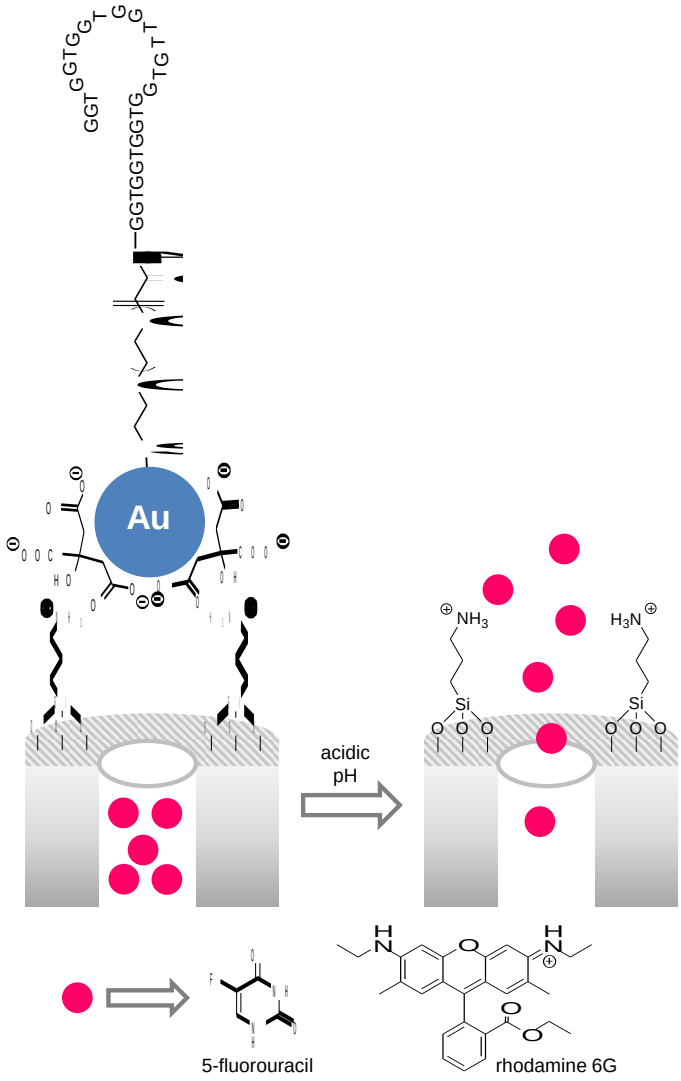

Figure 19. MSNs loaded with 5-fluorouracil or with rhodamine 6G and decorated with Au nanoparticles capped with citrate. The AuNPs were functionalised with PEG polymer conjugated to EpCAM aptamer. Cargo delivery is due to citrate protonation.

McNally et al, reported gold nanorods coated with a spherical mesoporous silica shell as potential nanosystems used for the detection and treatment of pancreatic tumours (Figure 20). Imaging was achieved using multispectral optoacoustic tomography by excitation of nanorods

with a NIR light that induced the emission of an acoustic signal.[29] For the preparation of the nanodevice, gold nanorods were coated with a mesoporous silica shell containing aminopropyl moieties using a co-condensation protocol. The external surface of the mesoporous silica shell was further functionalized with (3-glycidyloxypropyl)trimethoxysilane. In the next step CS was grafted onto the external surface through a Michael addition reaction between the epoxide moieties onto the nanoparticles' surface and the amino groups of the biopolymer. Then, the V7 peptide (which inserts non-specifically into phospholipid membranes in acidic environments) was reacted with the amino groups located onto the nanoparticles' surface using *N*-succinimidyl-4-(maleimidomethyl) cyclohexanecarboxylate as linker. Finally, the pores of the nanodevice were loaded with IR-780 or with gemcitabine. Drug release assays showed a negligible gemcitabine release at pH 7.4 (ca. 10% after 1 h) that was markedly enhanced at acidic pH (ca. 90% at pH 6.0 after 1 h). This release at acidic pH was ascribed to protonation of CS chains, which induced swelling of the polymer allowing drug delivery. Viability assays with S2VP10 and MiaPaca2 cells carried out with the gemcitabine-loaded nanoparticles showed a negligible cytotoxicity at neutral pH. However, a marked reduction in viability for both cell lines (up to ca. 97% cell death) was observed at pH 6.5, which was ascribed to nanoparticle endocytosis mediated by V7 peptide and endosomal drug release into the cytosol. Besides, female SCID mice implanted with orthotopic pancreatic adenocarcinoma tumours of S2VP10 and S2013 cells were treated with the IR-780-loaded nanoparticles. After 3 h of intravenous administration, multispectral optoacoustic tomography showed significant intratumoral accumulation of the nanoparticles with minimal accumulation in liver and kidney.

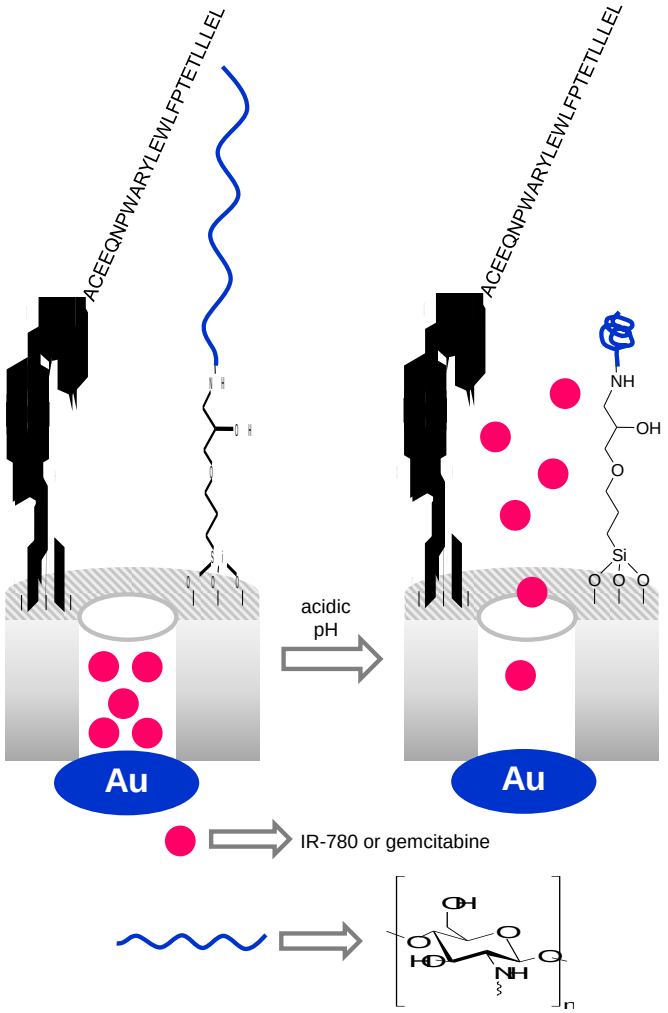

Figure 20. Gold nanorods coated with a mesoporous silica shell, loaded with IR-780 or gemcitabine, grafted with the V7 peptide and capped with CS. Release at acidic pH is due to protonation of CS chains, which induces swelling of the polymer.

Zhang and co-workers prepared MSNs that were loaded with the drug sorafenib or with C6 (a coumarin derivative acting as fluorophore). Then, the external surface of the loaded supports was functionalised with mercaptopropyl groups and the thiol moieties reacted with a maleimide-derivatised poly(L-histidine) though a Michael addition. Finally, the amino groups on the grafted poly(L-histidine) were reacted with PEG_{2000}-succinimidyl carboxymethyl ester through the formation of amide bonds (Figure 21).[30] PBS suspensions of the nanoparticles at neutral pH (7.4) showed a moderate cargo release (ca. 25% after 72 h) which was enhanced

(ca. 66% after 72 h) at acidic pH (5.0). The observed enhancement was ascribed to protonation of imidazole ring in the poly(L-histidine) backbone (pK_a = 6.1) which induced the polymeric layer to adopt an extended conformation with subsequent pore opening and cargo release. MTT assays carried out with the sorafenib-loaded nanodevices and HepG2 cells showed a marked reduction in cell viability in a dose-dependent manner due to nanoparticles' internalization and release of the entrapped drug. Besides, confocal microscopy studies carried out with the C6-loaded solid showed a marked C6 fluorescence in the cytoplasm due to the internalization of the nanoparticles and pore opening in the acidic environment on the lysosomes. Female Kunming mice were subcutaneously injected with H22 cells and then were administered with sorafenib-loaded nanoparticles via tail intravenous injection. This treatment induced a marked tumour growth inhibition due to the sorafenib release and the accumulation of the nanodevices in the tumour thanks to the EPR effect. Besides, histological analysis of tissues from the representative organs (kidneys, lungs, spleen, liver and heart) showed no obvious damage in mice treated with the unloaded nanodevice.

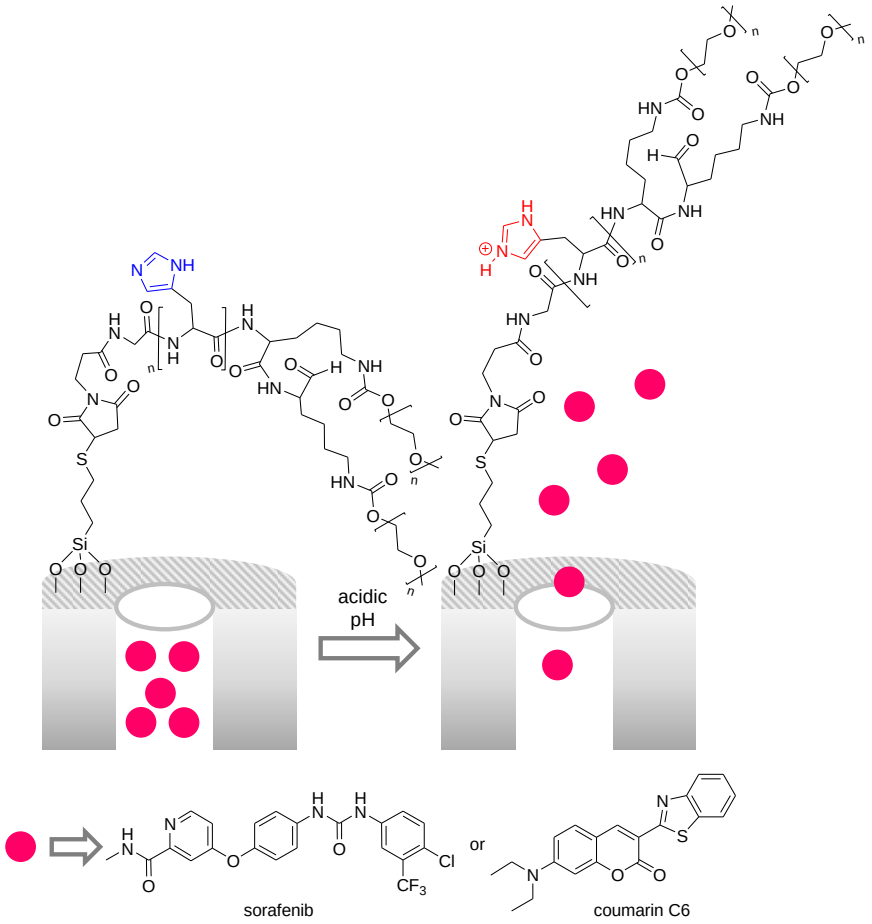

Figure 21. MSNs were loaded with sorafenib or coumarin C6 and capped with poly(L-histidine)-PEG. Protonation of the imidazole ring induced cargo release.

Zhang and co-workers prepared MSNs coated with an oligopeptide lipid liposome able to co-delivery erlotinib and Dox in the acidic environment of tumours (Figure 22).[31] The authors functionalised MSNs with aminopropyl moieties. Then Dox was loaded onto the pores and the nanoparticles coated with 1,5-dioctadeyl-L-glutamyl-2-histidyl-hexahydrobenzoic acid. Finally, erlotinib was adsorbed onto the external lipid coating yielding the final nanodevice. Controlled release studies showed that the nanoparticles remained tightly capped at neutral pH (7.4) whereas a marked delivery of both drugs (61 and 51% for erlotinib and Dox respectively after 48 h) at pH 4.5 was obtained. The observed delivery at acidic pH was ascribed to protonation of imidazole heterocycles and hydrolysis of the amide bonds (which linked hexahydrobenzoic acid) onto the lipid shell. Both reactions induced the appearance of

two positive charges in the lipid layer inducing the disruption of the coating shell by electrostatic repulsions. The prepared nanodevice was efficiently internalized by A549 cells via energy-mediated macropinocytosis and marked Dox fluorescence was observed in the cytoplasm after 1 h, whereas at longer times (8 h) drug emission was also observed in cell nuclei. Besides, MTT viability assays carried out at pH 6.5 showed a dose-dependent cytotoxic effect of the nanodecvices due to the co-delivery of both drugs. *In vivo* studies carried out in male C57/BL6 mice xenograft with LLC cells showed that nanodevices (administered through tail vein injection) were able to inhibit tumour growth and a marked reduction in volume through suppression of cell proliferation and induction of apoptosis was observed when compared to the free drug.

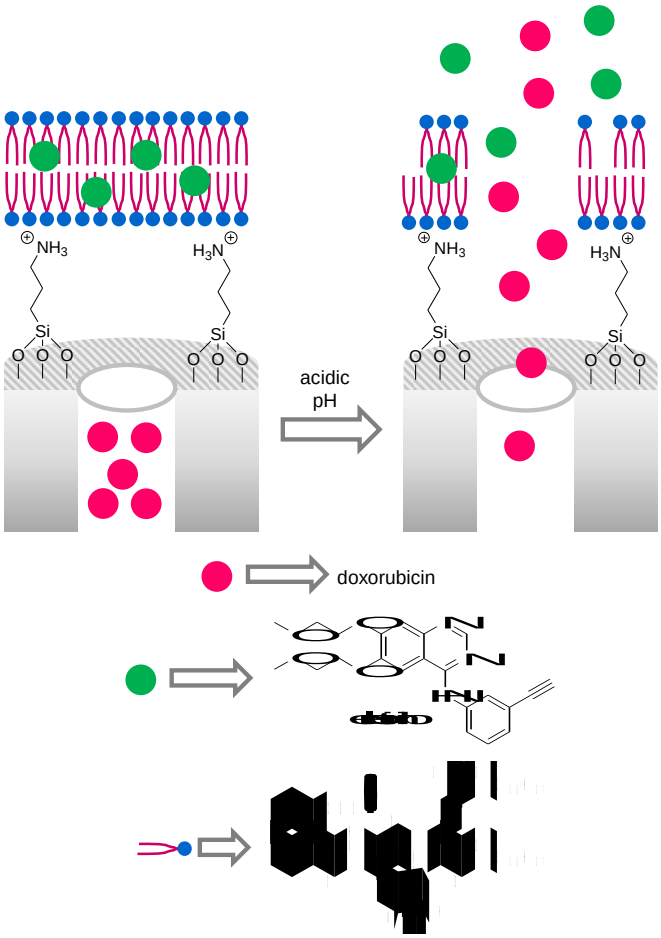

Figure 22. MSNs loaded with Dox and coated with an external lipid layer in which erlotinib was adsorbed. Cargo release is due to protonation of imidazole heterocycles and hydrolysis of the amide bonds.

Mesoporous titania nanoparticles were prepared and used as inorganic scaffold for the stimuli-responsive combined release of PTX and microRNA 708 (miR708 for c-FLIP protein suppression which is strongly expressed in several cancers).[32] For this purpose mesoporous titania nanoparticles were loaded with PTX and the surface functionalised with (3-glycidyloxypropyl)trimethoxysilane. Then, the epoxide moieties onto the surface were reacted with the positively charged poly(L-lysine) polymer. Next, miR708 was adsorbed, through electrostatic interactions, onto the positively charged polymeric shell. Afterward, nanoparticles were coated with the negatively charged methoxy-PEG-*b*-poly(L-aspartic acid) polymer (Figure 23). Aqueous suspensions of the nanoparticles showed a moderate PTX release at pH 7.4 (33% after 48 h) whereas at pH 5.0 a marked payload delivery was found (72% after 48 h). The observed enhancement at acidic pH was ascribed to methoxy-PEG-*b*-poly(L-aspartic acid) protonation which leads to the disassembly of the layer-by-layer coating. MTT assays carried out with the colorectal carcinoma cell lines HCT-116 and DLD-1 showed a marked reduction in viability in a dose-dependent fashion. Besides, CLSM studies, carried out with the nanoparticles loaded with coumarin-6 instead of PTX, showed the proper endocytosis of the nanodevice and their lysosomal localization. Western blot analysis of HCT-116 and DLD-1 cells treated with nanoparticles showed a marked inhibition of c-FLIP expression. Finally, an intravenous administration of the capped nanoparticles to DLD-1 xenograft tumour-bearing mice induced a marked inhibition of tumour growth compared to free PTX. Besides, histopathological analysis showed a drastic reduction in tumour cell volume and no signs of organ damage.

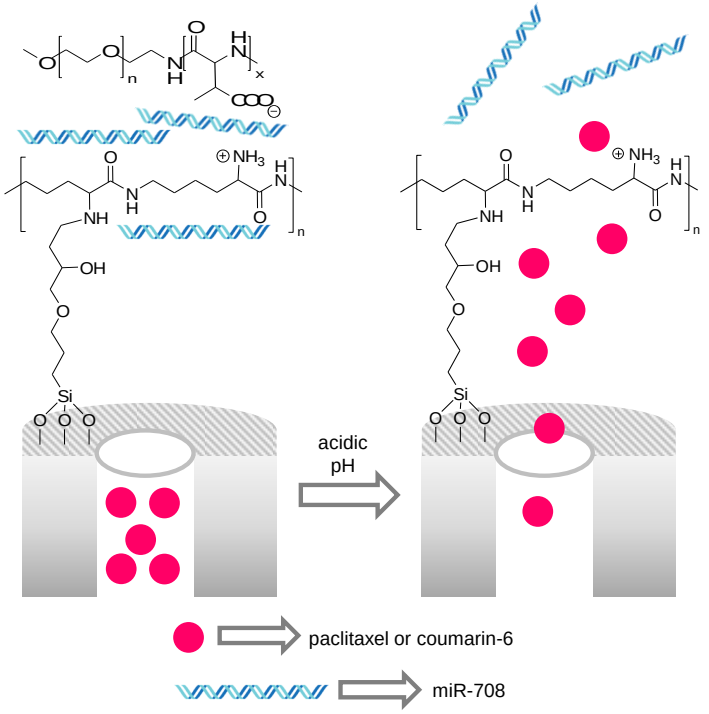

Figure 23. Mesoporous titania nanoparticles loaded with PTX or coumarin-6 and covalently functionalized with poly(L-lysine) polymer and finally capped with the methoxy-PEG-*b*-poly(L-aspartic acid) polymer. MicroRNA-708 was assembled between the polymer layers. Protonation of methoxy-PEG-*b*-poly(L-aspartic acid) induced cargo delivery.

The cytotoxicity of celastrol-loaded MSNs was tested in different cell lines and *in vivo* by Kim and co-workers (Figure 24).[33] For the preparation of the final nanodevices the authors mixed celastrol, CTAB and NH_4F and allowed the crude to react for 1 h. Then TEOS was added yielding, after 2 h, celastrol-loaded MSNs. Finally pores were capped with the negatively charged poly(L-aspartic acid)$_{10}$-*b*-PEG$_{5000}$ through electrostatic interactions with the positively charged surface of celastrol-loaded MSNs. Suspensions of the nanoparticles in PBS buffer at pH 7.4 showed a moderate celastrol release (ca. 10.5% after 48 h) which was enhanced to 16.5% after 48 h when pH was lowered to 5.0. This moderate enhancement was ascribed to the detachment of poly(L-aspartic acid)$_{10}$-*b*-PEG$_{5000}$ from the nanoparticle surface after protonation of the carboxylate moieties in an acidic environment. MTS viability assays

showed that nanoparticles were able to efficiently kill BT-474, SCC7 and SH-SY5Y cells. Besides, nanoparticles injected by tail vein in mice xenograft with SCC7 cells inhibited tumour growth and reduced tumour weight and volume.

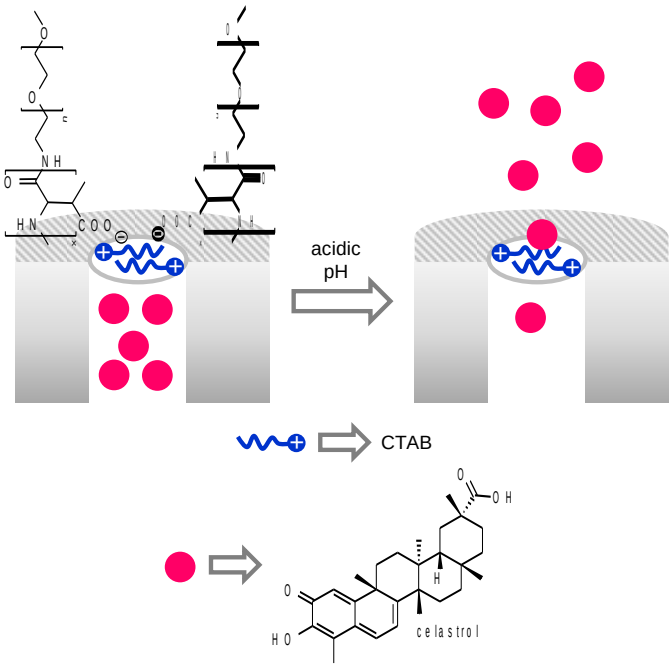

Figure 24. MSNs containing CTAB were loaded with celastrol and capped with poly(L-aspartic acid)$_{10}$-*b*-PEG$_{5000}$. Protonation of the carboxylate moieties in an acidic environment induced cargo release.

Co-delivery of Dox and gemcitabine was achieved using gold clusters-capped MSNs.[34] In a first step the authors functionalized MSNs with aminopropyl moieties. Moreover, gold clusters (AuNC) conjugated with bovine serum albumin (BSA) were synthesized by BSA-induced reduction of Au(III) salts. Using both components various types of solids were prepared by loading the pores of the MSNs with several cargos and by incorporating different molecules onto the BSA-AuNC ensemble by electrostatic interactions with the protein shell. The final nanodevices were obtained by capping the pores of the loaded MSNs with the BSA-AuNC through simple electrostatic interactions (Figure 25). Using this procedure three nanodevices were prepared containing (i) Dox in the MSNs and also in the BSA-AuNC, (ii)

Hoechst 33342 in the MSNs and Dox in the BSA-AuNC, and (iii) gemcitabine in the MSNs and Dox in the BSA-AuNC. Controlled release experiments showed negligible cargo release at pH 7.0 for the three nanodevices. As clear contrast, at pH 5.0, marked cargo delivery was observed for all three solids due to protonation of BSA (isoelectric point at 4.8) and subsequent detachment of the BSA-AuNC ensemble from the MSNs surface. CLSM carried out with the three nanodevices in A549 cancer cells showed internalization of the nanoparticles and the release of the entrapped cargos. Besides, release of Dox and Dox + gemcitabine induced an efficient cancer cell killing with nearly no cell survival at 100 μg/mL. Finally, for *in vivo* studies, other set of nanoparticles were prepared bearing only Hoechst 33342 in the MSNs. These nanoparticles were subcutaneously injected to nude mice xenograft with Human pancreatic cancer cells (MiaPaca 2) and, after certain time, the delivered dye and the detached BSA-AuNC accumulated mainly in the tumour due to EPR effect and partly in the liver and kidneys.

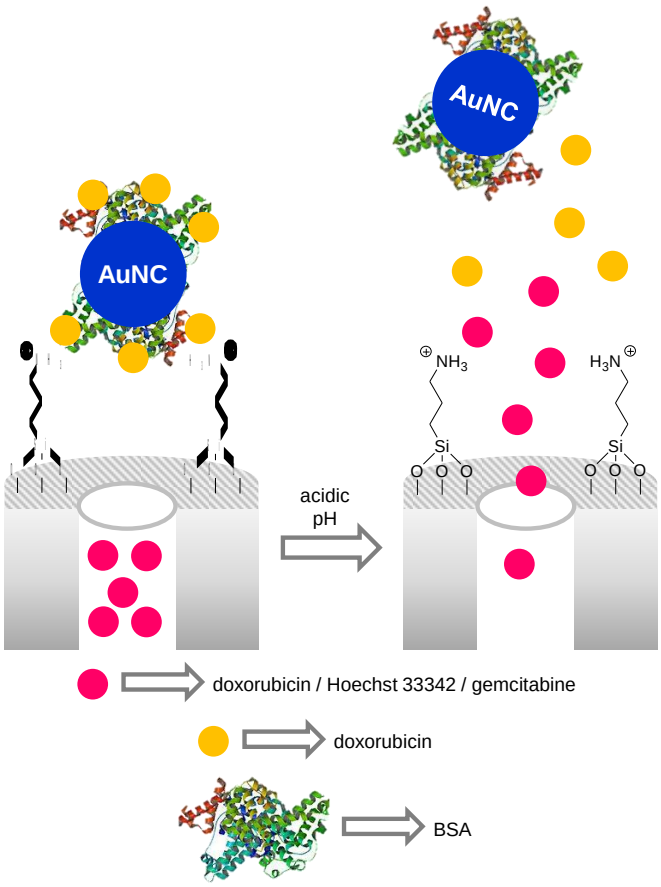

Figure 25. Gold clusters (AuNC) conjugated with BSA used as gatekeeper in MSNs loaded with Dox, gemcitabine or Hoechst 33342. Dox was additionally incorporated in the BSA-AuNC ensemble. Cargo delivery is attributed to protonation of BSA at acidic pH.

An appealing approach in pH-triggered drug delivery systems is the use of polyethylenimine (PEI) as coating for loaded nanomaterials. The cationic polymer PEI acts as proton sponge in acidic environments, thus facilitating the scape from the endocytic compartments with the subsequent drug release. Attending to this property, the use of this polymer has been widely described for gene delivery using different nanocarriers. Moreover, the amine groups of PEI can be easily conjugated with other molecules which could act as targeting ligands.[35] Following this approach, Chen and co-workers prepared MSNs with enhanced blood-brain barrier (BBB) permeability to treat human brain glioma (Figure 26).[36] The final

nanoparticles were prepared by loading the pores of the MSNs with a new selenium drug, prepared by the reaction between 4-carboxy-*o*-phenylenediamine and selenium dioxide, and then by coating the external surface of the nanoparticles with PEI and the RGD tripeptide. *In vitro* studies showed a moderate drug release at pH 7.4 (47% after 60 h) that was enhanced at acidic pH (ca. 86% after 60 h). This release at acidic pH was ascribed to the dissociation of the polymer from nanoparticles surface due to silanolate protonation. Co-cultures of bEnd.3 cells (mimicking brain capillary endothelial cells) on a culture insert of a transwell and U87 cells (human primary glioblastoma cells) located on the basolateral compartment were prepared in order to evaluate BBB permeability of the prepared nanoparticles. These studies showed a 61% permeability ratio than was ascribed to the presence of RGD peptide in the nanoparticles which facilitates transport. Once in contact with U87 cells, nanoparticles were endocytosed through the interaction of the integrin expressed in cells membrane with the RGD peptide, reaching first lysosomes and then released to the cytoplasm. MTT viability assays carried out with U87 cells showed a marked growth inhibition due to apoptosis induction and reactive oxygen species (ROS) generation by the released selenium drug. Besides, the same nanoparticles uptake was observed for glioma U87 tumour spheroids with a strong growth inhibition. Finally, Sprague-Dawley mice were intravenously injected with the prepared nanoparticles and histological studies of the different organs showed that there was no apparent damage in liver, lungs and kidneys.

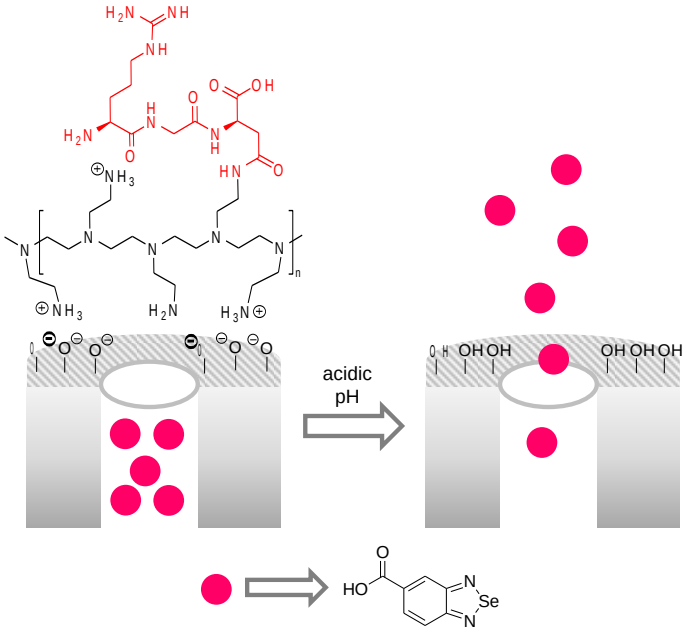

Figure 26. MSNs loaded with a selenium drug and capped with PEI and the RGD tripeptide. Cargo release at acidic pH was ascribed to silanolate protonation.

Gupta and co-workers designed core-shell silica-supported mesoporous titania nanoparticles (MTNs) for Dox delivery in breast cancer (Figure 27).[37] The nanoparticles were loaded with Dox and coated with poly-(L-lysine) polymer (PLL), through electrostatic interactions, onto the nanoparticle surface. Finally HA was electrostatically adsorbed onto the PLL layer to stabilize the carrier and target the CD44 receptor expressed in tumour cells. Drug release was confirmed to occur at low pH values. At pH 5.0, the ionic interactions were broken due to MTNs (isoelectric point of TiO_2 is in the 4-6 interval) and HA protonation. The material was studied in MDA-MB-231 xenograft tumour-bearing mice, as breast cancer model. The nanoparticles were intravenously administered confirming an enhanced inhibition of tumour growth compared to the free formulation.

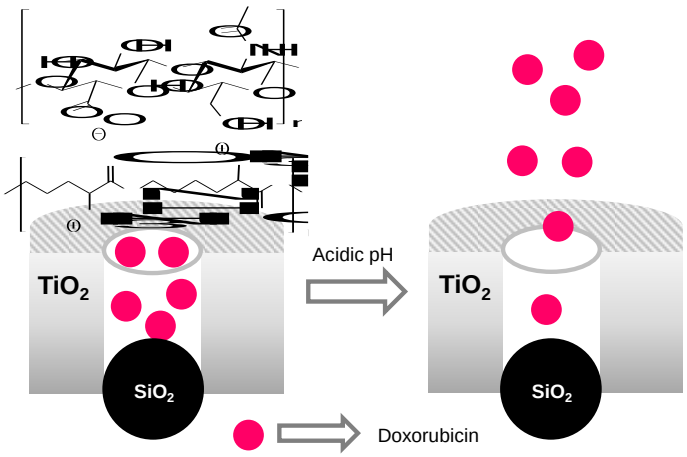

Figure 27. SiO_2 nanoparticles coated with a mesoporous TiO_2 shell, loaded with Dox and capped with pH-sensitive poly-L-Lysine and HA layers. Delivery was attributed to MTNs and HA protonation.

Ma and co-workers evaluated different sized MSNs (20, 40 and 80 nm diameter) for precise drug delivery in cancer therapy.[38] The different MSNs were loaded with an anticancer ruthenium polypyridyl complex and their external surface coated, through electrostatic interactions, with PEI functionalised with FA (Figure 28). After the FA receptor recognition by the cell, the nanocarrier was endocytosed, the acidic pH in the endocytic compartments facilitated PEI disassembly and the drug was delivered. Drug release studies were carried out in PBS at pH 7.4, emulating blood circulation, and compared with cell lysates to simulate the environment of cancer cells. The results demonstrated a significant drug release under intracellular conditions. The nanosystem was tested *in vitro* in HepG2 hepatocellular carcinoma cells and Dox-resistant HepG2 cells and *in vivo* in HepG2 tumour-bearing nude mice. *In vitro* experiments showed an anti-cancer activity of the prepared nanoparticles being the smaller (20 nm) more sensitive to HepG2 cells whereas the larger (80 nm) presented a higher inhibitory effect in Dox-resistant HepG2 cells. *In vivo* biodistribution studies showed preferential accumulation of the nanoparticles in the tumour after intravenous injection. Besides, the smaller sized nanoparticles (20 nm) accumulated in tumour more than the larger

nanoparticles (40 and 80 nm). On the other hand, all prepared nanoparticles promoted tumour regression *in vivo* without obvious toxicity (tumour growth inhibition of 46.16, 43.24 and 38.31% for nanoparticles of 20, 40 and 80 nm, respectively). Histopathological staining showed no significant damage in heart, liver, spleen, lung and kidney whereas tumour tissues presented marked necrosis.

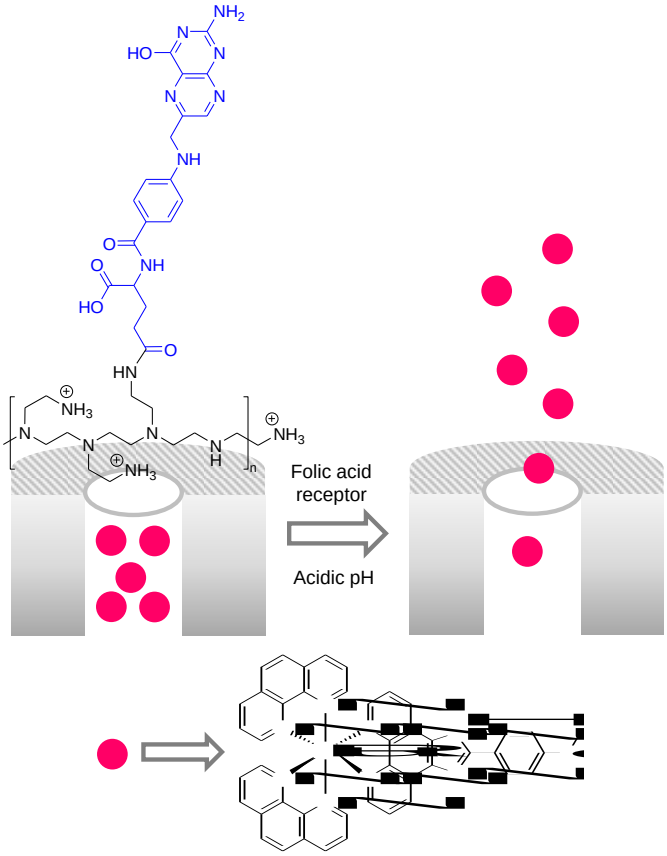

Figure 28. MSNs loaded with a ruthenium polypyridyl complex and coated with PEI polymer functionalized with FA (FA). Acidic pH induces PEI disassembly and drug delivery.

Multifunctional magnetic core-shell MSNs able to deliver simultaneously let-7a micro interfering RNA (miRNA), which has the ability to repress DNA repair mechanism and downregulate drug efflux pumps, and Dox in cancer cells were prepared by Lee and co-workers (Figure 29).[39] Magnetic $ZnFe_2O_4$ nanoparticles were coated with a mesoporous silica shell. The mesoporous coating was functionalised with trihydroxysilylpropylmethyl phosphonate and the pores loaded with Dox. Afterward, PEI was absorbed through

electrostatic interactions onto the external negatively charged surface of the Dox-loaded nanoparticles. Next, let-7a miRNA was adsorbed, through electrostatic interactions, onto the PEI layer. Lastly, the external surface was again coated with a PEI layer in which PEG containing the internalizing RGD peptide (which binds with α_v integrins) was covalently linked. MTT assays carried out using MDA-MB-231 cells (which overexpressed integrins) incubated with the prepared nanodevices showed a dose-dependent decrease in cell viability (ca. 90% with 100 μg/mL of nanoparticles). This marked reduction in cell viability was ascribed to nanoparticles internalization and let-7a miRNA and Dox delivery. Finally, MDA-MB-231 xenografted BALB/c nude mice were treated by tail vein injection with the prepared nanoparticles, and compared to the free drug, resulting in significant decrease in tumour volume due to the combined action of let-7a miRNA and Dox. Fluorescence imaging and MRI measurements showed the accumulation of nanoparticles in tumours.

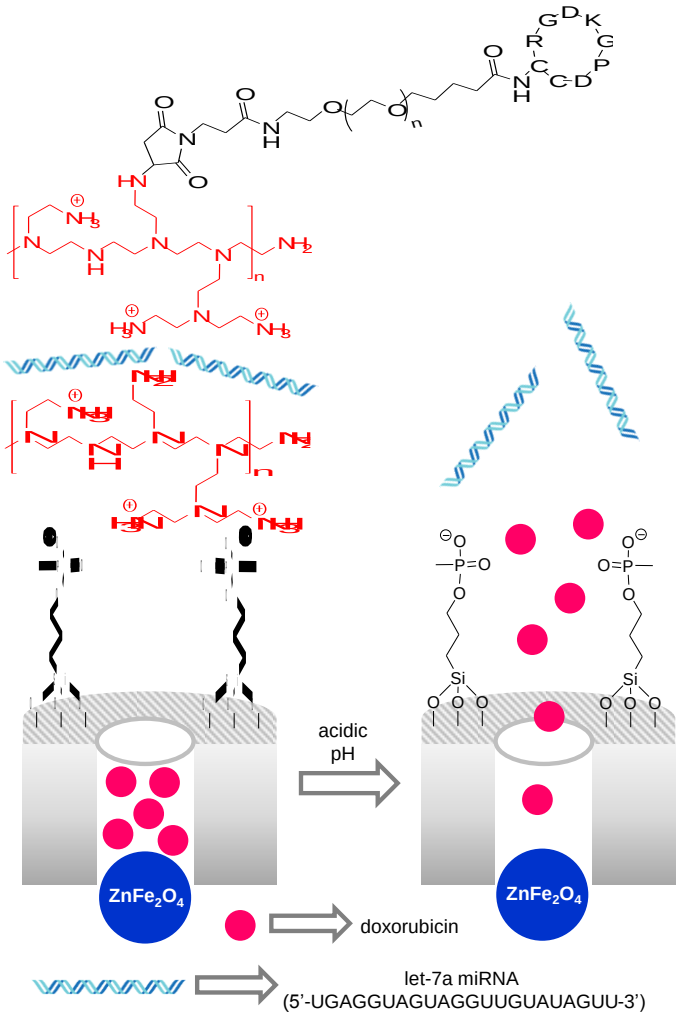

Figure 29. $ZnFe_2O_4$ core-shell MSNs loaded with Dox, grafted with PEI in which let-7a miRNA was adsorbed. Finally there is a PEI layer modified with PEG containing the RGD peptide. Acidic pH induces PEI disassembly and drug delivery.

Mamaeva et al. developed a system to target the glucose receptor in breast cancer stem cells (CSCs) for efficient release of stem cells inhibitors (ϒ-secretase inhibitors).[40] It is known that the glycolytic activity is increased in cancer cells and the glucose receptors are exposed at the cell membrane. To reach glycolytic cancer cells, the authors used carboxylic acid decorated MSNs loaded with ϒ-secretase inhibitors (GSI) and capped with PEI functionalised with glucuronic acid through the formation of amide bonds (Figure 30). Drug release was promoted after nanoparticles recognition by the glucose-receptor, which mediated their

endocytosis and thus the disassembly of the coating in the acidic cell compartments. Cellular uptake of the nanoparticles was studied in breast cancer models (MCF7 and MDA-MB-231) *in vitro*, the results showing a preferentially uptake of the nanoparticles by CSCs with a high glycolytic profile. *In vivo* studies were performed in murine xenograft models of breast cancer (using MDA-MB-231 cells) and MDA-MB-231 transplants on chick embryo chrioallantonic membranes. The results demonstrated the ability of the GSI-loaded glucose-functionalized MSNs to target the tumour and to reduce the CSCs population.

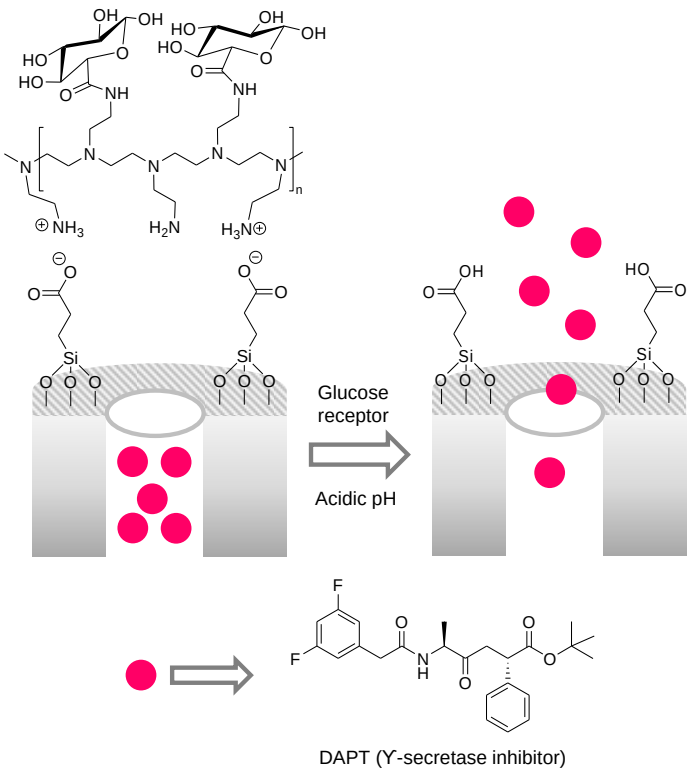

Figure 30. MSNs loaded with ϒ-secretase inhibitors (GSI), grafted with carboxylic groups and capped with PEI polymer functionalized with glucose moieties. Acidic pH induces carboxylate protonation and PEI disassembly.

Shen and co-workers prepared capped nanodevices for the efficient co-delivery of Dox and siRNA for the treatment of triple negative breast cancer.[41] For this purpose, MSNs were functionalised with isocyanatopropyl moieties, the pores were loaded with Dox and the external surface functionalised with a β-CD-PEI conjugate through the formation of urea

bonds. Finally, Dox was included into the β-CD hydrophobic cavity and PKM2 siRNA (sense and anti-sense sequences used CCA UAA UCG UCC UCA CCA A[dT][dT] and UUG GUG AGG ACG AUU AUG G[dT][dT] respectively) was adsorbed through electrostatic interactions onto the PEI layer (Figure 31). Aqueous suspensions of the nanodevice at pH 7.4 showed a moderate cargo release (10% of Dox and 30% of siRNA) after 72 h. As marked contrast, a remarkable delivery of Dox (80%) and siRNA (60%) was observed at pH 5.2 after the same time period. The authors ascribed the enhanced Dox release at pH 5.2 to PEI protonation. This PEI protonation induced the disruption of the cap and also generated electrostatic repulsion with the Dox included into the hydrophobic cavity of the β-CD. Flow cytometry and confocal microscopy studies revealed internalization of the nanodevices through endocytosis in MDA-MB-231 cells. At shorter times (up to 2 h) the released cargos were located in the lysosomes whereas after 6 h some of the Dox and siRNA were present in the cytoplasm and nucleus. Lysosomal escape was ascribed to PEI protonation. MTT assays carried out with the nanodevice and MDA-MB-231 cells showed a marked reduction in viability (ca. 80%) because the released siRNA was able to sensitize cells to Dox. *In vivo* studies were carried out with an orthotopic mouse model of MDA-MB-231 breast cancer treated with the nanoparticles or with free Dox intravenously administered. A major therapeutic effect was achieved with the nanoformulation when compared with the free drug. The nanoparticles induced a marked decrease in tumour weight and immunohistochemistry analysis confirmed the suppression of PKM2 expression in tumour tissues.

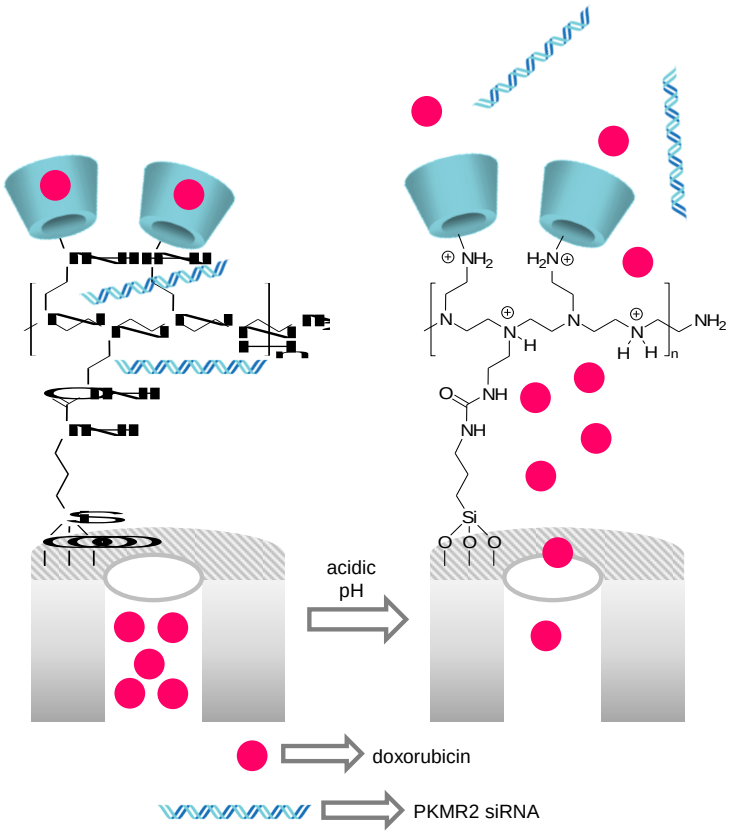

Figure 31. MSNs loaded with Dox and capped with β-CD-PEI conjugate. PKMR2 siRNA adsorbed through electrostatic interactions onto the PEI layer. Cargo delivery was attributed to PEI protonation.

MSNs functionalized with FA (folate receptors (FR) are overexpressed in cancer cells) or with methionine (tumour cells required higher amounts of this amino acid than normal cells) were used for the targeted release of docetaxel (Figure 32).[42] For the preparation of both nanodevices the authors used MSNs functionalised with aminopropyl moieties using a co-condensation procedure. The amino groups of the inorganic support were then reacted with FA using EDC/NHS as coupling agents. For the preparation of the methionine-functionalised MSNs the amino groups were first reacted with epiclon B-4400 (3a,4,5,7a-tetrhydro-7-methyl-5-(tetrahydro-2,5-dioxo-3-furanyl)-1,3-isobenzofurandione. This reaction yielded MSNs with carboxylic acid groups onto the external surface. Then, methionine was linked to

the carboxylic groups using NHS/EDC as coupling agents. The pores of both types of nanoparticles were loaded with docetaxel. Both nanoparticles showed marked and sustained docetaxel release at neutral pH (ca. 60% after 10 h) that was moderately enhanced (ca. 80% after 10 h) at acidic (5.5) pH. At neutral pH docetaxel interacted with the amino moieties onto the internal pore surface through hydrogen bonds. However, at acidic pH, the percentage of protonated amino moieties was increased which induced a reduction in the hydrogen bond interactions with the consequence of a moderate enhancement in drug release. MTT assays carried out with both types of nanoparticles and MCF-7 cells showed a dose-dependent reduction in cell viability with a marked reduction in the IC_{50} values (5.72 and 6.99 nM for FA and methionine functionalised materials respectively) when compared with that of free docetaxel (81.8 nM). Flow cytometry studies showed that both nanoparticles induced cell apoptosis through receptor-mediated cell internalization. *In vivo* studies were carried out with the FA- and methionine-functionalised nanoparticles derivatised with FITC and with empty pores. BALB/c mice xenografted with MCF-7 cells were intravenously treated with the nanoparticles and its biodistribution in the excises organs studied by fluorescence. Nanoparticles accumulated mainly in the tumour and in a lesser extent in the kidney.

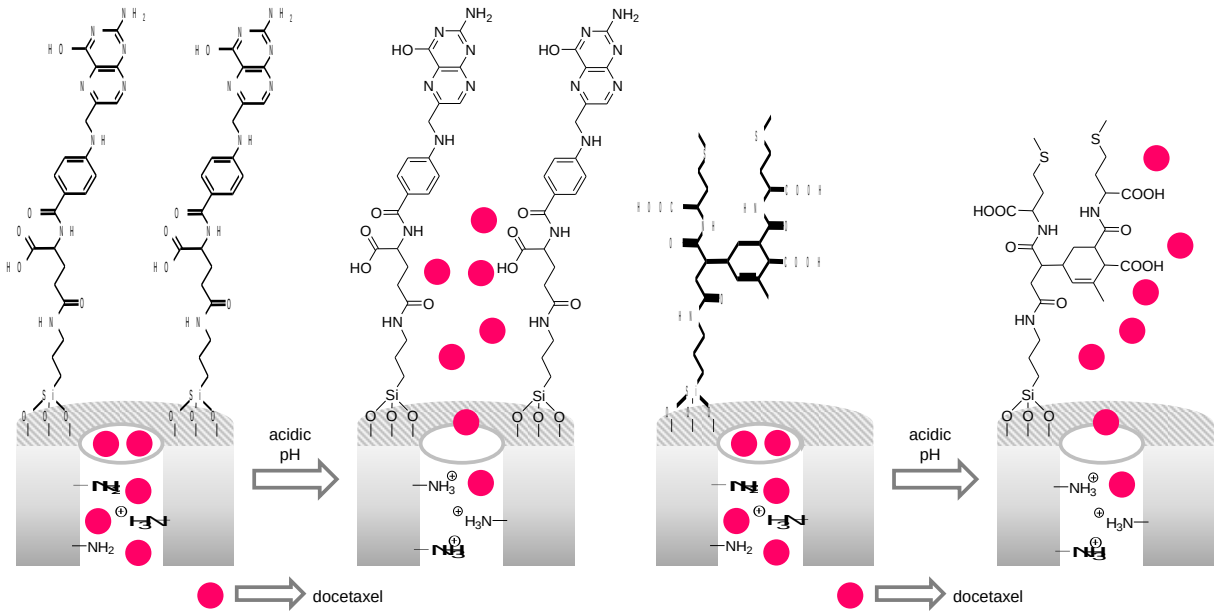

Figure 32. MSNs loaded with docetaxel and capped with FA (left) or methionine (right). Delivery is attributed to protonation of the amino groups.

Chen and coworkers prepared a new gated system activated by a combination of pH conditions, optical hyperthermia and ROS generation.[43] Amino-functionalized MSNs were loaded with Dox and mixed with L-cysteine-stabilized AuNPs in the presence of $FeCl_2$ to obtain an AuNPs-capped nanodevice by the formation of a Fe^{2+} coordinating bridge between cysteine and amino groups of the MSNs surface (Figure 33). The system showed negligible release in PBS buffer at pH 7.4 while Dox was efficiently released at pH 5.5 reaching a 95% in 24 h. This pH-dependent release can be explained in terms of the protonation of amine group in the surface of MSNs, which causes the dissociation of the metal complex, uncapping the materials and allowing Dox release. Moreover, AuNPs dissociation from the mesoporous surface favored their aggregation in clusters that can absorb NIR light. Thus, when the pH of a suspension of the capped MSNs in PBS was adjusted to 5.5 and irradiated for 5 min with a 808 nm laser light (0.75 W) a temperature increase from 37.5 to 69 ºC was registered, while capped nanoparticles at pH 7.4 only exhibited a slight temperature increase. Additionally, released Fe^{2+} ions take advantage of the high concentration of hydrogen peroxide in tumor cells to generate highly toxic hydroxyl radicals through a Fenton reaction. Capped nanoparticles were tested in a human oral squamous carcinoma cell line (WSU-HN6). The unloaded capped MSNs showed certain viability reduction (until 70% at 48 h) due to the release of Fe^{2+} ions and subsequent Fenton reaction. After irradiation, cell viability decreased until 30% at 48h. When nanoparticles were additionally loaded with Dox, cell viability after irradiation was reduced until 18% after 48 h. Nanoparticles were intravenous injected in tumor-bearing mice and Dox fluorescence in an IVIS fluorescence imaging system was registered at 0, 6, 24 and 48 h. At 6 h, Dox fluorescence was mainly accumulated in tumor tissue showing the strongest signal at 24h. Some liver accumulation was detected in *ex vivo*

fluorescence images, but in tumor tissue fluorescence conserved the higher signal intensity. In a step forward, Sprague-Dawley rats were treated with the gated MSNs and gold amount in blood was used to assess clearance and residence time of the particles. Dox-loaded MSNs showed higher prolonged blood circulation time with respect to the free drug. Finally, *in vivo* therapeutic efficacy was tested in WSU-HN6 tumor-bearing nude mice. A suspension of the Dox-loaded nanoparticles were intravenously injected and 24h later the animals were exposed to 808 nm laser light (0.75 W) for 10 min. Tumor treated temperature raised up to 48 ºC in comparison to the control tumor. A higher tumor inhibition growth (90% at 14 days) and higher survival rate was found in mice treated with the nanoparticles and irradiated with NIR light.

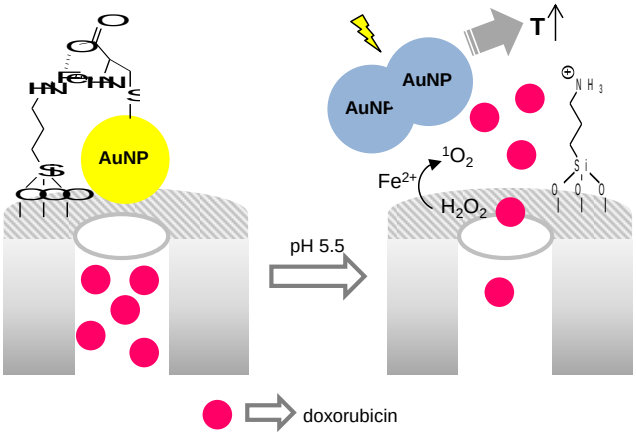

Figure 33. MSNs loaded with Dox and capped with AuNPs through a Fe^{2+} bridge with amine moieties. At pH 5.5 amines were protonated and coordinating bridge was broken inducing Dox release. NIR light favored Dox release by aggregated AuNPs photothermal effect. Fe^{2+} cations enhanced ROS production.

2.3. pH-induced cap degradation or dissolution

pH-triggered degradation of certain polymers or inorganic coatings have also been used as mechanism to induce cargo release. At this respect, PDA has also been extensively used as biocompatible coating for the preparation of pH-sensitive gated nanodevices because this

polymer suffers degradation at acidic pH. Its versatility arises from the fact that can be easily deposited onto organic or inorganic surfaces. Besides, the physical and chemical properties of the PDA coating can be easily tuned using Michael addition reactions or Schiff-base formation.[44] Calcium carbonate coatings have also been used as capping agents due to its fast degradation at acidic pH which generated carbon dioxide. Besides, some examples in which the porous inorganic scaffold is degraded at acidic pH have been reported.

For instance, Li et al. described a PDA modified MSNs system, loaded with the anti-miR-155 and containing the aptamer AS1411 to target drug delivery into colorectal cancer (Figure 34).[45] The anti-miR-155 loaded MSNs were coated with PDA through oxidative self-polymerization in weak alkaline conditions and finally, the SH-terminated AS1411 aptamer was attached to PDA through a Michael addition reaction. The nanomaterial recognized the nucleolin receptor present in cancer cells, which mediated the endocytosis, with the subsequent degradation of PDA cap by lysosomal pH. The efficiency of the nanodevice was studied in SW480 cells and in nude mice bearing SW480 tumour xenograft as colorectal cancer model. The animals were divided in different groups and the treatments were administered intravenously by tail vein injection to study the *in vivo* accumulation and anti-tumour activity. The results demonstrated that the nanoparticles reached efficiently the tumorous cells and the specific controlled release of the anti-miR-155 in the tumour site enhanced its therapeutic effect compared to the free drug.

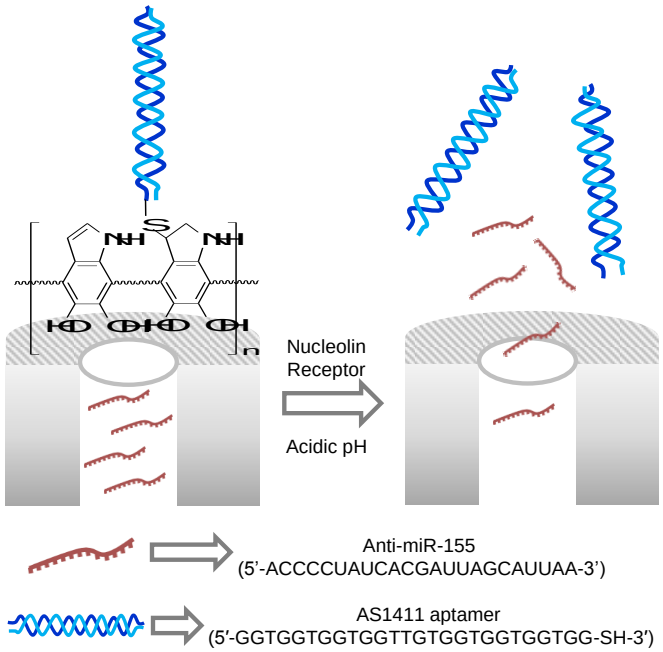

Figure 34. MSNs loaded with anti-miR-155 and coated with PDA films functionalised with a modified AS1411 aptamer covalently attached to PDA. Delivery was due to degradation of PDA cap by lysosomal pH.

Zeng and co-workers prepared PDA coated MSNs for targeted cancer therapy.[46] For the preparation of the functional material MSNs were loaded with Dox and then coated with a PDA shell. Then, a PEG derivative containing FA and thiol moieties was linked onto the PDA shell through a Michael addition reaction (Figure 35). Aqueous suspensions of the prepared nanoparticles showed a moderate Dox release at pH 7.4 (28.5% after 190 h) that was increased at acidic pH (38.3 and 49.5% at pH 5.0 and 2.0 and after 190 h) due to the rupture of the PDA coating. Confocal microscopy and flow cytometry studies showed a marked uptake of the prepared nanoparticles by HeLa cells mediated by FA. Besides, MTT assays carried out with the Dox-loaded capped nanoparticles and HeLa cells showed a dose-dependent reduction in cell viability. *In vivo* studies carried out with athymic nude mice bearing HeLa cells and intravenously injected with the nanoparticles showed accumulation of the solid in the tumour due to EPR effect. Also, a marked reduction in tumour size was

observed due to Dox release confirming the therapeutic benefit of the nanoformulation compared to the free drug. Histological analysis of the excised tumours showed that most cells were destroyed and became necrotic whereas no noticeable damage was observed in tissues of other organs.

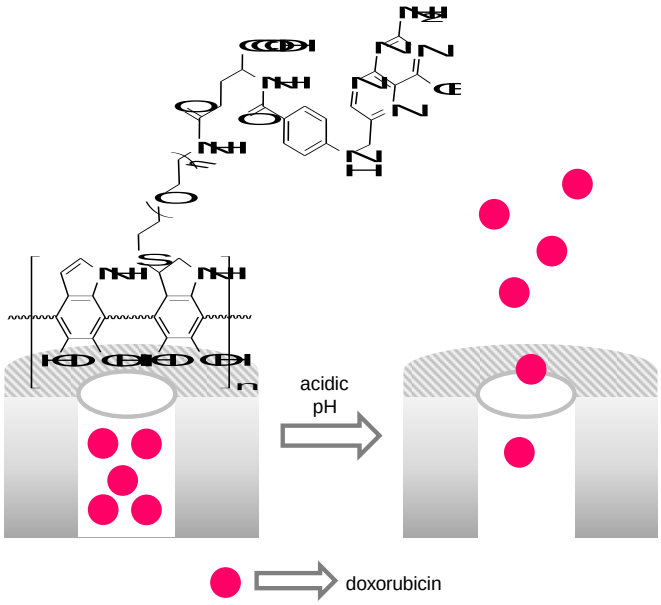

Figure 35. MSNs loaded with Dox, capped with PDA attached to a PEG derivative containing FA.

MSNs loaded with Dox and functionalised with PDA were also developed by Mei et al.[47] In a first step, D-α-tocopheryl PEG_{1000} succinate was reacted with carbonyldiimidazole and, subsequently, the obtained product was modified with ethylenediamine. On the other hand, MSNs were prepared and externally functionalised with aminopropyl moieties, the pores loaded with Dox and, finally, coated with a PDA shell. The final nanodevice was prepared by the covalent linking, through a Michael addition reaction, of the D-α-tocopheryl PEG_{1000} succinate derivative onto the PDA coating (Figure 36). Dox delivery from the prepared nanoparticles at pH 7.4 was moderate showing a 19.5% of drug release after 6 days. However, at acidic pH, the amount of Dox release reached 39 and 48% at pH 6.5 and 5.0 and after 6 days. The authors ascribed cargo release to the degradation of PDA coating at acidic pH.

CLSM studies showed internalization of the nanoparticles in A549 and A549/MDR cells. MTT assays in A549 and A549/MDR cells showed a marked reduction in viability in both cell lines. The results showed that D-α-tocopheryl PEG moieties helped to overcome the multi drug resistance of A549/MDR cells through the inhibition of P-gp pumps enhancing Dox accumulation. *In vivo* biodistribution studies, carried out with female sever combined immunodeficient mice xenograft with A549/MDR cells treated with the nanodevice (intravenously injected via tail), showed a marked accumulation of the nanoparticles in the tumour. Besides, nanoparticles induced a remarked reduction in tumour growth compared to free drug treatment. Finally, histopathological analysis of tissues of the major organs showed a marked damage in tumour and normal morphology in heart, liver, spleen, lungs and kidneys.

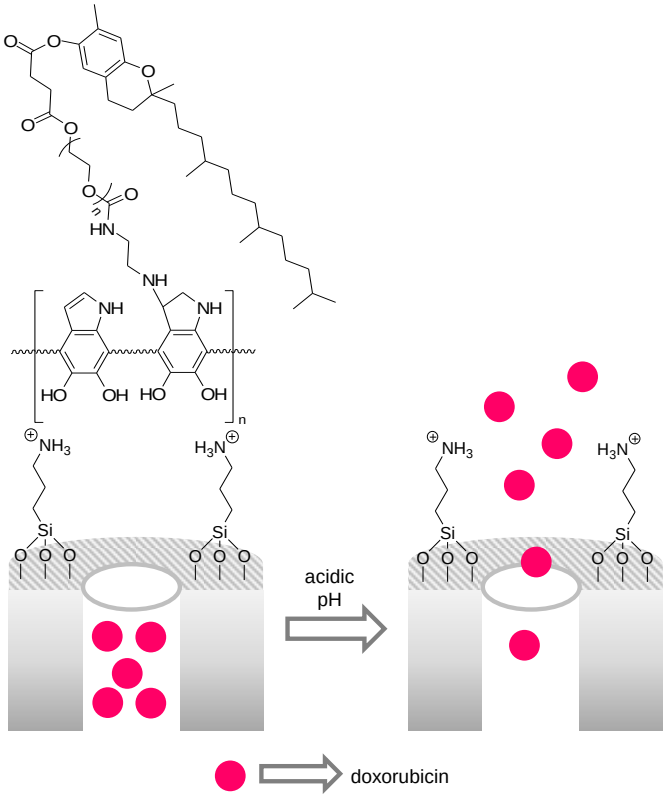

Figure 36. MSNs were loaded with Dox and coated with PDA containing a D-α-tocopheryl PEG_{1000} succinate derivative. Delivery is due to degradation of PDA at acidic pH.

MSNs loaded with Dox and coated with PDA and PEG were prepared by Chen et al.[48] As seen above, the PDA coating acted as pH-sensitive gating ensemble whereas the PEG shell was used to increase stability and biocompatibility of the final Dox-loaded nanodevice (Figure 37). At neutral pH a moderate sustained release of the entrapped Dox was observed (ca. 35% after 20 h) whereas at pH 5.0 ca. 60% of drug was delivered after the same time. The prepared nanoparticles were efficiently endocytosed by MCF7 and MDA-MB-231 cells inducing a marked reduction in cell viability. Besides, the anti-tumour efficacy of the prepared nanodevice was tested in nude mice bearing subcutaneous MCF7 tumours. Administration of the Dox-loaded capped nanoparticles induced a major inhibition of tumour growth, compared to free drug administration, attributed to the EPR effect and Dox controlled release in the acidic environment of the tumour. Moreover, mechanistic studies indicated that Dox released from the PDA coated nanoparticles induced a strong pro-death autophagy by the inhibition of the ATK-mTOR-p70S6K signalling pathway when compared with the free drug.

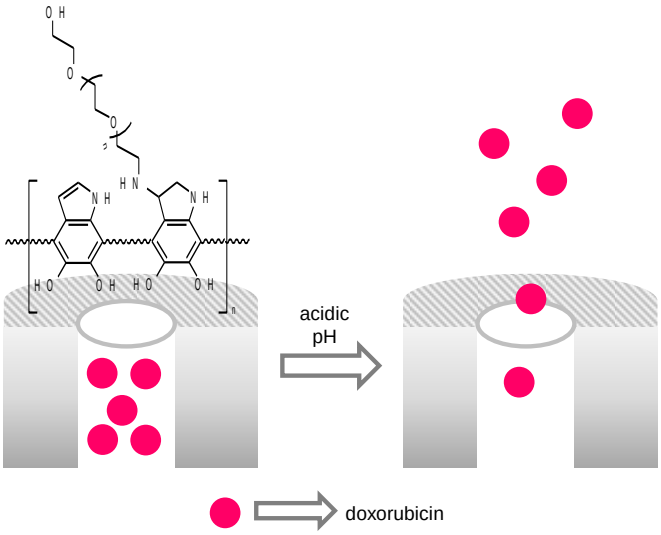

Figure 37. MSNs loaded with Dox and capped with PDA bearing a PEG derivate. PDA degradation at acidic pH induced cargo release.

Y. Li et al. prepared MSNs loaded with miR-238, coated with PDA, and finally grafted with a VEGF aptamer (Apt) and the Bevacizumab (Bev) antibody to target colorectal cancer cells

(Figure 38).[49] For this purpose, the pores of amino-functionalised MSNs were loaded with miR-328 and the outer surface coated with PDA. Then, Apt-SH and Bev-SH derivatives were reacted with NH_2-PEG-maleimide using Michael addition reactions and the obtained Apt-PEG-NH_2 and Bev-PEG-NH_2 were grafted onto the PDA layer. The nanomaterial targeted the VEGF receptor present in cancer cells, through VEGF aptamer and Bevacizumab (which can bind with this receptor), with the further destabilization of PDA polymer by lysosomal pH. No delivery studies at different pHs were performed by the authors. The nanocarrier was studied *in vitro* in SW480 cells and *in vivo* in a SW480 xenograft tumour model of colorectal cancer. The animals were divided in different groups and treatments were injected intravenously to compare the nanoformulation with the free drug administration. The results demonstrated that this multifunctional nanosystem efficiently delivered miR-328, with the subsequent gene silencing, guided an active targeting to colorectal cancer cells and enhanced the antitumour effect with low systemic toxicity.

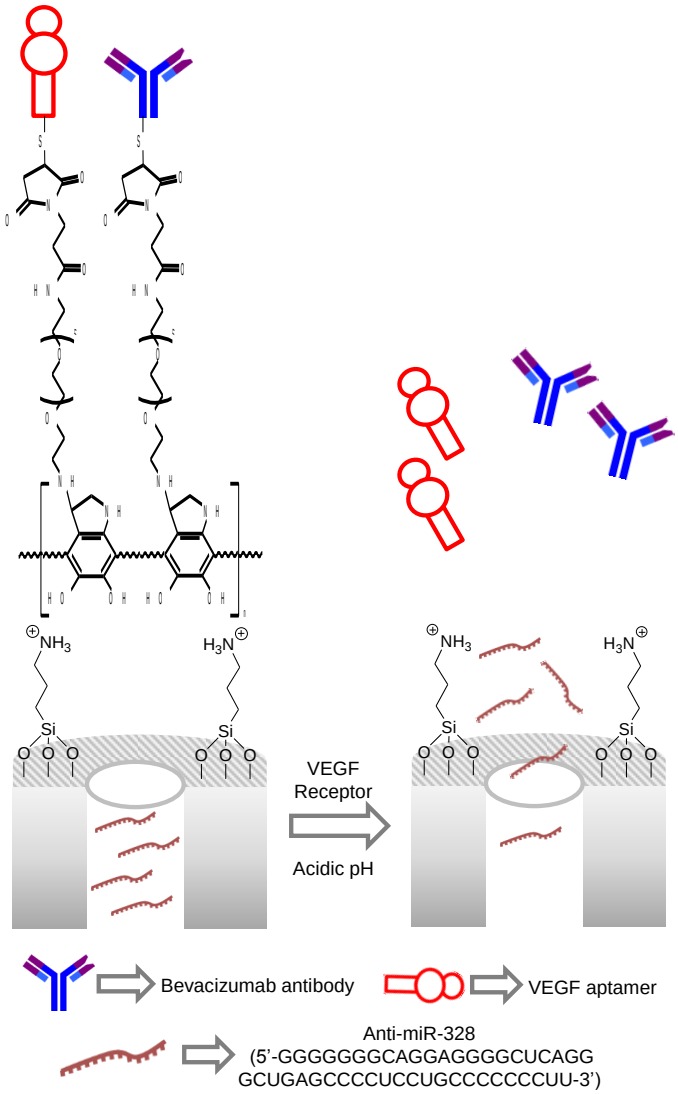

Figure 38. MSNs loaded with anti-miR-328 and coated with PDA functionalised with PEG derivatives containing a VEGF aptamer and the Bevacizumab antibody. Destabilization of PDA polymer by lysosomal pH induced cargo delivery.

PDA-coated MSNs functionalised with the Asn-Gly-Arg (NGR) tripeptide were used by Cheng et al. for the treatment of brain glioma in rats.[50] The authors loaded MSNs with Dox and capped the pores with a PDA layer obtained by oxidative self-polymerization of dopamine. Finally, the targeting NGR peptide was covalently linked, through a Michael addition reaction, onto the PDA shell (Figure 39). NGR is known to bind with aminopeptidase CD13 overexpressed in cancerous tissues. At neutral pH a negligible cargo release was

observed (less than 10% after 24 h), whereas at pH 5.0 a marked Dox delivery (ca. 50% after 24 h) was found. CLSM and flow cytometry studies showed internalization of the nanodevices in BCEC cocultured with C6 cells and C6 cells, both overexpressing the CD13 receptor. Besides, nanodevice uptake induced a dose-dependent reduction in the viability of BCEC-C6 and C6 cells due to NGR-mediated clathrin-dependent endocytosis and Dox release due to the acidic environment of lysosomes. *In vivo* studies were carried out using a C6 cell orthotopic glioma nude mouse model stablished by injecting C6 cells into the right brain of the mouse. Non-invasive fluorescence imaging measurements showed the preferential accumulation of the nanoparticles in brain tumours after intravenous tail injection. Histological evaluation of tumour tissues of mice treated with the nanodevice showed apoptotic and necrotic regions due to the targeting ability of the nanoparticles and to Dox release. Besides, the survival time for the mice treated with the nanodevice was enhanced to 32 days when compared with animals treated with saline (19 days).

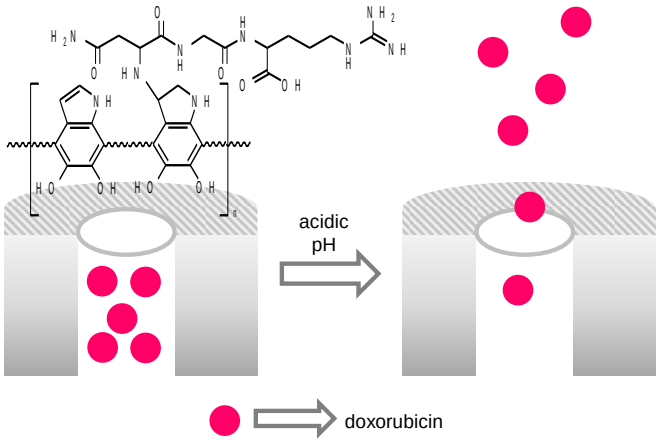

Figure 39. MSNs loaded with Dox and capped with PDA functionalised with the Asn-Gly-Arg, NGR) tripeptide. PDA destabilization by lysosomal pH induced cargo delivery.

C.F Weng et al. loaded Cu(II)-containing MSNs with 16-hydoxycleroda-3,13-dien-15,16-olide (HCD) and capped the nanoparticles with Eudragit S100 co-polymer (which is insoluble at acidic pH but highly soluble at neutral pH) through electrostatic interactions between the

negatively charged polymer and the positively charged Cu(II) ions located onto the nanoparticles' surface (Figure 40).[51] Controlled release studies at acidic pH (1.2 and 5.0) showed negligible HCD delivery (ca. 10% after 48 h) from the nanoparticles, whereas a remarkable HCD release was found at neutral pH (ca. 95% after 48 h) due to the dissolution of the polymeric coating. MTT viability assays carried out with the HCD-loaded Eudragit-coated MSNs on C6 cells showed a dose-dependent reduction in cell viability due to the effective internalization through endocytosis of the nanoparticles and HCD release. Finally, the efficacy of nanoparticles in an *in vivo* xenograft C6 glioma mouse model was assessed by intraperitoneal administration compared to orally administration of the free drug. The results demonstrated that Eudragit-coated nanoparticles were able to decrease tumour volume and micro-sections of the excised tumour revealed chromatin condensation and larger areas of cell death. A better therapeutic effect was accomplished with the nanoformulation.

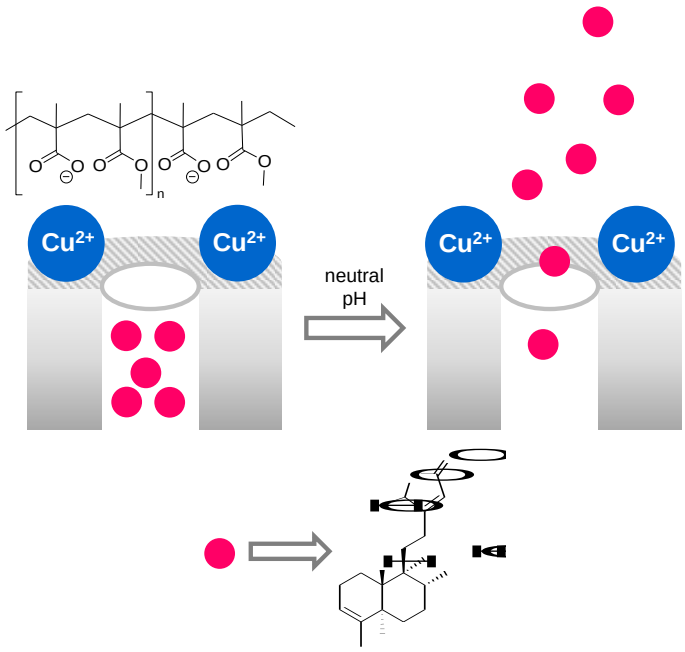

Figure 40. Cu(II)-containing MSNs loaded with HCD drug and capped with the Eudragit S100 co-polymer. Dissolution of the polymer at neutral pH induced cargo delivery.

P. Srivastava and co-workers developed adenosine triphosphate (ATP)-functionalised MSNs with a calcium carbonate coating for cancer drug delivery against aggressive lymphoma (Figure 41).[52] ATP could serve as modulator ligand binding purinergic receptors (P2 receptors), which are overexpressed in diverse cancer cells types thus suppressing tumour cell growth. MSNs were functionalised with carboxylic acid groups to conjugate ATP moieties through the formation of amide bonds. Moreover, the anticancer drug Dox was loaded onto the pores of the ATP-functionalised support and finally nanoparticles were capped with a calcium carbonate layer. The pores were closed by molecular interactions between the ATP and $CaCO_3$ established in the bio-mineralization process. Pore opening mechanism was studied in suspensions of the nanoparticles at different pH (7.4, 6.2 and 5.4) by monitoring Dox release. In physiological conditions a negligible drug release was observed, whereas in mild acidic conditions a significant Dox delivery was assessed. Cargo delivery was attributed to the melting down of the $CaCO_3$ coating in acidic pH conditions. The anti-tumour activity of the nanodevice was studied in aggressive and highly metastatic murine lymphoma called DL and in the Dox-resistant DL variant (DLR). The cellular *in vitro* experiments demonstrated the capability of the nanomaterial to reach cancer cells and cargo release. The synergistic effect of ATP and Dox release was observed in both DL and DLR cells, with high effective cytotoxicity against DL cells and DLR cells despite the resistance to Dox. The therapeutic effect of the nanoparticles (intraperitoneally injected) was demonstrated *in vivo* in DL tumours transplanted in AKR mice. The nanoformulation showed *in vivo* biocompatibility with nanoparticle accumulation in tumour site and an enhancement in tumour burden reduction compared to free drug administration. Besides, the lifespan of mice treated with the nanoformulation was significantly improved when compared with animals treated with Dox and Dox + ATP.

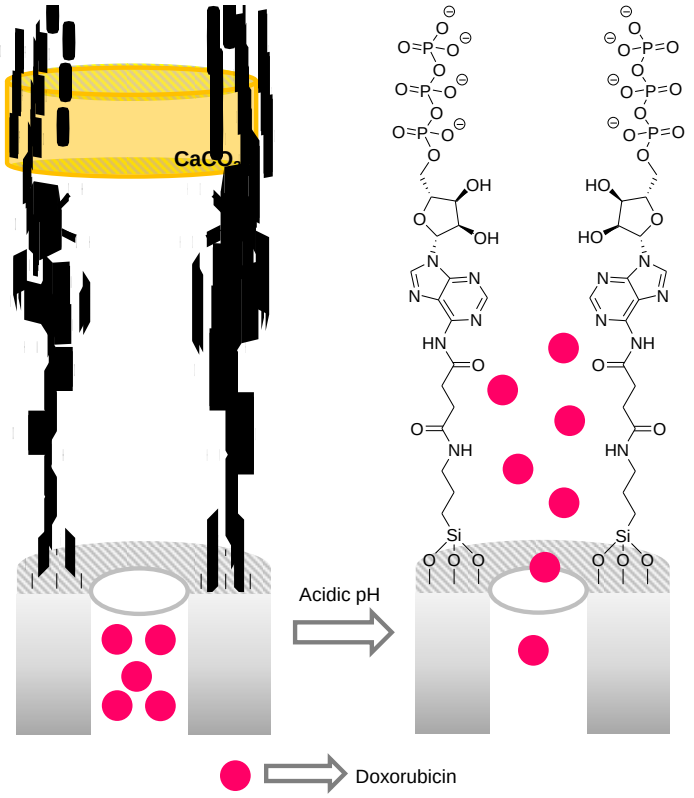

Figure 41. MSNs loaded with Dox, decorated with ATP and capped with a pH-sensitive calcium carbonate shell. Cargo delivery is due to the melting down of the $CaCO_3$ coating in acidic pH conditions

Deng et al. embedded Dox into MSNs by incorporating the drug in the synthesis mixture of the nanoparticles.[53] Moreover, the external surface was functionalised with aminopropyl moieties and then the nuclear localization signal peptide (NLS with the KRKRK sequence to achieve nuclear targeted drug release) was covalently anchored, through an amide bond using EDC/NHS as coupling agents. Afterward, the unreacted amines were blocked by reaction with citraconic anhydride to lower the positive surface charge and the pores were loaded with methylene blue a photosensitizer for photodynamic therapy (Figure 42). Incubation of the prepared nanoparticles in PBS at pH 5.0 for 24 h induced the dissolution of the solid with the subsequent Dox and methylene blue release. CLSM showed internalization of the nanoparticles in U87MG cells. After 12 h, nanoparticles accumulated in the cytoplasm

whereas after 24 h were located in the cell nuclei due to the interaction of the grafted NLS peptide with α and β importins. Cancer cell killing efficiency of U87MG cells upon incubation with the nanoparticles and under irradiation using a 660 nm laser (100 mW/cm^2 for 5 min) was tested using MTT assays. The viability of U87MG cells decreased significantly after the combined treatment due to the efficient release of Dox and the methylene blue-induced ROS generation. Finally, U87MG tumour-bearing mice were treated through tail vein injection with the nanoparticles and then irradiated with a 660 nm laser. This dual treatment induced a marked tumour growth inhibition thus resulting in a better therapeutic effect of the nanoformulation. Besides, negligible tumour growth inhibition was observed for mice treated with nanoparticles without the NLS peptide or methylene blue loading. Furthermore, histopathological staining of tumour tissues showed severe damages whereas no obvious lesions in other organs (heart, kidney, spleen, lung and liver) were found.

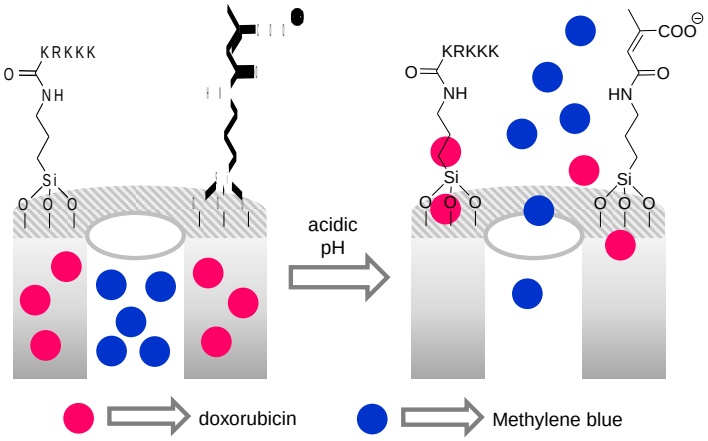

Figure 42. MSNs with embedded Dox, loaded with methylene blue and capped with the peptide KRKRK. Unreacted amines were additionally blocked with citraconic anhydride. Acidic pH induced the dissolution of the solid with the subsequent cargo release.

2.4. Bilayer disruption

Phospholipid bilayers have been extensively used as capping agents in the preparation of biologically compatible capped materials. Several simple or complex phospholipids can be

used for the preparation of bilayers (see Figure 43) which coat the loaded nanoparticles inhibiting cargo release. Moreover, lipids on the bilayer can be functionalised with certain polymers for enhance biocompatibility of the nanodevice (such as PEG derivatives) or with targeting biomolecules. Besides, these lipid bilayers have been reported to facilitate the cellular uptake of nanoparticles and drug release upon cell membrane fusion and disruption of the lipid bilayer in the acidic environment in lysosomes.

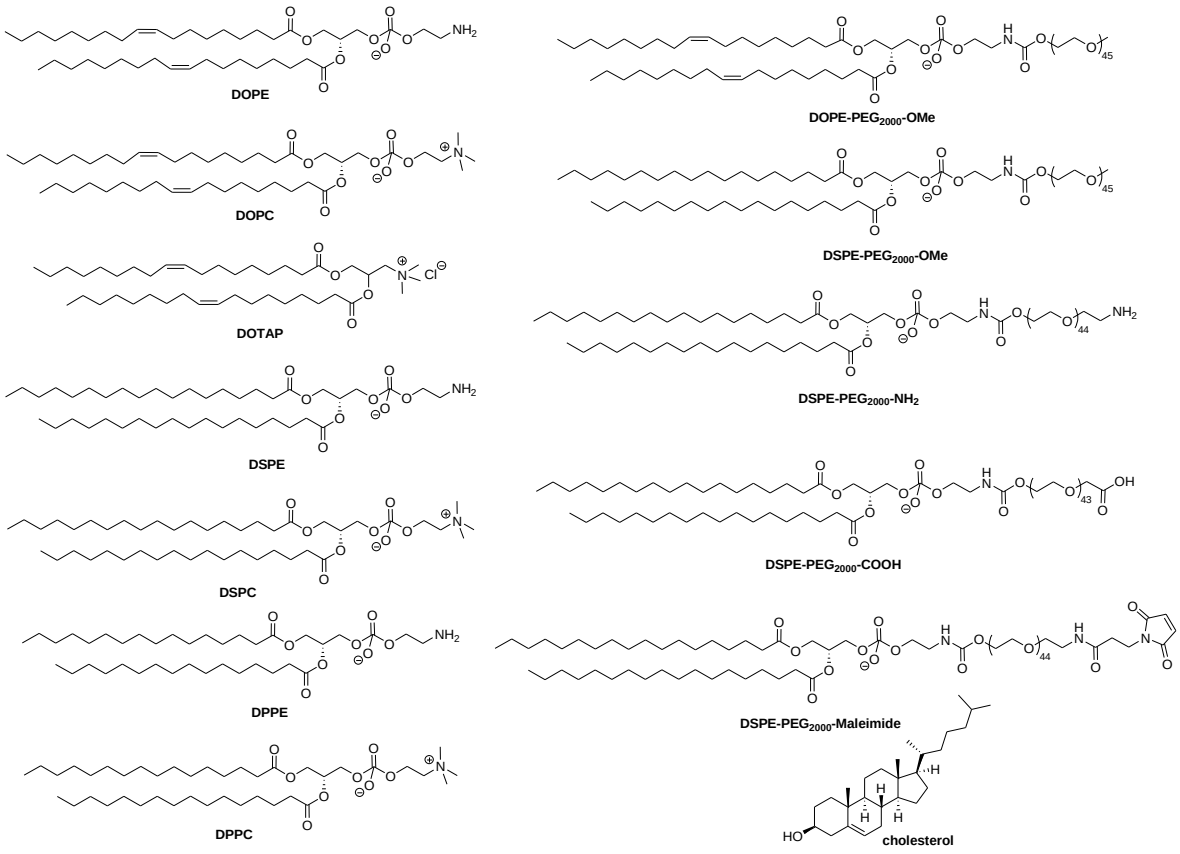

Figure 43. Chemical structures of the lipids used in the preparation of gated materials.

Mishra and co-workers prepared MSNs loaded with metformin and TPT and studied the controlled co-delivery of both drugs in BALB/c mice bearing 4T1 tumours.[54] The author used MSNs loaded with the pamoate salts of metformin and TPT and the pores were capped with a lipid bilayer formed by a mixture of DSPE-PEG_{2000}-OMe/cholesterol/soya phosphatidylcholine (Figure 44). The prepared nanodevice was able to release both drugs *in*

vitro in a sustainable fashion for 48 h with more marked delivery at acidic pH (ca. 90% cumulative release) when compared with neutral pH (ca. 70%). MTT assays showed that nanoparticles induced a marked viability reduction for 4T1 and MDA-MB-231 cells due to the efficient co-delivery of both drugs. Flow cytometry studies carried in MDA-MB-231 cells indicated the internalization of the nanovehicle and the release of both drugs. This co-delivery induced mitochondrial membrane depolarization that led to cell cycle arrest and apoptosis. Besides, the effect of the prepared nanoparticles was tested in BALB/c mice bearing 4T1 tumours. The nanoparticles were intravenously injected and compared to free drug administration. The controlled co-delivery of metformin and TPT induced a marked reduction in tumour size (i.e. 13.9-fold when compared with an untreated animal and 4.06-fold when mice were treated with a mixture of free metformin and TPT) and showed a major survival rate of the animals.

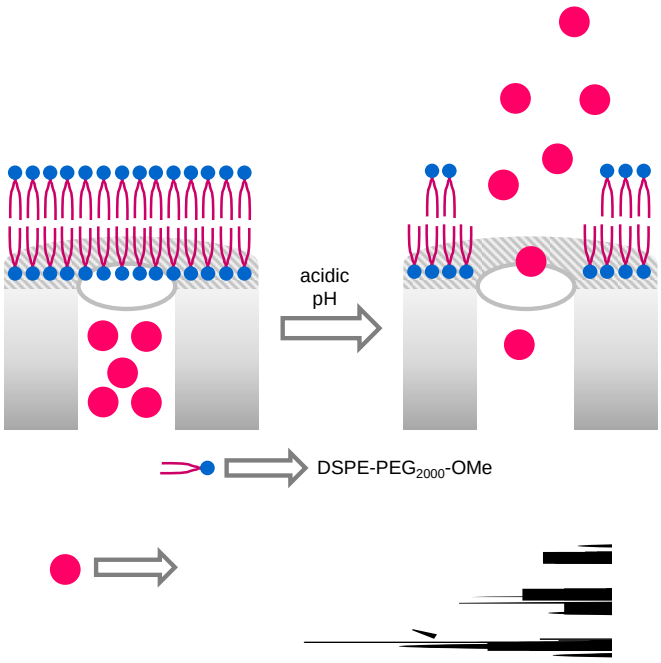

Figure 44. MSNs loaded with metformin and TPT and capped with a lipid bilayer formed by a mixture of DSPE-PEG_{2000}-OMe/cholesterol/soya phosphatidylcholine

Zoledronic acid is a nitrogen containing bisphosphonate that is extensively used for the treatment of osteoporosis and bone metastases. Zoledronic acid induces apoptosis of tumour cells and inhibits tumour cell growth *in vivo* in several types of cancers. Rosenholm and co-workers prepared lipid bilayer-gated MSNs for tumour-targeted delivery of zoledronic acid (Figure 45).[55] For this purpose, MSNs functionalized with aminopropyl moieties using a co-condensation procedure were firstly prepared. Then, aziridine was polymerized onto the external surface of the nanoparticles yielding a covalently linked hyperbranched PEI coating. Afterward, the pores of the PEI-coated nanoparticles were loaded with zoledronic acid (or with calcein) and the amines of the PEI were reacted with DOPE previously derivatised with *N,N'*-disuccinimidyl carbonate. A lipid bilayer was formed onto the externa surface of the nanoparticles by adding DOPC and DSPE-PEG_{2000}-Maleimide. Finally, FA, as targeting ligand, was covalently linked to the maleimide groups onto the lipid bilayer. The calcein-loaded nanoparticles were efficiently internalized by MDA-MB-231 cells, escaped from the endosomes and released calcein in the cytoplasm. Water soluble tetrazolium salt (WST-1) assays carried out with the zoledronic acid-loaded nanoparticles and MDA-MB-231 cells showed a dose-dependent reduction in cell viability due to drug release. Besides, nanoparticles were intravenously injected in mice xenograft with TLR9 siRNA MDA-MB-231 cells and a significant reduction in tumour size was observed compared to the free drug.

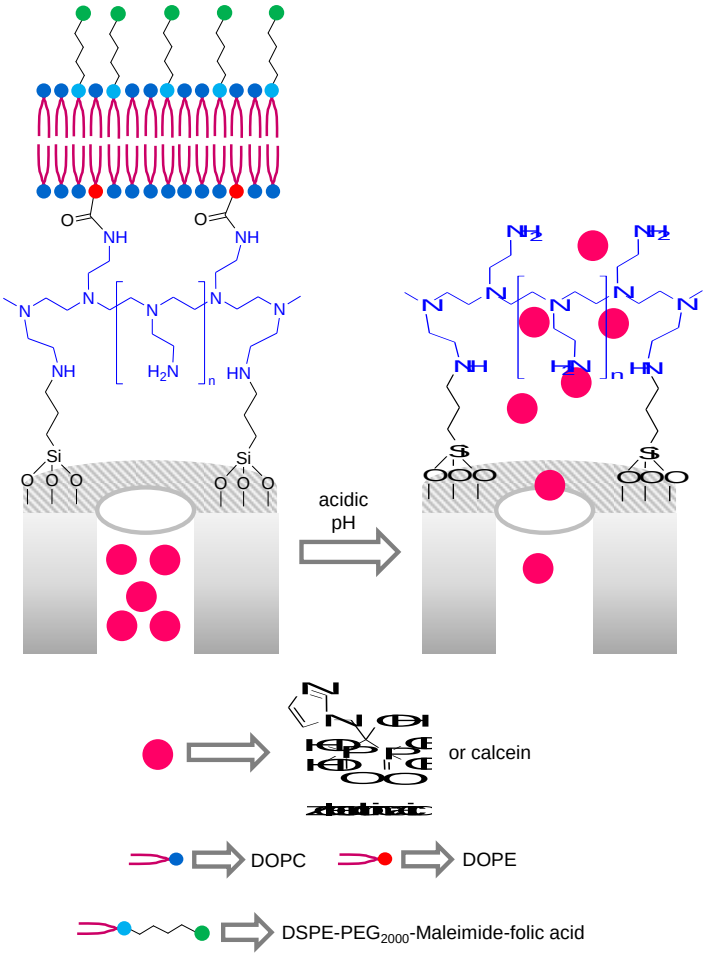

Figure 45. MSNs loaded with zoledronic acid or calcein and capped with a lipid bilayer formed by DOPC, DOPE and DSPE-PEG_{2000}-Maleimide-FA.

Hollow MSNs coated with a lipid bilayer were used by Xu and co-workers for the co-delivery of miR-375 and Dox to overcome multi drug resistance in hepatocellular carcinoma (Figure 46).[56] Hollow MSNs were loaded with Dox and the external surface was coated with a cationic lipid bilayer formed by DOTAP, cholesterol, and DSPE-PEG_{2000}-OMe. Finally, miR-375 was adsorbed onto the external cationic lipid bilayer through electrostatic interactions. The sequence of miR-375 was 5'-CCC GCG ACG AGC CCC UCG CAC AAA ACG C-3' and 5'-GCG UUU UGU UCG UUV GGC UCG CGU GAG G-3'. At neutral pH moderate drug (ca. 20% after 30 h) and miR-375 release was observed whereas a marked delivery of both cargos was observed at acidic pH (ca. 50% of Dox after 30 h). Flow cytometry studies

carried out with HepG2/ADR cells (resistant to Dox) showed internalization of the prepared nanodevice and co-delivery of Dox and miR-375 (which inhibited P-gp with subsequent reduction in drug efflux). Besides, MTT assays, carried out with the prepared nanodevice and HepG2/ADR cells, showed a marked reduction in cell viability due to a synergistic effect of the Dox and miR-375 co-delivery. Finally, HepG2/ADR tumours were implanted in BALB/c nude mice and then treated with the prepared nanodevice or the free drug by tail vein injection. The treatment with the nanoparticles remarkably inhibited tumour cell proliferation and increased the rate of apoptosis compared to the free drug.

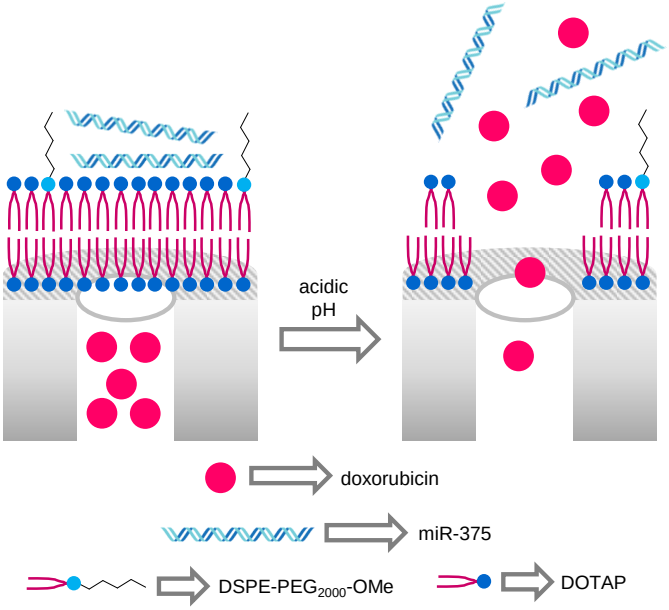

Figure 46. MSNs loaded with Dox and capped with a lipid bilayer formed by DOTAP, cholesterol, and DSPE-PEG_{2000}-OMe in which miR-375 was adsorbed.

The antiviral ML336 was encapsulated onto lipid bilayer-coated MSNs and the prepared nanodevices used for the treatment Venezuelan equine encephalitis virus (VEEV) infections.[57] Pores of MSNs were loaded with ML336 and the pores coated with a lipid bilayer formed by cholesterol, DSPC and DSPE-PEG_{2000}-Ome (Figure 47). Aqueous suspensions of the prepared nanoparticles at pH 5.0 showed a marked delivery of the entrapped antiviral drug due to the disruption of the coating bilayer in the acidic environment.

In vitro studies carried out with HeLa cells infected with TC-83 virus, used as VEEV substitute, and treated with the prepared nanodevice showed a marked reduction in viral load (6 orders of magnitude after 48 and 72 h). This reduction was ascribed to cell internalization of the nanoparticles through a clathrin-mediated endocytosis and subsequent drug release. Besides, administration of nanoparticles (through an intraperitoneal injection) to C3H/HeN mice murine model of VEEV infection induced a marked reduction of viral load in liver, kidney, serum and brain after 4 days. This marked reduction in viral load was not observed when mice were treated with free ML336. The efficacy of the nanodevice in reduction of viral load was ascribed to protection of ML336 and to an increase in circulation time of the drug.

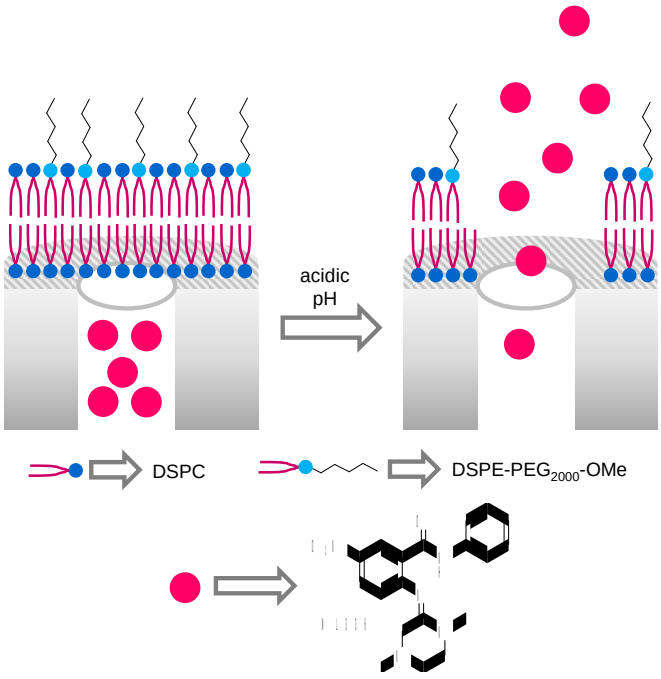

Figure 47. MSNs loaded with the antiviral ML336 and capped with lipid bilayer formed by cholesterol, DSPC and DSPE-PEG_{2000}-OMe.

2.5. Miscellaneous

Cui and co-workers prepared MSNs loaded with both Dox and sodium bicarbonate and incorporated the loaded nanoparticles onto a poly(L-lactide) fibrous scaffold (Figure 48).[58] Nanocomposites at pH 7.4 showed a moderate Dox release (ca. 20% after 20 days), whereas

at pH 4.0 an enhancement in drug release was observed (ca. 50% after 20 days). The enhanced release at acidic pH was ascribed to the reaction of sodium bicarbonate with protons which induced CO_2 formation. This gas created channels in the fibrous structure facilitating Dox diffusion. Confocal microscopy studies in the presence of MDA-MB-231 cells showed a marked reduction in cell viability. Besides, female BALB/c mice were inoculated with MDA-MB-231 cells and, after 8-9 days, tumours were partially resected and the nanocomposite implanted into the remnant tumour. After 10 weeks a marked apoptosis and necrosis in tumours was observed. The efficacy of elimination of cancer cells was confirmed by the decrease in Bcl2 and tumour necrosis factor alpha (TNF-α) levels.

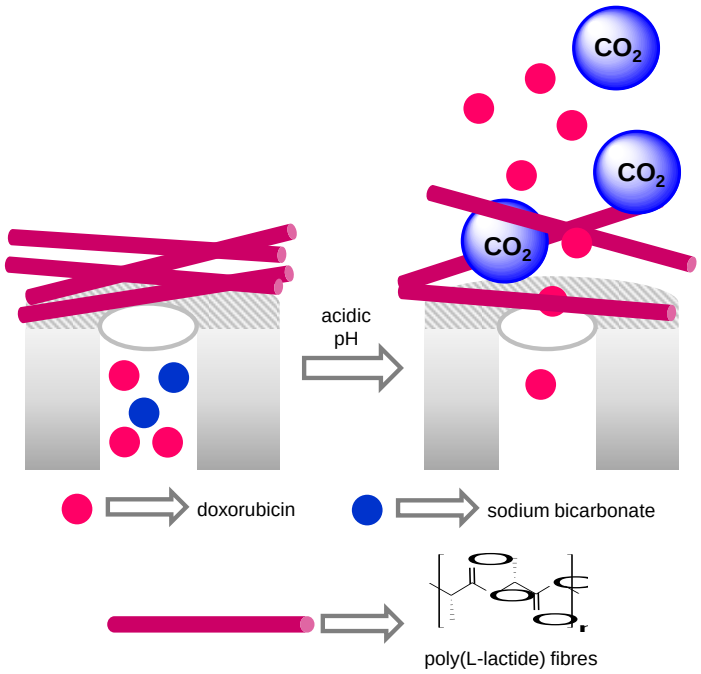

Figure 48. MSNs loaded with Dox and sodium bicarbonate and capped with poly(L-lactide) fibres. Release at acidic pH was ascribed to the reaction of sodium bicarbonate with protons which induced CO_2 formation.

Quercetin, a natural flavonoid, was used by Sil and co-workers as payload in the development of pH-triggered gated nanodevices for targeted delivery in a breast cancer model.[59] MSNs functionalized with aminopropyl moieties were prepared by a co-condensation protocol and

then FA was covalently linked using EDC/NHS as coupling agents. Finally, the pores of the FA decorated nanoparticles were loaded with quercetin (Figure 49). Aqueous suspensions of the prepared nanoparticles at pH 7.4 showed a weak quercetin release (ca. 10% after 60 h) that was enhanced at pH 5.0 (ca. 25% after 60 h). The authors did not indicate the gating mechanism. MTT analysis carried out with the prepared nanoparticles and MDA-MB-231 cells showed a dose-dependent reduction in cell viability (50% cell death at 10 μg/mL concentration) due to FA-mediated endocytosis of the nanoparticles. Western blots indicated that endocytosis of nanoparticles and quercetin release in MDA-MB-231 cells induced apoptosis associated to an increase in the expression of Bax and caspase 3 together with a decrease in p-Akt levels. Finally, MDA-MB-231 cells were inoculated in 10-days old chicken embryos which developed a tumour after 15 days. Treatment of embryos with nanoparticles at 5 μg/mL concentration, showed a marked reduction in tumour size. Besides, BALB/c mice bearing 4T1 tumours were intravenously injected with FA-functionalised and quercetin loaded nanoparticles and mice were sacrificed after 48 h. *Ex vivo* bio-imaging measurements showed preferential accumulation of the marked nanoparticles on the tumours due to the presence of FR and, to a lesser extent, in the kidneys.

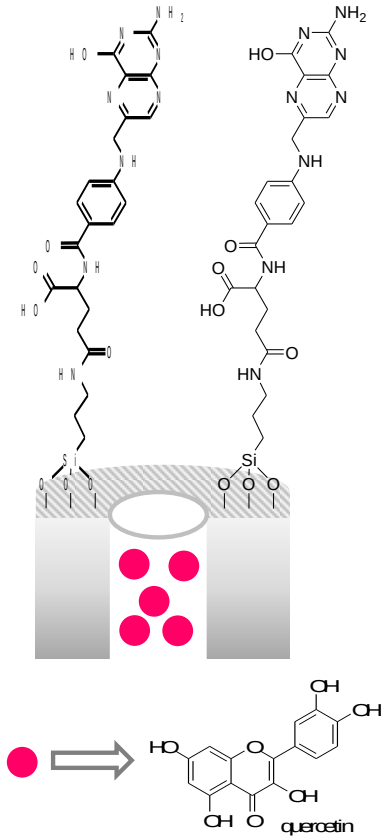

Figure 49. MSNs loaded with quercetin and capped with FA.

Dendritic MSNs were used as inorganic scaffold by Wang and co-workers for the development of nanodevices able to release the insoluble drug curcumin for breast cancer therapy (Figure 50).[60] The authors functionalised the dendritic MSNs with aminopropyl moieties which were subsequently reacted with succinic anhydride. Then, FA was covalently grafted onto the external surface using EDC/NHS as coupling agents. Afterward, the prepared nanoparticles were soaked with an aqueous solution containing calcium hydroxide. As a consequence the inner surface of the pores was decorated with Ca(II) ions. Finally, curcumin was loaded into the pores by the formation of complexes with the grafted Ca(II) ion. PBS suspensions of the nanoparticles at pH 7.4 showed a moderate curcumin release (35% after 1 h) that was enhanced at pH 5.0 (ca. 80% after 1 h). The enhancement in drug release was ascribed to the dissociation of Ca(II)-curcumin complex under acidic environment. MTT viability assays carried out with MCF-7 cells (FR positive cells) showed a dose-dependent

profile when cells were incubated with the prepared nanoparticles. Cell viability reduction was ascribed to folate-induced nanoparticles internalization, which was assessed by CLSM studies, and curcumin release which induced cell apoptosis by G2/M cell cycle arrest and ROS generation. Finally, the authors treated BALB/c mice bearing MCF-7 tumours with the nanoparticles by vein tail injection and observed high plasma levels of the solid and remarkable accumulation in the tumour compared to free drug administration.

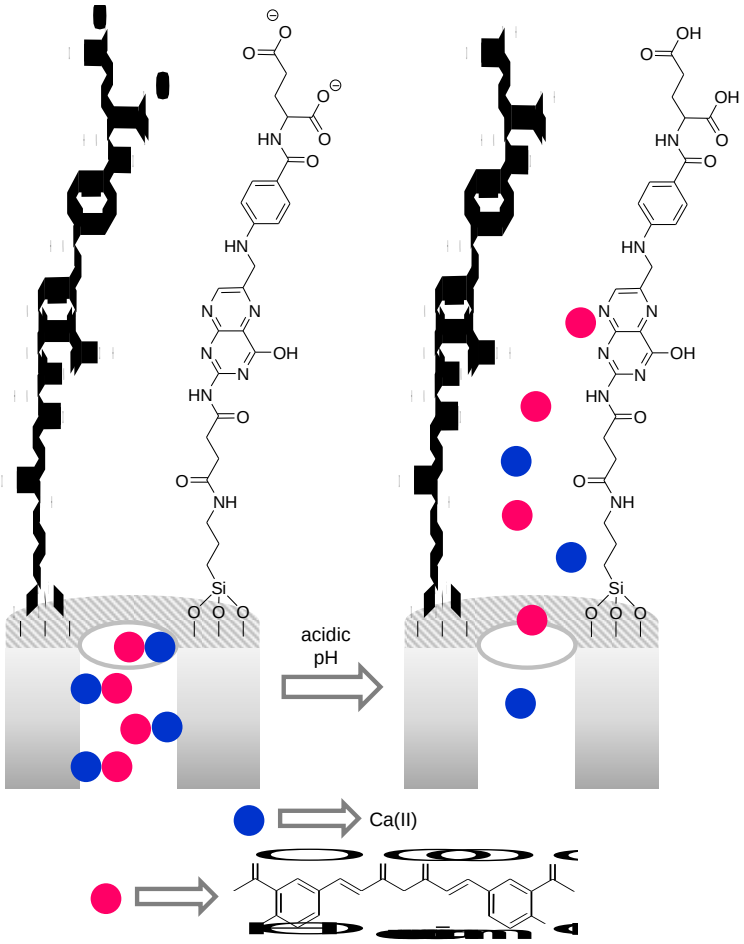

Figure 50. MSNs loaded with calcium hydroxide and curcumin and capped with FA. Drug release was ascribed to the dissociation of Ca(II)-curcumin complex under acidic environment.

3. Redox-responsive drug delivery systems

Oxidation and reduction reactions have an important role in the design and development of gated nanomaterials. In biological applications, the different concentration of reducing agents

within the intracellular environment and the bloodstream can be exploited to release drugs efficiently by their encapsulation in nanocarriers equipped with redox-responsive (supra)molecular capping machinery. In addition, it is known that in tumours and cancer cells there is a significant increase in redox activity compared to normal cells for instance due to a higher concentration of GSH. In the examples described below the mechanisms which control pore uncapping are basically two, (i) the cleavage of disulphide bonds, and (ii) bonds cleaved by the presence of ROS.

3.1. Reduction of disulphide bond

The most commonly used redox capping ensembles are formed by bulky (bio)molecules containing disulphide linkages. These bulky capping ensembles block mesopores, yet in the presence of reducing agents (such as glutathione, GSH) the disulphide bonds are cleaved with the subsequent cap detachment and cargo delivery. The first example of this gating mechanism was described by Lin and co-workers, who developed redox-sensitive MSNs functionalised with CdS nanocrystals through disulphide bonds.[61] Since then, this has been a rather popular approach to design gated nanosystems. For instance, Tian et al. reported GSH-responsive MSNs with transferrin (Tf) acting as gatekeeper to control drug delivery and targeting tumour site (Figure 51).[62] Hollow MSNs were functionalized with SH groups that were reacted with 2,2'-dipyridyl disulphide. Dox was loaded onto the nanomaterial and Tf functionalized with thiols groups was anchored to the nanocarrier via the formation of disulphide bonds. When GSH was added, the release of Dox from the MSNs was triggered. The system was studied *in vitro* in A549 lung cancer cells, the targeting specificity of the Tf functionalized nanoparticles was corroborated and a higher cytotoxic was achieved with the nanoparticles in comparison with the free Dox. Finally, tumour-targeted delivery and therapeutic efficacy of the nanoparticles was studied in A549 tumour-bearing mice after intravenous injection. The results confirmed the preferentially accumulation of the

nanoparticles in tumours. Moreover, a higher anti-tumour activity was observed with the nanoformulation, when compared with free Dox.

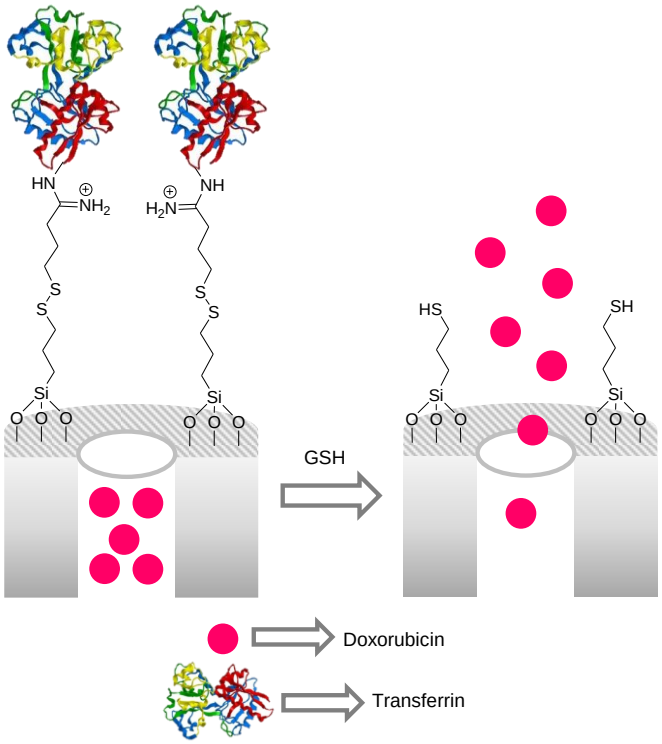

Figure 51. MSNs loaded with Dox and capped with Tf through disufide bonds. Drug delivery is triggered in the presence of GSH.

Fang and co-workers prepared MSNs for chemotherapy and miRNA delivery in a colorectal cancer model.[63] MSNs were functionalised with mercaptopropyl groups and the thiol moieties were reacted with 2,2'-dipyridyldisulphide. Moreover the nanoparticles were loaded with Dox. In a next step, PEI bearing thiol groups was covalently grafted onto the external surface of the loaded nanoparticles through the formation of disulphide bonds. Finally, a mixture of orthopyridyldisulphide-PEG-WL8 and orthopyridyldisulphide-PEG were grafted onto the external surface (Figure 52). WL8 is a targeting peptide with high affinity for GRP78 receptor overexpressed in the surface of colorectal cancer cells such as SW480. Finally, miRNA-145 (downregulated in colon cancer tissues) was adsorbed onto the external layer of

the nanoparticles. PBS suspensions of the nanoparticles at pH 7.4 showed a moderate Dox release (ca. 20% after 12 h) that was moderately enhanced at acidic pH (ca. 40% after 12 h). Besides, due to the presence of disulphide bonds in the coating of the nanodevice a marked release of Dox at pH 7.4 (ca. 65% after 12 h) in the presence of GSH was also observed. Confocal microscopy studies showed the efficient nanoparticle uptake by SW480 cells mediated by GRP78 receptor, the localization in the lysosomes after 1.5 h and then lysosomal escape after 3h due to the PEI-mediated proton sponge effect. Cytotoxicity studies carried out with the prepared nanoparticles and SW480 cells showed a marked reduction in cell viability due to the release of Dox and miRNA-145, which supressed the expression of prosurvival protein VEGF. *In vivo* studies, carried out with female BALB/c nude mice with an orthotopic colorectal cancer model using SW480 cells, showed preferential accumulation of nanoparticles in tumours attributed to the targeting ability of WL-8 peptide. Bioluminescence imaging studies (carried out with the same nanoparticles but with fluorophore Cy5.5 covalently anchored onto the PEI layer through the formation of an amide bond) showed a strong tumour growth inhibition of mice treated with the nanoparticles. Besides, metastases were inhibited (in liver, lung and spleen) due to miRNA-145 delivery which supressed the expression of VEGF and HIF-1α proteins in tumours. The combined nanoformulation therapy enhanced a major therapeutic effect compared to drug administration.

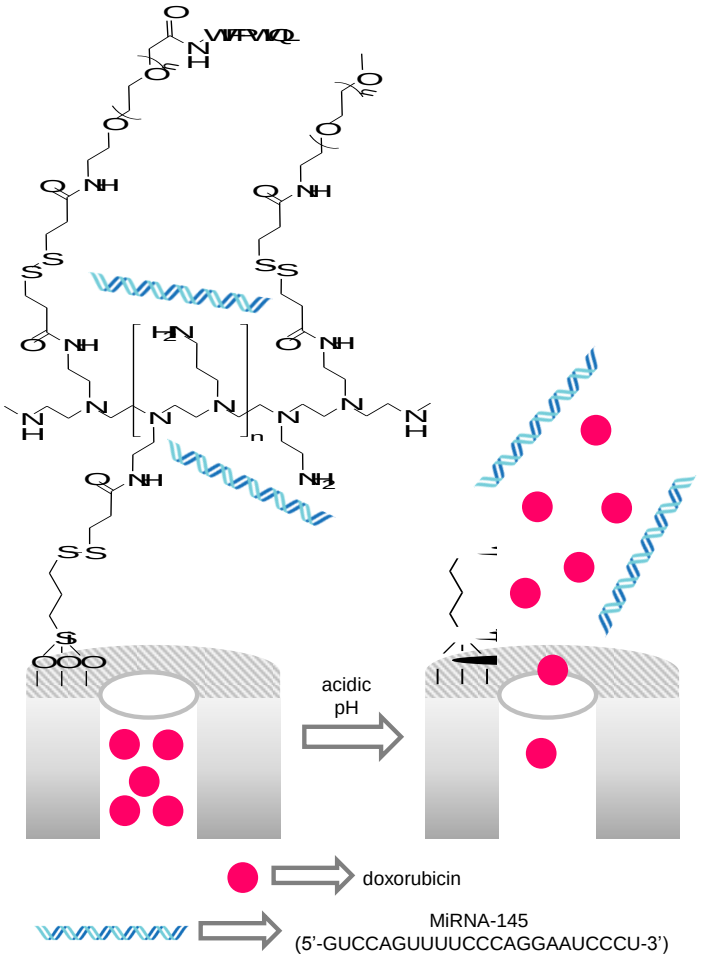

Figure 52. MNSs loaded with Dox, functionalized with PEI and capped with a mixture of orthopyridyldisulphide-PEG-WL8 and orthopyridyldisulphide-PEG in which miRNA-145 was adsorbed. Delivery was due to the rupture of the disulphide bonds.

Huang and co-workers described a multifunctional nanocarrier for dual-responsive delivery in cancer cells.[64] MSNs were modified with carboxylate groups to anchor cystamine through the formation of amide bonds. This protocol yielded MSNs functionalised with amine terminated stalks containing disulphide bonds. Then, phenylboronic acid (CPA) was conjugated by the formation of amide linkages and the anticancer drug Dox was loaded onto the pores. Finally the cytochrome C conjugated with LA (CytC-LA) was attached, through boronate esters bonds as gatekeeper yielding the final nanodevice (Figure 53). LA is a targeting motif able to bind an asialoglycoprotein receptor overexpressed in tumours. The

authors found that the presence of GSH or acidic pH triggered cargo delivery, due to the reduction of the disulphide linkages or to the hydrolysis of boronate ester bonds. Moreover, when both conditions were combined (GSH and acidic pH) the system demonstrated an enhanced Dox release. The therapeutic efficacy of the material was tested *in vitro* and *in vivo* in a liver tumour model in HepG2 cells. The nanoparticles were endocytosed by the HepG2 cells and a remarkable cytotoxic effect was observed. In addition, samples were administered in HepG2 tumour-bearing mice intravenously by tail vein injection. The results showed a significant tumour growth inhibition with the nanoformulation when compared with the free drug.

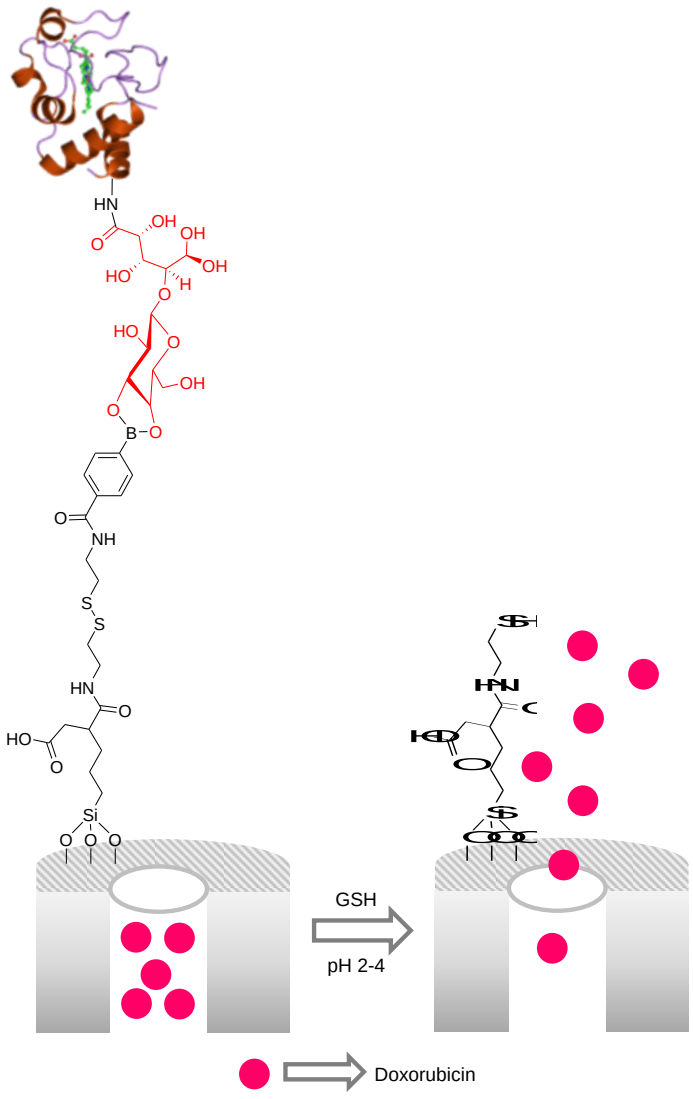

Figure 53. MSNs loaded with Dox and capped with stalks containing disulphide and boronate ester bonds anchored to cytochrome C conjugated with LA (structure in red). Delivery was due to the rupture of the disulphide bonds.

Zhao et al. developed a dual delivery drug/siRNA system based on redox-responsive MSNs for cancer therapy.[65] MSNs were loaded with Dox, modified with thiol moieties which were reacted with 2,2'-dithiodipyridine and final capped with thiol-modified Bcl-2 siRNA via the formation of disulphide bonds (Figure 54). The sequences used to form Blc-2 siRNA mimics were sense strand 5'-CCG GGA GAU AGU GAU GAA GdTdT-3' and antisense strand 5'-CUU CAU CAC UAU CUC CCG GdTdT-3' modified with thiol groups in 3' end. The authors found a poor cargo release in the absence of GSH, whereas in the presence of this tripeptide a significant release of Dox was observed. Besides, the GSH-induced release of Bcl-2 siRNA induced a marked inhibition of Bcl2 protein expression. Moreover, the efficient capping of the nanoparticles was also tested in blood samples (2 mM GSH), detecting small amounts of released Dox. The therapeutic efficacy of the system was tested *in vitro* in the breast adenocarcinoma cell line MCF-7 and *in vivo* in MCF-7 tumour xenograft bearing-mice. Cellular studies demonstrated the accumulation of the nanoparticles in cancer cells and the subsequent siRNA and Dox delivery. Finally, MCF-7 tumour xenograft bearing-mice were treated with the nanoparticles or with the free drug by tail vein injection. The nanoparticles accumulated preferentially in tumour through EPR effect and induced a significant inhibition in tumour growth compared to free drug administration.

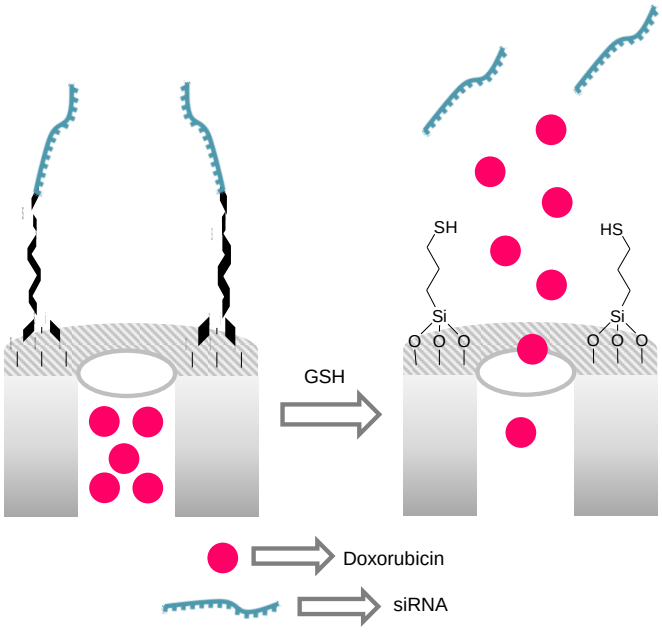

Figure 54. MSNs loaded with Dox and capped with Bcl-2 siRNA derivatised with disulphide bonds. Drug delivery is triggered by SGH that induced the rupture of the disulfide bonds.

Chen and co-workers prepared MSNs able to co-deliver Dox and a shRNA to sensitize cancer cells resistant to chemotherapy (Figure 55).[66] It is know that CSCs overexpressed ABCG2 (ATP binding cassette family G2 protein member) and contribute to drug resistance. The authors used a shRNA anchored onto MSNs to silence ABCG2 and reverse Dox resistance. MSNs were functionalised with –SH groups then reacted with 3-mercaptopropionic acid. Dox was loaded into the mesopores and PEI was grafted onto the external surface through the formation of amide bonds. Finally, the shRNA-ABCG2 was anchored by electrostatic interaction with the cationic polymer. In the absence of GSH, the Dox was entrapped in the pores, whereas when GSH was added a remarkable release of Dox was observed due to the cleavage of the disulphide bonds. The nanoparticles were evaluated *in vitro* and *in vivo* in the human hepatoma Hep3B CSCs. The cellular experiments showed that the nanoparticles internalized in cancer cells, with the subsequent release of the shRNA and Dox. ABCG2 was efficiently blocked and Dox sensitivity was restored thus contributed to higher toxicity to

remove CSCs. The potential of the nanosystem was also tested in tumour xenograft mice models by intravenously administration. Delivery of shRNA and Dox from the nanoformulation was demonstrated and tumours were efficiently reduced with no obvious side effects in mice compared to free drug.

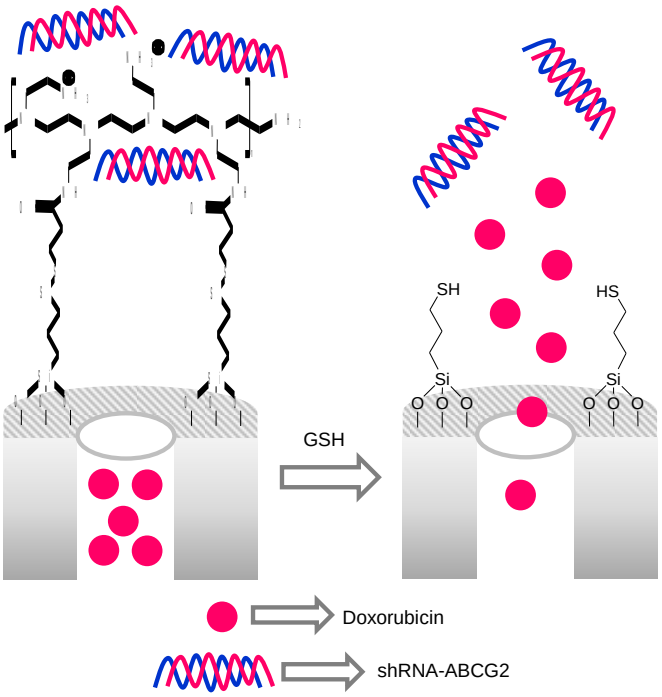

Figure 55. MSNs loaded with Dox and capped with PEI anchored to the surface through disulphide bonds. shRNA-ABCG2 was adsorbed onto the PEI layer. Drug delivery is triggered by SGH that induced the rupture of the disulfide bonds.

Xie et al. described a multifunctional delivery system based on MSNs for pain relief in pathological neuroinflammation.[67] The authors loaded MSNs with the analgesic Δ9-tetrahydrocannabinol (THC) and functionalised the external surface with thiol moieties to anchor the anti-inflammatory peptide ARA290 (an erythropoietin-derived peptide) by disulphide bonds. Finally, SH-PEG-SH, than acted as capping ensemble, was also anchored by disulphide bonds (Figure 56). Cargo delivery form the nanomaterial was triggered by the cleavage of the disulphide bonds by redox modulators at the site of inflammation. The system

showed a stable retention of the drugs under physiological conditions. However, when dithiothreitol (DTT) was added, the peptide ARA290 and the PEG detached from MSNs surface resulting in TCH release. The nanoparticles were tested in primary murine microglial cells as *in vitro* model of neuronal inflammation, showing a remarkably suppression of inflammatory response. The therapeutic effect of the nanodevice was evaluated in a chronic constriction injury of the sciatic nerve in mice as peripheral nerve pain model. The nanoparticles showed a great potential in the suppression of inflammation *in vivo*, the neuropathic pain responses were significantly attenuated and protective effects were higher with the nanoformulation compared to single drug controls.

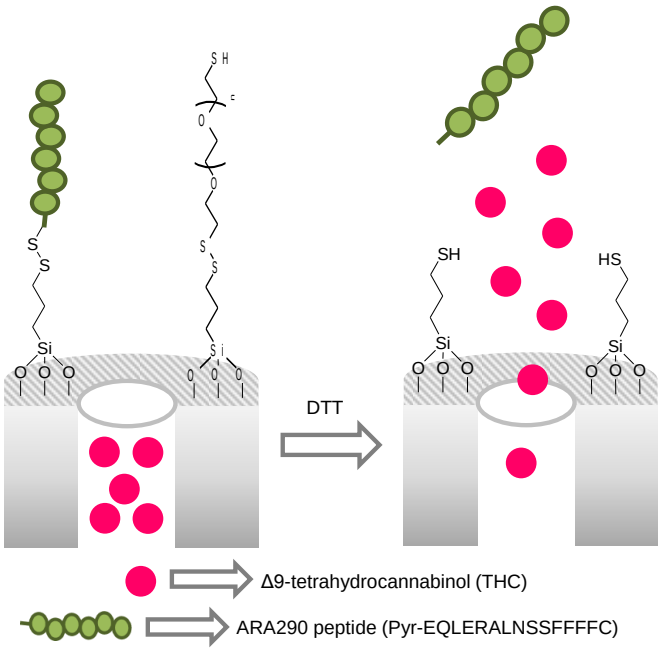

Figure 56. MSNs loaded with Δ9-tetrahydrocannabinol (THC) and capped with the ARA290 peptide and PEG through the formation of disulphide bonds. Cargo delivery was triggered by the cleavage of the disulphide bonds

Lu and co-workers reported biodegradable GSH-depletion dendritic mesoporous organosilica nanoparticles (GDMON) capable of co-delivering an antigen protein (ovalbumin) and a toll like receptor 9 (TLR9) agonist to enhance cancer immunotherapy (Figure 57).[68] The direct

killing of cancer cells via cytotoxic T lymphocytes (CTL) plays an important role in therapies based on the use of immune system to battle tumour cells. The GDMON nanoparticles contained GSH-responsive tetrasulphide moieties (-S-S-S-S-) incorporated in the structure of the inorganic scaffold and propyl methylphosphonate moieties grafted onto the external surface. The ovalbumin (OVA) and oligoDNA TLR9 agonist (CpG) were loaded into the large dendritic mesopores and the nanoparticles were finally coated with PEI polymer by electrostatic interactions. After the cellular uptake the nanoparticles disintegrated intracellularly due to high GSH levels which induced the rupture of the tetrasulfide bonds, resulting in OVA and CpG release. The redox-responsive properties of the nanomaterial were tested in intracellular and extracellular conditions. In the absence of GSH, cargo release was minimized whereas in the presence of GSH a significant release was observed due to the GSH-depletion of the nanoparticles. Cellular uptake, GSH-induced degradability and capability of the nanoparticles to activate immune cells were confirmed in macrophages RAW 264.7 cells. Moreover, the activity of the nanomaterial, as a vaccine formulation, was studied *in vivo* in C57BL/6 treated mice, and the activation of cytotoxic T lymphocytes was confirmed. Finally, the antitumour immunity of the nanoparticles was evaluated in an aggressive B16-OVA melanoma tumour bearing mice. The nanoparticles were intravenously administrated to compare their therapeutic effect with the free drug treatment. The nanoformulation showed a significantly improved antitumour activity due to the proliferation of CTLs, with the subsequent reduction of tumour growth and enhancement survival rate.

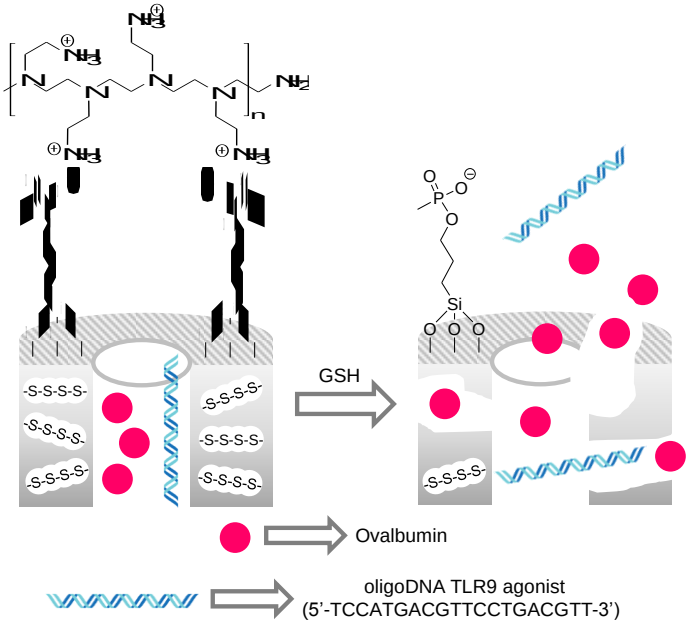

Figure 57. Mesoporous organosilica nanoparticles containing tetrasulphide bonds, loaded with Dox and with a toll like receptor 9 (TLR9) agonist and functionalised with methyl phosphonate units. Pores are capped with PEI polymer through electrostatic interactions. GSH induced the rupture of the tetrasulphide bonds resulting in cargo delivery.

Chen and co-workers prepared CuS-capped mesoporous organosilica nanoparticles for multi-responsive drug delivery in chemo-photothermal therapy.[69] For this purpose, thioether bridged yolk-shell structured mesoporous organosilica nanoparticles (YSPMOs) were synthetized and functionalised with thiol groups. The linker cysteamine was used to introduce disulphide bonds onto the external surface of YSPMOs. Dox was loaded and the material was finally capped with CuS nanoparticles containing L-cysteine upon amide bond formation (Figure 58). In the absence of any reducing stimulus, at pH 7.4 and 5.8, negligible Dox release was observed. In contrast, drug release was increased when GSH was added into the suspension. Drug release was attributed to the GSH-induced cleavage of disulphide bonds which induced the detachment of the CuS nanoparticles and pore opening. The photothermal drug release properties were also analysed, observing a small Dox delivery upon NIR

irradiation. In contrast, at acidic pH, NIR irradiation and GSH addition the highest amount of Dox was released due to the combination of the triple stimulation. The chemo-photothermal properties of the nanoparticles was analyzed in MDA-MB-231 breast cancer cells *in vitro* and *in vivo* in S180 sarcoma-bearing nude mice. Cellular studies showed an enhancement of the antitumour efficacy with the combination of the nanoparticles with photothermal therapy compared with other groups. These findings were confirmed *in vivo*; the nanoplatform accumulated in tumours and the nanoparticles + NIR combination exhibited the highest anti-tumour efficacy in terms of tumour growth inhibition with the lower systemic toxicity.

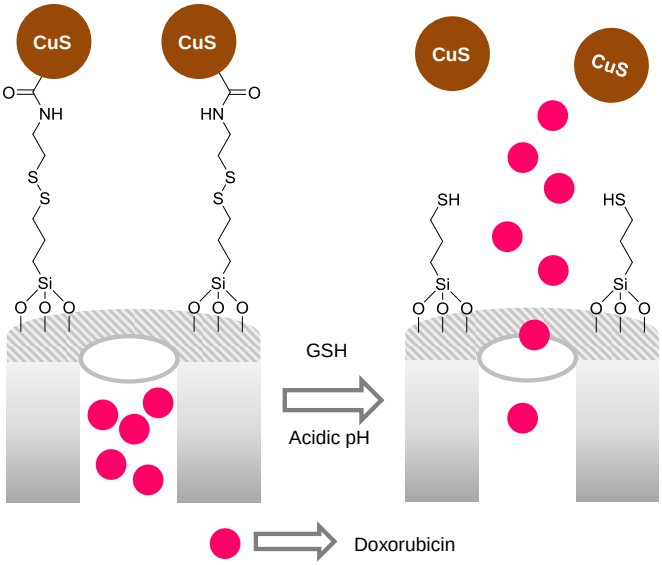

Figure 58. Thioether bridged yolk-shell structured mesoporous organosilica nanoparticles loaded with Dox and capped with L-cysteine-CuS using a disulphide-containing linker. Drug release was attributed to the GSH-induced cleavage of disulphide bonds.

Zhou et al. designed Tf-conjugated MSNs for targeted tumour therapy with minimal immune response activation.[70] Tf receptor is overexpressed in many cancer types. Hollow MSNs were used as inorganic scaffold to load Dox and then their external surface was modified with thiol groups, which were further reacted with 2-carboxyethyl-2-pyridyldisulfide yielding a loaded support functionalised with carboxylate moieties grafted onto the outer surface through

disulphide bonds. Carboxylate groups were reacted with 3-butinyl-1amine using EDC/NHS as coupling agents. Finally, an azide-modified Tf was anchored onto the external surface using a Cu(I)-catalysed alkyne-azide coupling reaction (Figure 59). Drug delivery was mediated by the specific cleavage of the disulphide bonds in the redox environment of cancer cells. A negligible amount of Dox release was observed in physiological conditions, while in the presence of GSH a remarkable drug delivery was found. Anti-tumour activity of the nanomaterial was evaluated in breast cancer MDA-MB-231 cells. The Tf-targeted effect of the nanoparticles was confirmed to occur preferentially to cancer cells that resulted in an enhanced cytotoxic effect. Moreover, non-immunotoxicity of the nanoplatform was observed in combination with macrophages cells, attributed to the biocompatibility of Tf. The authors also evaluated the potential therapeutic effect of the nanoparticles *in vivo* in MDA-MB-231 tumour-bearing mice as breast cancer model by intravenous injection of the nanoparticles. The tumour-targeting ability of the nanomaterial was demonstrated and enhanced tumour growth suppression was accomplished compared to the free drug, without induced inflammation.

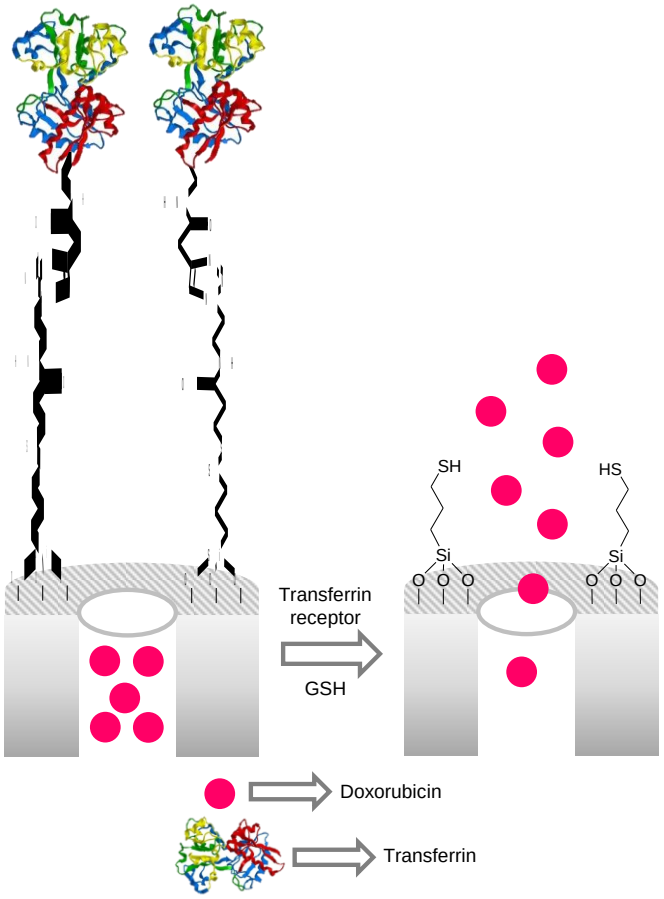

Figure 59. MSNs loaded with Dox and capped with Tf using a disulphide bond. Drug delivery was mediated by the specific cleavage of the disulphide bonds.

Wang et al. designed redox-responsive MSNs as drug delivery carrier to overcome drug resistance in lung cancer.[71] Drug resistance to tyrosine kinase inhibitor (TKI) is the main drawback for an efficient treatment of EGFR-mutant lung cancer. To overcome this drug resistance, MSNs were used for the design of a nanodevice to target EGFR with the anti-EGFR antibody cetuximab (CET) as cap and loaded with the anticancer drug Dox or the TKI drug gefitinib (GEF). For the preparation of the nanodevice the surface of MSNs was modified with mercaptopropyl groups and then Dox or GEF were loaded. Finally, the CET antibody was anchored onto the external surface through the formation of disulphide bonds (Figure 60). After the CET binding to EGFR on the cell surface the nanoparticles internalized

and the capping ensemble was disrupted through the cleavage of disulphide bonds by intracellular GSH. In the absence of GSH, a negligible Dox release was registered whereas in the presence of high levels of GSH or DTT an increased delivery of the drug was observed. The specific targeting mediated by CET was confirmed in PC9 lung cancer cells, which overexpressed EGFR in comparison with epithelial Beas2B lung cells. Dox loaded nanoparticles functionalised with CET antibody were preferentially internalised by PC9 lung cancer cells, when compared with epithelial Beas2B lung cells, inducing a marked growth inhibition. The therapeutic application of the GEF loaded nanoparticles was analysed *in vivo* in PC9-DR tumour bearing mice after intravenously administration of the free drug or the nanoparticles. The nanoparticles showed a significant effect in targeting the tumour site with the subsequent inhibition of the PC9-DR tumour growth. The results showed a better therapeutic effect of the nanoformulations and reduced undesired side effects, when compared with the free drugs.

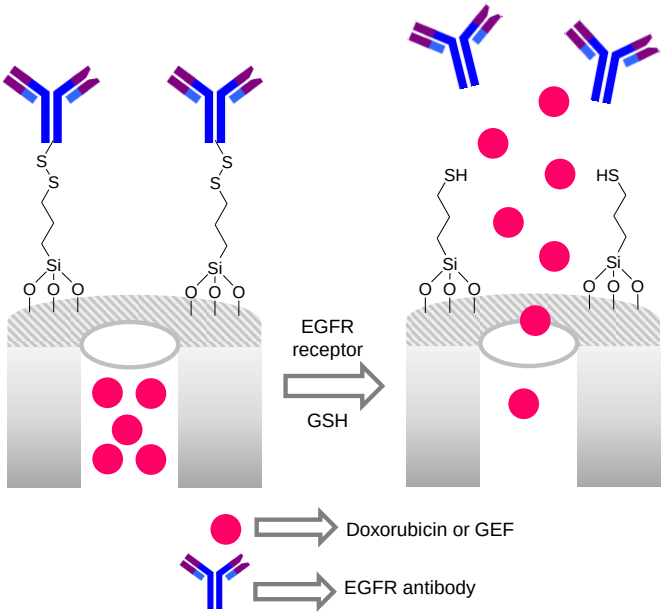

Figure 60. MSNs loaded with Dox or with gefitinib (GEF) and capped with anti-EGFR antibody cetuximab (CET) attached by disulphide bonds. Delivery is due to the cleavage of disulphide bonds.

3.2. Bonds cleaved by ROS

ROS are increased in pathological conditions such as in cancer cells. In the field of nanomedicine, this biochemical property has been exploited to design capped materials with sensitive groups which are broken in the presence of ROS. The molecules acting as gatekeeper are based on bonds such as thioketals, ketals and diselenides that are cleaved in the presence of ROS species such as hydrogen peroxide H_2O_2, superoxide anion O_2^- and hydroxyl radical HO. Examples of such ROS-responsive nanomaterials have been reported in the literature although very few examples have been tested in *in vivo* models. For instance, Hu and co-workers used MSNs for the preparation of a ROS-cleavable nanodevice.[72] For this purpose, MSNs were functionalized with aminopropyl moieties. Then the amino groups were reacted with a thioketal linker which was synthesized by the reaction between acetone and 3-mercaptopropionic acid. Afterward, Dox and the ROS generator α-tocopheryl succinate (α-TOS) were co-encapsulated. Finally, the nanoparticles were functionalised with β-CD derivatised with amino groups, through the formation of amide bonds, and then the pores capped upon addition of adamantane-containing PEG via host-guest interactions (Figure 61). The system was designed to respond to intracellular ROS present in cancer cells, which mediated the release of Dox and α-TOS from the inner pores after ROS-induced thioketal cleavage. The α-TOS delivered had the capability of self-regenerate the intracellular ROS, which facilitated the cleavage of the thioketal linkers and the subsequent release of more α-TOS, self-accelerating the release of Dox. The ROS-responsive properties of the nanoparticles were tested in the presence of H_2O_2 (as a typical ROS). The results demonstrated that in the presence of different concentrations of H_2O_2; the thioketal linkage was cleaved and the supramolecular inclusion complex removed with subsequent Dox and α-TOS delivery. The ROS generating capability and ROS-triggered release was confirmed in MCF-7 breast cancer cells (with high amounts of ROS) compared to normal cells as control group. The high efficiency of drug release of the nanoparticles in ROS abundant tumour MCF-7 cells was

demonstrated. Finally, the antitumour efficacy was studied in MCF-7 tumour-bearing nude mice with the intravenously administration of nanoparticle samples compared to the free drug treatments. The material showed a high inhibition in tumour growth promoted by the self-accelerating drug release strategy, which maximized the antitumour activity resulting in a higher apoptosis of cancer cells compared to the free drug, with lower side effects.

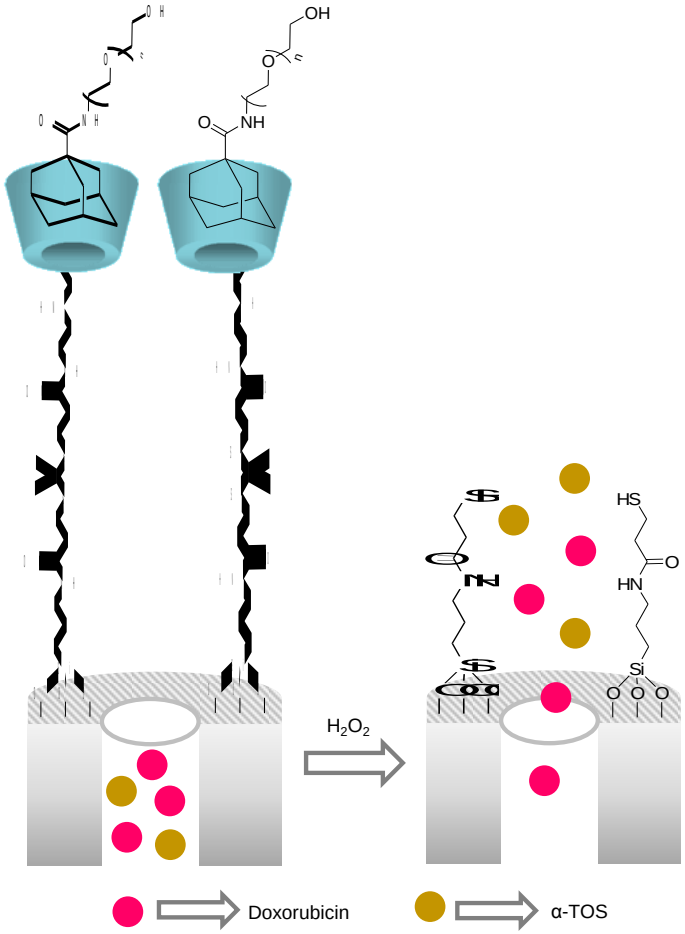

Figure 61. MSNs loaded with Dox and α-tocopheryl succinate (α-TOS) and capped with β-CD-adamantane-containing PEG and a ROS-cleavable thioketal linker. Delivery is due to ROS-induced thioketal cleavage.

Shao et al. described a controlled delivery system based on diselenide bridged MSNs of potential application in cancer therapy.[73] MSNs were modified with diselenide bonds and then the pores loaded with the cytotoxic ribonuclease A (RNase A). Then, the external surface

of the loaded nanoparticles was coated with HeLa cancer cell membrane vesicle (CM) yielding the final nanodevice (Figure 62). Controlled release from the nanoparticles was tested in media mimicking the tumour microenvironment. When nanoparticles were stirred in the presence of ROS or GSH a high RNAse release was observed attributed to diselenide bond rupture with subsequent degradation of the inorganic scaffold. The cellular uptake and drug release of the nanoparticles was demonstrated in HeLa cells. The antitumour efficacy of the system was also evaluated in HeLa tumour-bearing nude mice after intravenous injection of different treatments. The presence of the cancer-cell membrane in the nanoparticles enhanced their accumulation in the tumour and a higher therapeutic effect was observed in terms of tumour suppression compared to the free drug.

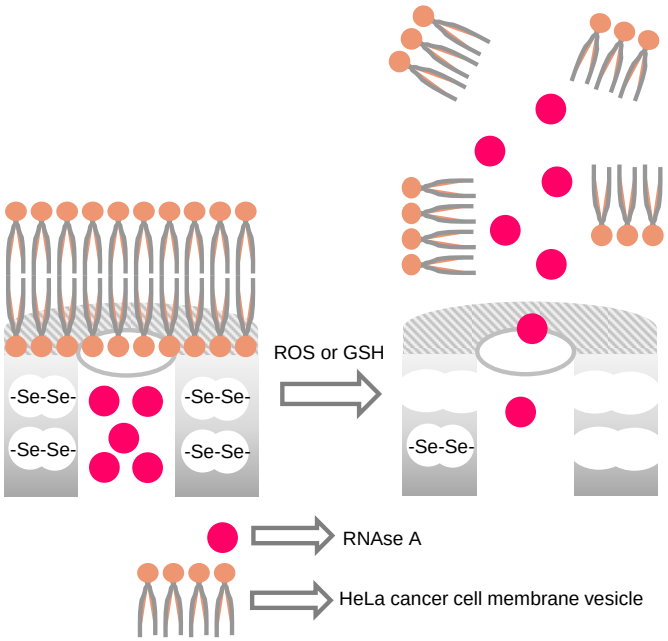

Figure 62. Diselenide bridged MSNs loaded with RNAse A and coated with HeLa cancer cell membrane vesicles. Cargo release is triggered by ROS-induced diselenide cleavage.

Tan and co-workers reported ROS-responsive MSNs for hydrogen peroxide detection and drug delivery in heart failure treatment.[74] For this purpose MSNs were modified with amino groups and maleic anhydride was covalently grafted through the formation of amide bonds. Then, 2-mercaptoethylamine was also grafted onto the carboxylate-functionalised scaffold

using a Michael addition reaction yielding free amino moieties. Afterward, a fluorescein derivative bearing boronate ester groups (FL2), which acted as H_2O_2 probe, was anchored through the formation of amide bonds. Finally, the therapeutic drug of heart failure captopril was loaded in the mesopores and the gatekeeper α-CD was used as cap via host-guest interaction with the boronic ester moieties of the FL2 probe (Figure 63). To validate the H_2O_2-induced turn-on of the FL2 probe and the triggered release of captopril, sensing and drug delivery studies were performed in the absence or presence of H_2O_2. The results demonstrated that in the absence of H_2O_2 no change in the fluorescence intensity or captopril delivery was observed. In contrast, under oxidative stress conditions, the boronic ester moieties were hydrolysed leading to the disassembly of the α-CD with the subsequent turn on of emission of FL2 and captopril release. High levels of toxic ROS, such as H_2O_2, are associated with chronic heart failure. The therapeutic effects of the ROS-responsive MSNs were evaluated in a hearth failure sqKR15 zebrafish model. After treatment with the nanoparticles a significant H_2O_2 detection was accomplished in the induced heart failure zebrafish compared to healthy controls. Moreover, the treatment with the nanoparticles induced an improvement in the heartbeat rate as well as cardiac output in comparison with the free-drug group. The better therapeutic effect was attributed to the controlled captopril release in the vicinity of the heart for a long period of time under oxidative stress conditions.

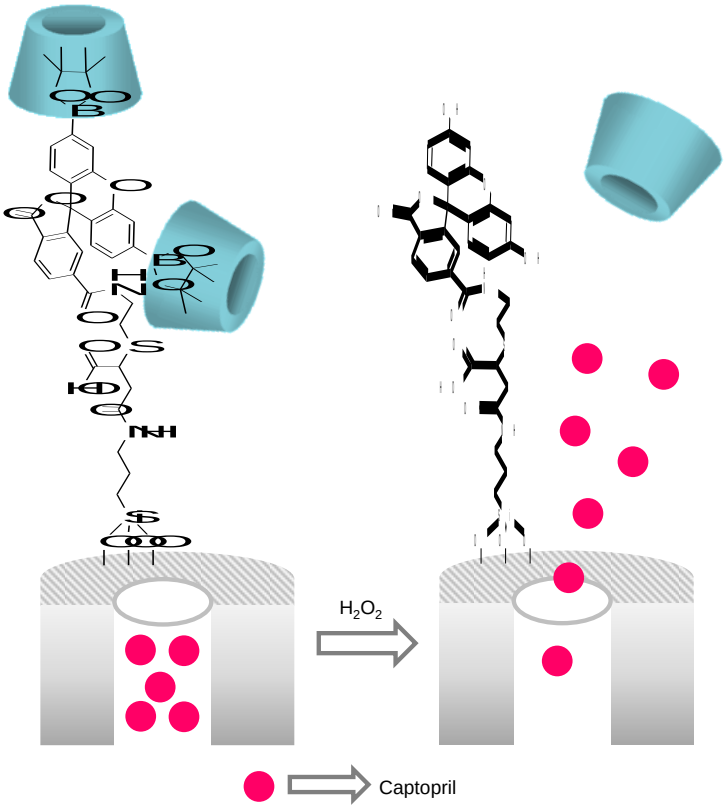

Figure 63. MSNs loaded with the drug captopril, functionalised with a fluorescein derivative bearing boronate ester groups and capped with α-CD. Cargo release is due to boronic ester cleavage under oxidative stress conditions.

3.3 Miscellaneous

Ren and co-workers designed a nanotheranostic system based on manganese oxide (MnO_x) coated superparamagnetic iron oxide nanoparticles (SPION) and MSNs loaded with camptothecin (CPT).[75] The SPION nanoparticles were covered with a thin layer of MnO_x and finally modified with carboxylic acid groups. On the other hand, MSNs were functionalised with amino groups and the anticancer drug CPT was loaded in the mesopores. Finally, the pores were locked with the MnO_x-SPION nanoparticles through the formation of amide bonds (Figure 64). The uncapping mechanism takes advantage of the presence of MnO_x that could be disintegrated under various concentrations of GSH, H^+/H_2O_2. To investigate delivery from the nanoparticles biodegradation studies under tumour-like

conditions were performed. In a neutral non-reductive environment, cargo release was insignificant compared to that observed in tumour-like condition (GSH, H^+/H_2O_2) in which a marked drug release was registered. The nanoformulation showed a marked cytotoxic effect in Panc-1 cells, attributed to drug delivery of the hydrophobic CPT. Moreover, the released MnO_x-SPION acted as contrast agent for *in vitro* and *in vivo* imaging. T1 and T2 MRI contrast images were acquired in a MRI scanner system using pancreatic xenograft-bearing mice with the administration by tail vein injection of the final theranostic nanodevice. The *in vivo* results demonstrated that the final theranostic nanodevice generated Mn ions due to the biodegradation of MnO_x in the tumour environment thus achieving greater T1 MRI contrast. In addition, *in vivo* antitumour effect of the nanoparticles was evaluated in pancreatic xenograft-bearing nude mice by intravenous tail injection. The results demonstrated a significant tumour regression without undesired effects attributed to the nanoformulation of CPT compared to the free drug. The nanoformulation increased half-life time of the CPT and targets the tumour with the subsequent specific release of CPT.

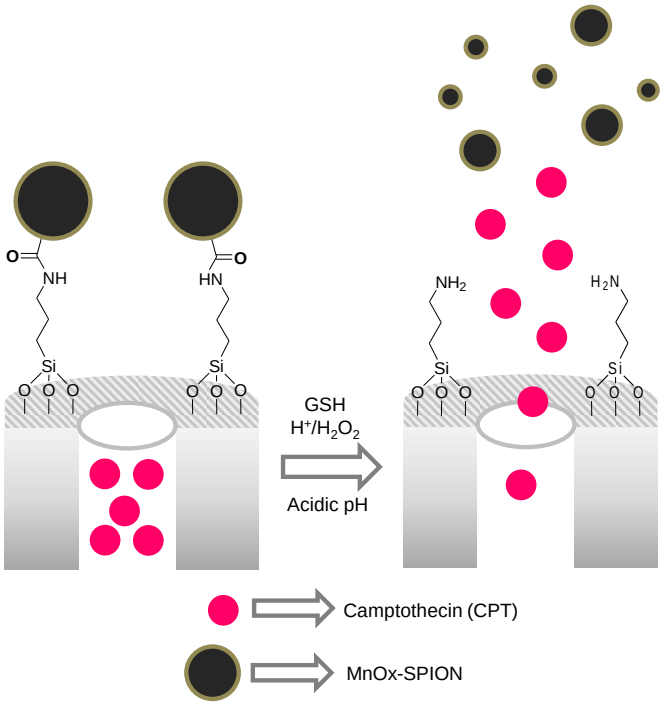

Figure 64. MSNs loaded with CPT and capped with MnOx-SPION through amide bonds. Drug is delivered due to disintegration of MnO_x in the presence of GSH, H^+/H_2O_2.

Li and co-workers developed non-porous silica nanoparticles coated with a mesoporous layer of $MnSiO_3$ as T_1-MRI contrast agent and drug delivery theranostic carrier.[76] The nanoparticles were loaded with Dox and the $MnSiO_3$ coating was PEGylated (using PEG_{5000}-NH_2) by ultrasound treatment (Figure 65). The authors demonstrated the multi-responsive delivery behaviour of the nanodevice in reducing or mild acidic conditions, mimicking the tumour environment. In the presence of high GSH levels, a redox reaction takes place and the manganese coating was dissociated. Moreover, in acidic pH (5.4-6.8) a sustained dissociation of the manganese layer was observed and the Dox release was also promoted. The nanoparticles were evaluated *in vitro* in MFC-7 cancer cells. The nanoparticles were able to internalize in MFC-7 cells, resulting in manganese ions release for T_1-MRI detection and subsequent drug delivery that effectively killed MCF-7 cancer cells. Moreover, the potential use of the nanoparticles was evaluated in MDA-MB-231 tumour-bearing nude mice as breast cancer model. The nanoparticles were administered by tail vein injection and the use of the theranostic nanomaterial was demonstrated for tumour detection. Toxicology of the nanoparticles was evaluated and the results showed lower side effects than those of free Dox and no detectable toxicity.

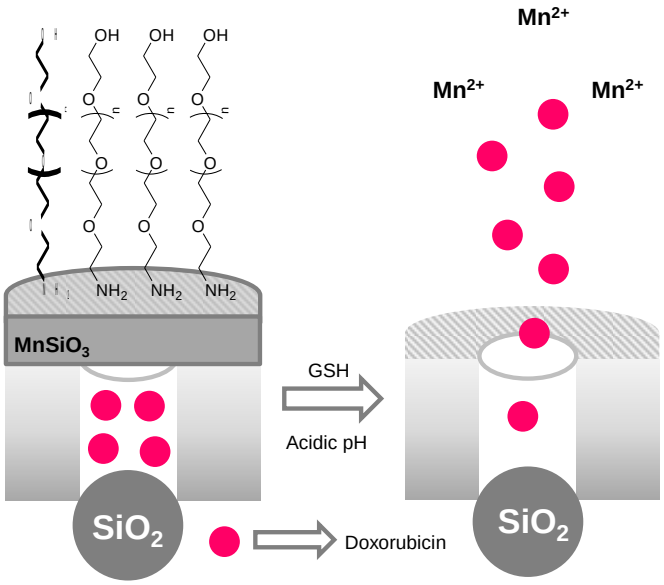

Figure 65. Mesoporous manganese silicate coated silica nanoparticles loaded with Dox and capped with PEG. Drug is delivered due to disintegration of $MnSiO_3$ in the presence of GSH, H^+/H_2O_2.

Yu and co-workers prepared biodegradable Mn-doped hollow MSNs as theranostic platform for tumour imaging and drug delivery.[77] MSNs were transformed into Mn-doped hollow MSNs under high-temperature treatment with $MnSO_4 \cdot H_2O$. Using this procedure Mn-doped silica layers onto the surface of MSNs were formed and their biodegradability properties were tested under reducing and mild-acidic microenvironment (Figure 66). Degradability of the nanoparticles in the presence of GSH, varied pH conditions and in an intracellular environment, was confirmed by inductively coupled plasma (ICP) and by TEM images. The results showed that in the presence of GSH and at acidic pH the Mn extraction from MSNs surface was accelerated. Moreover, the Mn-doped hollow MSNs nanomaterial was loaded with Dox and finally capped with a silane-PEG which contained an amide linkage. Drug-release profiles were registered in physiological conditions, in the presence of GSH, varied pHs and in combined acidic/reducing conditions. In the absence of any stimuli, the presence of Dox in solution was low whereas in suspensions containing GSH a high Dox release was observed. Moreover, when nanoparticles were stirred in acid conditions the Dox release also took place and was enhanced when combined with GSH. Dox release in the presence of GSH and in acidic environments was ascribed to the "extraction" of Mn from the inorganic scaffold which induced support disintegration. The cellular *in vitro* studies carried out with liver cancer Hep G2 cells demonstrated that the nanoparticles efficiently delivered Dox into the cells. The nanomaterial was also evaluated *in vivo* in Hep G2 tumour xenograft mice model. The tumour growth was significantly suppressed, attributed to the nanoparticles' accumulation in the tumour site, fast biodegradation and drug release in the tumour

microenvironment. Besides, biodegradation (due to GSH and acidic environment) of the nanodevice induced the release of paramagnetic Mn centres which enhanced longitudinal relaxivity allowing the MR imaging of the tumour.

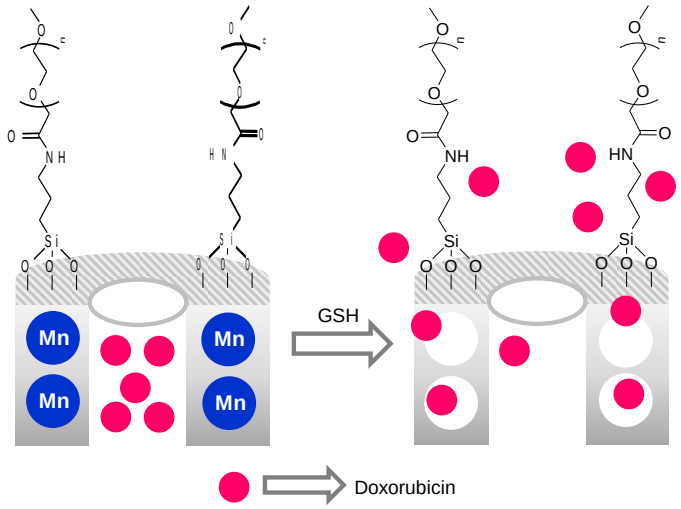

Figure 66. MSNs doped with manganese, loaded with Dox and capped with poly(ethyelene glycol). Rupture of the inorganic scaffold due to GSH-induced Mn extraction yielded cargo release.

4. Enzyme-responsive drug delivery systems

Enzyme-responsive gated materials have attracted much attention in the last years in drug delivery applications.[78] In pathological conditions, from cancer to inflammation disorders, the activity of some enzymes is upregulated and this fact could be used to design gated materials. Typical enzymes used to uncap the pores in different pathological scenarios are hydrolases, lipases, nucleases, phosphatases, glycosidases, oxidoreductases and transferases. In these nanoparticles bulky (bio)molecules, able to block the mesopores, contain functional groups that could be hydrolysed by selected enzymes. As we detail below, some of these nanomaterials have successfully been applied in realistic biological environments in *in vivo* models, being protease-responsive and hyaluronidase-responsive gated nanocarriers the most widely used.

4.1. Proteases

Proteases are enzymes involved in the hydrolysis of peptide bonds. In this context, proteases present in endocytic compartments could serve to hydrolyse polypeptidic chains acting as cap in gated nanodevices. Besides, specific proteases present in different tissues or cancer cells, such as cathepsins or metalloproteinases (MMPs), have been used to design tailor-made enzyme-sensitive gated systems. For instance, Li and co-workers reported an enzyme-responsive nanodevice for real-time diagnosis by magnetic resonance imaging (MRI) and tumour treatment in living animals.[79] For the preparation of the nanodevice the anticancer drug Dox was loaded onto magnetic iron oxide nanoparticles coated with a mesoporous silica layer. The surface of the nanoparticles was modified with mercaptopropyl moieties and the thiol groups were reacted with 3-(maleimido)propionic acid *N*-hydroxysuccinimide ester through a Michael addition reaction. This procedure yielded nanoparticles with the surface functionalized with *N*-hydroxysuccinimide ester groups. The system was finally capped, through the formation of amide bonds with the *N*-terminus, with a peptide substrate of the matrix metallopeptidase-2 (MMP-2), overexpressed in cancer cells (Figure 67). The authors found that the nanodevice remained capped in the absence of MMP-2 enzyme, whereas Dox release was clearly observed when the MMP-2 enzyme was present. The antitumoural activity and selectivity of the nanomaterial was evaluated *in vitro* in HT-1080 cancer cells. Moreover, MRI-chemotherapy experiments were carried out in HT-1080 tumour-bearing mice by nanoparticle administration by tail vein injection. T_2-weight MRI imaging measurements showed accumulation of the nanoparticles in tumours which was enhanced after the application of a magnet. Besides, a marked inhibition of tumour growth was observed for mice treated with the nanoparticles alone or with nanoparticles + magnet.

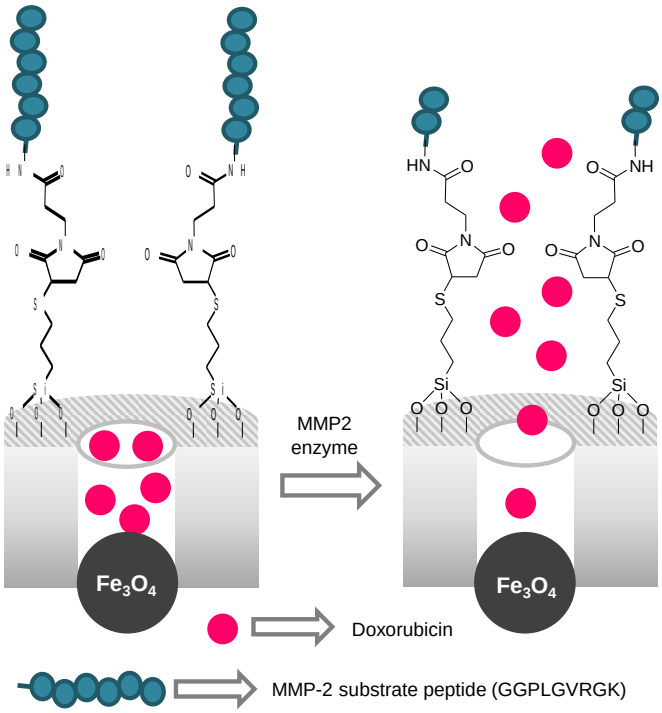

Figure 67. Fe_3O_4 nanoparticles coated with a mesoporous silica shell loaded with Dox and capped with a peptide substrate of the matrix metallopeptidase-2 (MMP-2) enzyme. Delivery is achieved upon peptide cleavage by MMP-2.

García-Fernández and co-workers prepared poly-L-lysine capped MSNs to target inflamed tissues by controlled release of anti-inflammatory drugs (Figure 68).[80] MSNs were loaded with the anti-inflammatory drug VX-765. The surface was then modified with (3-isocyanatopropyl)triethoxysilane and ε-poly-L-lysine was linked covalently through urea bonds. The poly-L-lysine coating can be degraded by the proteases present in the endocytic compartments inside cells. The authors corroborated that pore opening took place when pronase (mixture of several nonspecific endo and exo-proteases) was incubated with the nanoparticles and a significant drug release was observed due to the hydrolysis of the peptide bonds in the polymeric coating. In contrast, in the absence or pronase and or in the presence of the denatured enzyme a near zero release was observed indicating a specific enzyme-opening of the gated MSNs. The anti-inflammatory activity of the solid was evaluated *in vitro*

in the THP-1 human leukemic monocytes cells and *in vivo* in an air pouch mouse as model of inflammation first in a local approach and then systematically by intravenous tail injection of the nanoparticles. The results indicated an enhancement in the therapeutic effect of the encapsulated anti-inflammatory drug when compared with the free drug.

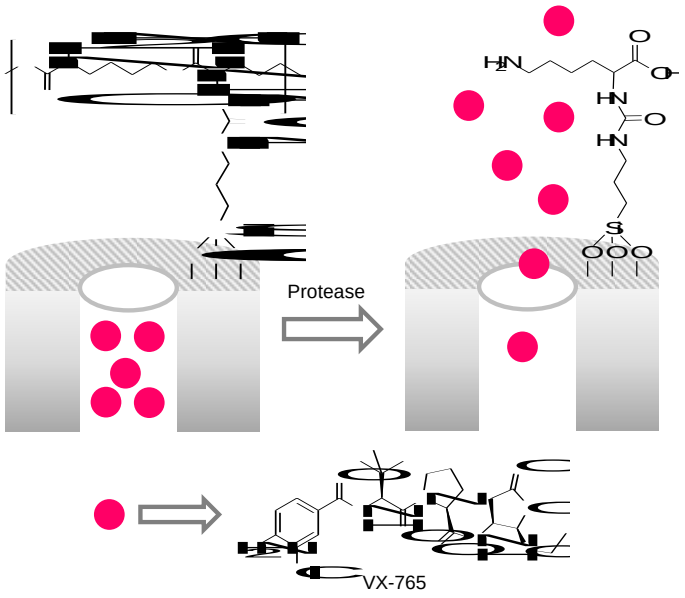

Figure 68. MSNs loaded with the anti-inflammatory drug VX-765 and capped with ε-Poly-L-Lysine. Proteases induced cargo delivery.

Srivastava et al. developed a protease responsive nanosystem for drug release in a colon cancer model.[81] The nanocarrier was based on MSNs loaded with Dox and modified with amino groups to which the antioxidant molecule bilirubin was anchored through the formation of amide bonds. The final nanodevice was obtained after coordination of BSA with the grafted bilirubin (Figure 69). The authors demonstrated stability of the solid at physiological conditions and Dox release in the presence of trypsin. Controlled release of the final nanodevice was studied *in vitro* using MC-38 (murine) and HCT-116 (human) colon carcinoma cells. The results demonstrated Dox release in the cells lines and a high inhibition in cell growth. Finally, *in vivo* toxicity and distribution studies were carried out in BALB/c mice. These studies showed accumulation of the nanoparticles in kidney and liver. Besides,

lymphocytes and monocytes were tolerant to nanodevice as MTT assays showed that viability was unaffected.

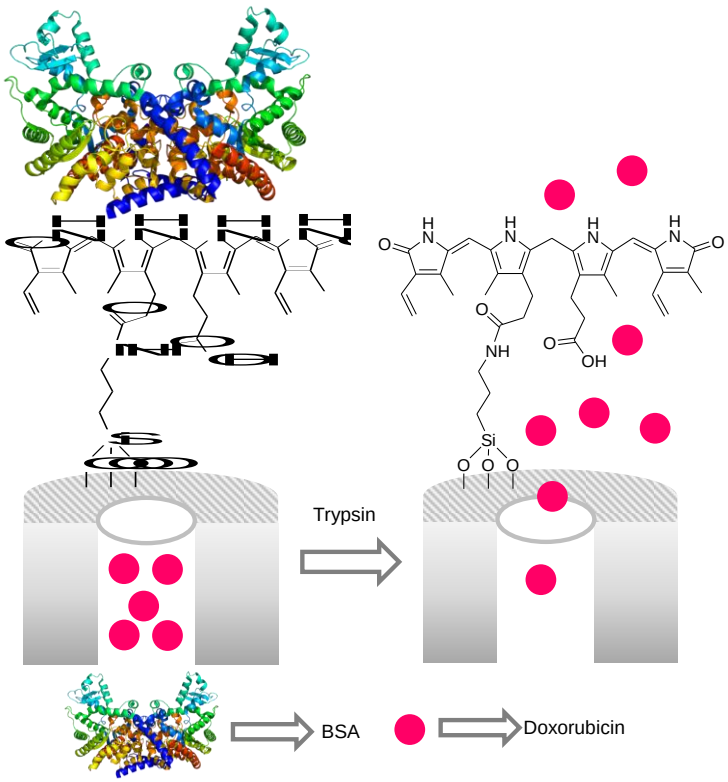

Figure 69. MSNs loaded with Dox, functionalised with bilirubin and capped with BSA. Cargo delivery was achieved in the presence of trypsin.

4.2. Hyaluronidases

Hyaluronidases (HAses) are enzymes involved in the degradation of HA and their activity has been reported to be increased in some pathological conditions such as in cancer. HA-capped nanomaterials have widely used in biomedicine due to its good biocompatibility and the targeting properties of HA. In this scenario, it has been reported that members of the HA signalling pathway (HYAL-1 hyaluronidase, HA synthases and HA receptors) are overexpressed in a variety of carcinomas. For instance, Jiang et al. prepared HA-capped MSNs loaded with the anticancer drug 5-fluoracil (5-FU) for the effective cargo delivery in a colon cancer model.[82] After loading 5-FU, the mesoporous nanoparticles were modified with

amino groups and then HA was covalently attached through the formation of amide bonds (Figure 70). HA played a dual role, to target the CD44 receptor overexpressed in cancer cells, and to act as a cap, which is degraded by HAase abundant in colon. The authors demonstrated that in the presence of HAase, HA was hydrolysed and a high drug delivery was observed compared to the control conditions in the absence of the enzyme. The anti-tumour efficacy of the nanoparticles was studied *in vitro* in HT29 colon cancer cells. These studies showed that the nanoformulation was preferential uptake by cancer cells. Moreover, the nanoparticles were also evaluated *in vivo* in a HT-29 cancer-cell bearing xenograft tumour model. The nanoparticles exhibited a significant anticancer effect reducing the tumour burden (3-fold) compared to the free drug. The remarkable anticancer effect *in vivo* of the nanodevice was ascribed to the targeting efficiency of HA toward the CD44 receptor. This preferential internalisation allowed to reach a high intracellular drug concentration than that obtained with 5-FU alone. Besides, histopathological studies showed a remarkable apoptosis levels in tumour tissues.

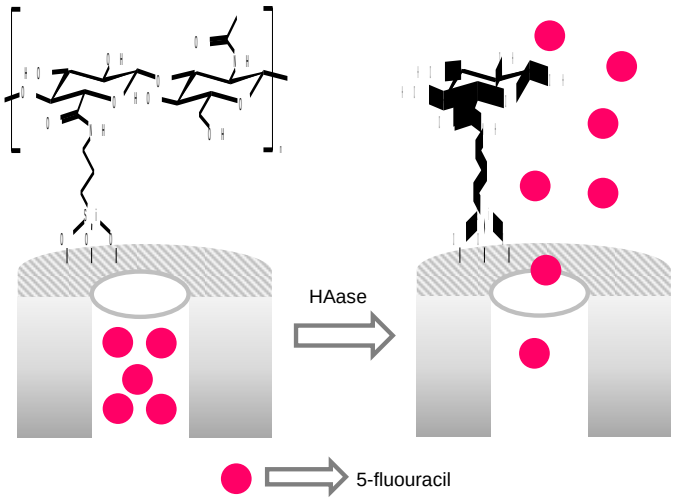

Figure 70. MSNs loaded with 5-fluouracil and capped with HA through amide bond formation. Cargo delivery is due to HA degradation by HAses.

Huang and co-workers designed a dual-responsive delivery system based on hollow MSNs capped with HA to target tumour cells.[83] Mercaptopropyl functionalized hollow MSNs were reacted with S-(2-aminoethylthio)-2-thiopryridine hydrochloride to yield nanoparticles functionalised with amino groups. The anticancer drug Dox was loaded and the HA was anchored to the nanoparticles through the formation of amide bonds (Figure 71). Drug release experiments demonstrated the uncapping of the nanoparticles in the presence of HAase and reducing agents. Samples were suspended in different pH conditions (pH 7.4, 6.8 and 5.0) with various concentrations of GSH (1 and 10vmM) and HAase at 150 U/mL. The experiments demonstrated a higher Dox release when the material was exposed to HAase under GSH 10 mM conditions in an acidic environment. The hydrolysis ability of HAase detached HA that exposed the disulphide links to GSH. *In vitro* cell experiments were performed in murine mammary carcinoma 4T1 cells and *in vivo* studies in 4T1 xenograft tumour-bearing mice as breast cancer model. The intravenously injection of the nanoparticles targeted efficiently breast cancer cells and improved suppression of tumour growth compared to the effect of the free drug.

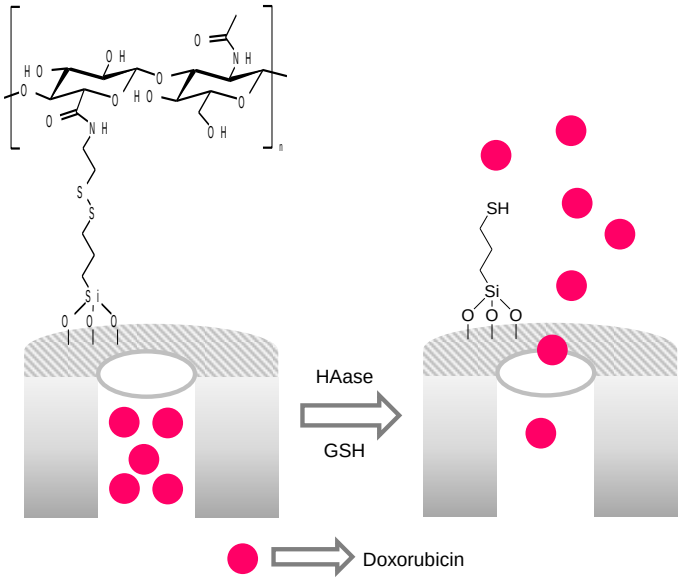

Figure 71. MSNs loaded with Dox and capped with HA through disulphide bonds. Drug release is triggered in the presence of HAase and reducing agents.

Ding et al. developed an enzyme-triggered system to delivery anticancer drug and siRNA to overcome drug resistance in breast cancer.[84] MSNs were loaded with Dox and coated electrostatically with PEI polymer. Then, siRNA was adsorbed by electrostatic interactions onto the PEI matrix and the PEI-nanoparticles were further coated with HA. Finally, the breast tumour cell-penetrating peptide (PEGA-pVEC) was linked via covalent amide bond formation with the carboxylic acids of the HA coating (Figure 72). Enzyme-triggered studies showed that HA coating prevented Dox release whereas the presence of HAase induced a significant drug delivery. *In vitro* cytotoxicity was studied in MDA-MB-231 breast cancer cells. The obtained results demonstrated the ability of the nanoparticles to internalize in cancer cells via HA recognition of the CD44 cell receptor, and the delivery of the siRNA which effectively silenced the gene associated with drug resistance thus restoring Dox-induced cytotoxicity. The therapeutic effect of the nanocarrier was confirmed in breast cancer bearing mice. Animals were injected with the prepared nanoparticles and compared with those treated only with free Dox. The nanoformulation induced a marked tumour growth inhibition when compared with the results obtained with the free drug. Histological studies showed that major organs (heart, liver, spleen, lung, kidney and brain) displayed no pathological changes whereas tumour tissues presented marked apoptosis.

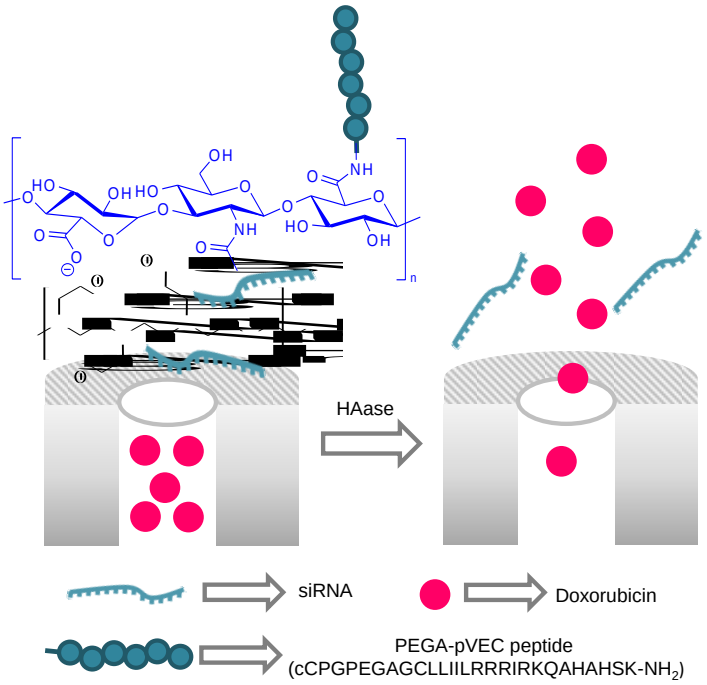

Figure 72. MSNs loaded with Dox and coated with a PEI layer which contained adsorbed siRNA molecules. Finally PEI surface was coated by HA functionalized with the breast tumour cell-penetrating peptide (PEGA-pVEC). Drug release is triggered by HAase.

Yang et al. prepared sulfhydryl and amino-co-functionalized MSNs loaded with Dox and capped upon addition of a HA derivative (HA-Histidine-SS-Pyridine) through a disulphide bond exchange reaction (Figure 73).[85] As in the case above, the nanoparticles were designed to respond to the presence of intracellular hyaluronidase (HAase), which degrades HA, and GSH that reduces disulphide bonds. In fact, the authors found that the nanoparticles were able to release the entrapped Dox in the presence of HAase or GSH. Besides, when both stimuli are present, a more marked Dox release was observed. In contrast, when nanoparticles were suspended in water in the absence of any stimuli a negligible Dox release was found, confirming the function of the HA as a cap to prevent premature drug release. The targeting ability and antitumour efficacy of the nanoparticles was demonstrated *in vivo* in a Dox-resistant human breast adenocarcinoma (MCF-7/ADR) mouse model. For this purpose mice were administered with the prepared nanoparticles (through intravenous injection) or with free

Dox. Nanoparticles showed a stronger cytotoxicity in the MCF-7/ADR cells and enhanced therapeutic effect to reverse multi drug resistance in a MCF-7/ADR tumour-bearing xenograft mouse model compared to the free drug, attending to the superior pharmacokinetics and targeting effect to reach the tumour site.

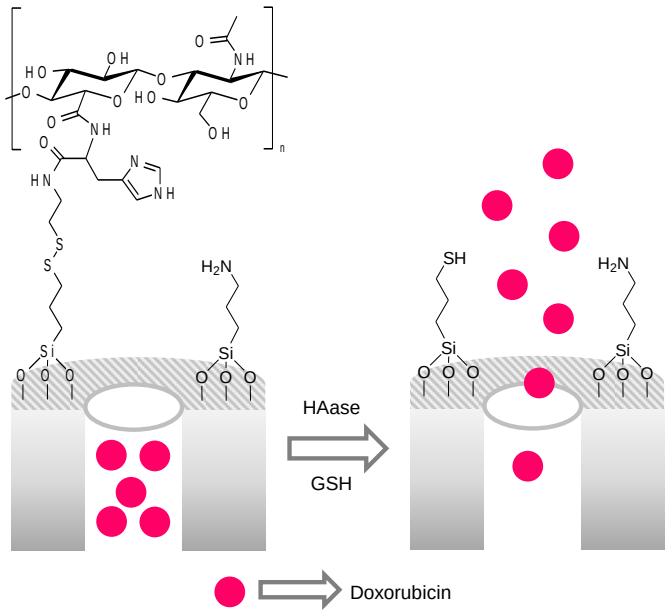

Figure 73. MSNs loaded with Dox and capped with a HA derivative through disulphide bonds. Drug release is triggered in the presence of HAase and reducing agents.

Ding and co-workers prepared gated MSNs for a combined chemotherapy-sonodynamic therapy (SD) synergistic function for cancer treatment.[86] MSNs were loaded with Dox and modified with amino groups. On the other hand, HA was modified with methacrylic anhydride and assembled onto the MSNs surface by phothoinitiated polymerization in the presence of irgacure 2959 and UV light irradiation (Figure 74). The obtained material was designed to release Dox in the presence of HAase, which is overexpressed in the tumour microenvironment. Drug delivery studies were performed under physiological conditions in the absence and presence of HAase. The studies demonstrated a HAase-dependent Dox release due to HA polymer degradation. Moreover, Dox release was significantly enhanced under sonication in combination with HAase. *In vitro* biocompatibility and anticancer effect

of the system was demonstrated in MDA-MB-231 breast cancer cells. In addition, MDA-MB-231 cells were xenografted in BALB/c nude mice which were treated with the nanoparticles by tail intravenously injection. The nanoparticles were capable of reach the tumour site and release the entrapped drug by HAase activity in the tumour environment. Besides, higher suppression of tumour growth was observed when chemotherapy by nanoparticles was combined with ultrasounds (US) treatment. A major therapeutic benefit was achieved with the nanoformulation, compared to the free drug administration. The nanoformulation also displayed lower side effects.

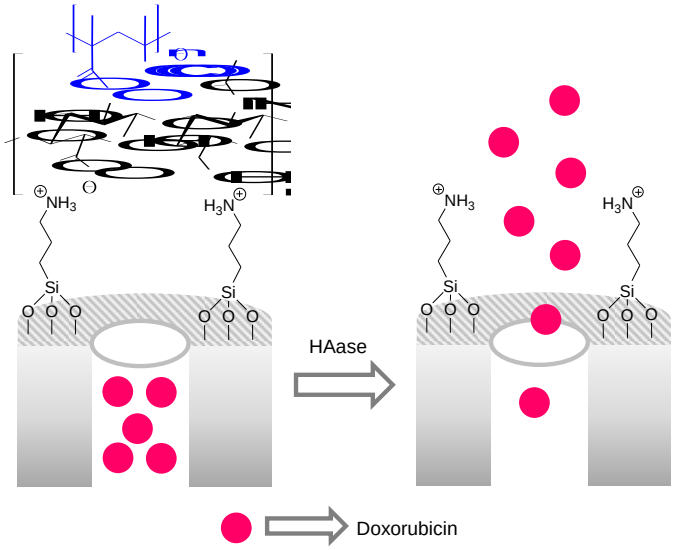

Figure 74. Amino functionalised MSNs loaded with Dox and capped with a HA derivative through electrostatic interactions. Cargo delivery is achieved by HA hydrolysis in the presence of HAase. Cargo delivery was also enhanced by US treatment.

Zhou et al. designed dual enzyme-responsive nanoparticles for drug delivery in cancer therapy based on MSNs coated with extracellular matrix components.[87] The external surface of the nanoparticles were modified with amino groups and loaded with Dox. Then, the extracellular matrix components collagen I and HA were linked onto nanoparticles surface via amide bonds yielding the final nanodevice (Figure 75). The extracellular matrix components can be degraded gradually by HAase and MMP-2. Moreover, HA recognize the CD44 receptor

overexpressed in cancer cells, facilitating the endocytosis of the nanomaterial. Aqueous suspensions of the final nanoparticles showed negligible cargo release in the absence of HAase and MMP-2 enzymes. However, a marked Dox release was observed in their presence. The *in vitro* cytotoxicity and specific uptake of nanoparticles was assessed in cancer cells (HeLa and HepG2) and *in vivo* in HeLa tumour-bearing mice. In the *in vivo* study mice were separated in different groups and the effect of free Dox compared to nanoparticles was evaluated by intravenous administration. The results demonstrated an enhancement in the drug half-life with the nanoparticles, a preferentially tumour accumulation and a major tumour growth suppression.

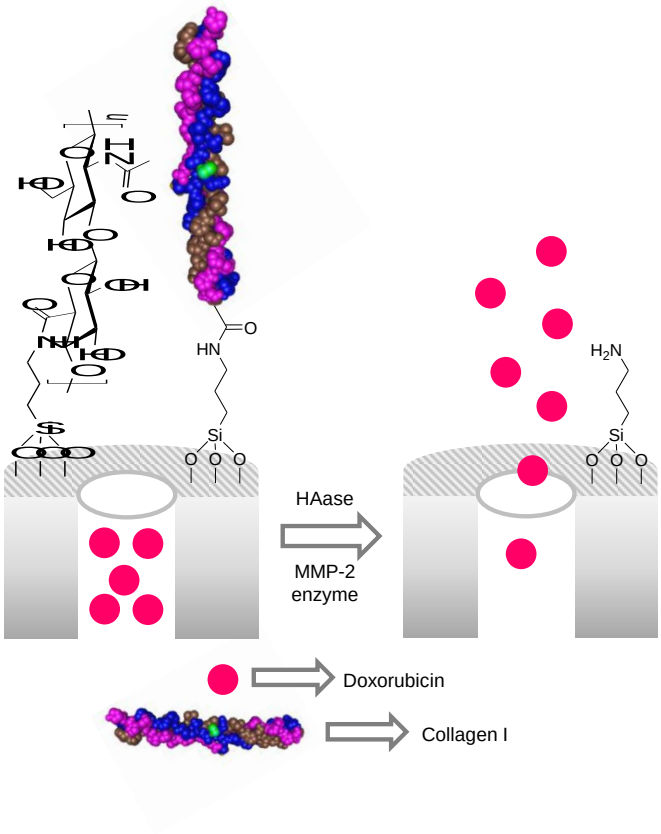

Figure 75. MSNs loaded with Dox and decorated with HA and collagen. Cargo delivery is triggered by HAase and MMP-2.

4.3. NAD(P)H dehydrogenase quinone 1 (NQO1)

Nanovalves, based on the formation of supramolecular complexes with cyclic molecules and stalks grafted onto the nanoparticles surface, have been widely used to block mesopores in mesoporous silica supports and inhibit cargo release.[88] Moreover, these supramolecular nanovalves can be designed with bulky stoppers containing enzyme-cleavable linkers.[89] Upon enzymatic hydrolysis, the stopper is removed with subsequent pore opening and cargo release. Based in this approach some recent examples using NAD(P)H:quinone oxidoreductase 1 enzyme (NQO1), which is overexpressed in cancer cells, as stimuli have been reported.

Gayam and co-workers developed a system is based on MSNs loaded with Dox and capped with a rotaxane nanovalve equipped with a benzoquinone stopper head group.[90] The authors functionalized MSNs with aminopropyl moieties and reacted the amino groups with a tosylated PEG-alkyne derivative. Then, pores were loaded with Dox and α-CD coordinated with the PEG stalk. Finally a benzoquinone stopper was added through a click chemistry reaction (Figure 76). Gate opening was controlled by the cleavage of the benzoquinone stopper induced by the presence of NQO1. In the absence of enzyme, suspensions of the nanoparticles showed a negligible cargo release, whereas in the presence of NQO1 and NADH a marked Dox delivery was observed. The nanocarrier was evaluated in the NQO1 positive cells lines, A549 (adenocarcinomic human alveolar basal epithelial cells) and MCF-7 (breast cancer cells) and HL-60 (human promyelocytic leukaemia cells) which does not express NQO1. The system demonstrated a great selectivity and drug delivery in cancerous cells in which NQO1 enzyme is overexpressed, decreasing cell viability. The nanoparticles were validated *in vivo* by subcutaneous administration in nude mice bearing A549 lung cancer cells. The nanoformulation exhibited a higher tumour inhibition activity, compared with the free drug, due to the effective accumulation and Dox delivery at the tumour site.

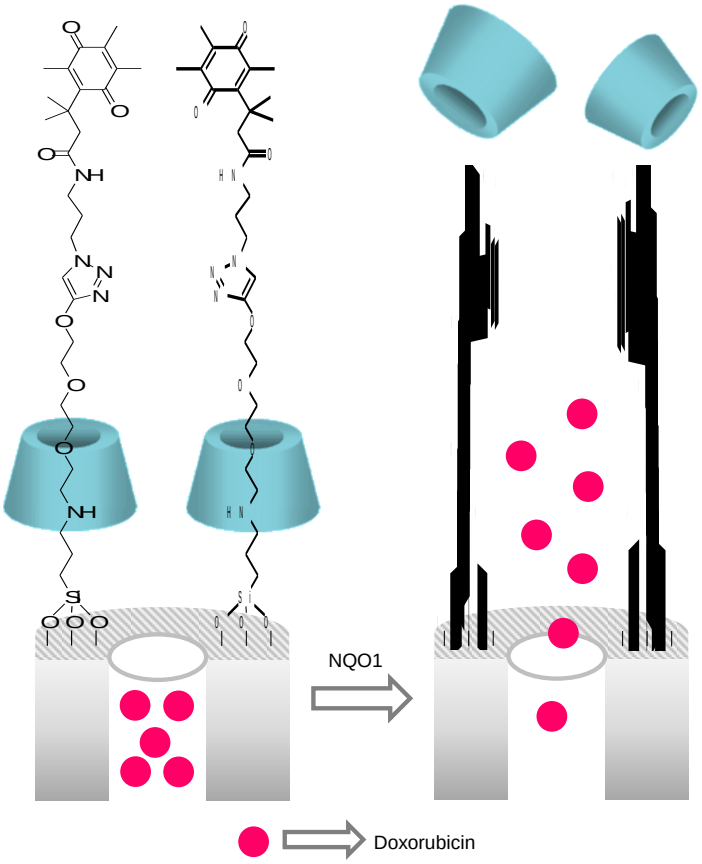

Figure 76. MSNs loaded with Dox and capped with rotaxane nanovalves containing benzoquinone stoppers. Cargo release is triggered by NQO1 enzyme.

Lee et al also designed a drug delivery system based on gated MSNs triggered by NQO1 enzyme in hypoxia conditions in cancer cells.[91] Hypoxia conditions are found in most of tumours and in this environment the activity of some bioreductive enzymes, such as NQO1, has been reported. The authors used MSNs which were previously functionalised with aminopropyl moieties. Then, an azoderivative functionalised with carboxylic acids and with a terminal alkyne chain was prepared and grafted onto the external surface of the MSNs through the formation of amide bonds. The pores were loaded with Dox and mono-6-azido-6-deoxy-β-CD anchored using an alkyne-azide coupling reaction. Finally, PEG-isocyanate was covalently grafted onto CD through formation of carbonate ester bonds (Figure 77). Dox release was studied in physiological conditions under normoxic (20 % O_2) and hypoxic (0.1%

O_2) conditions under the NQO1 stimuli. Dox remained entrapped inside the nanodevice at physiological conditions. Moreover, under NQO1 addition in normoxic conditions a minimal Dox release was observed. On the contrary, Dox release was enhanced under hypoxic conditions and in the presence NQO1. These results are attributed to the rupture of NQO1-sensitive azo bonds in the hypoxic conditions with subsequent gatekeeper removal. The antitumoural activity of the system was evaluated in NQO1-expressing cancer cells (MDA-MB-231/pNQO1 and A549) under hypoxic conditions. The obtained results confirmed the ability of the material to kill NQO1-positive cancer cells under hypoxic conditions. Moreover, the solid was also tested *in vivo* as platform to deliver drugs to hypoxic regions of tumours in a MDA-MB-231/pNQO1 xenograft mouse model. The nanoparticles were administered by tail vein injection in MDA-MB-231 bearing mice (as normoxic conditions) and MDA-MB-231/pNQO1 bearing mice (as hypoxic conditions) and compared to free drug administration. The results demonstrated that free Dox was mainly distributed in the liver, kidney, lung, and spleen indistinctly in MDA-MB-231 and MDA-MB-231/pNQO1 mice. In contrast, a significant Dox accumulation was found in hypoxic conditions in tumours of MDA-MB-231/pNQO1 but not under normoxic conditions. The efficient delivery of Dox at the tumour site under NQO1 activity was confirmed and a remarkable inhibition of the tumour growth observed with the nanoformulation.

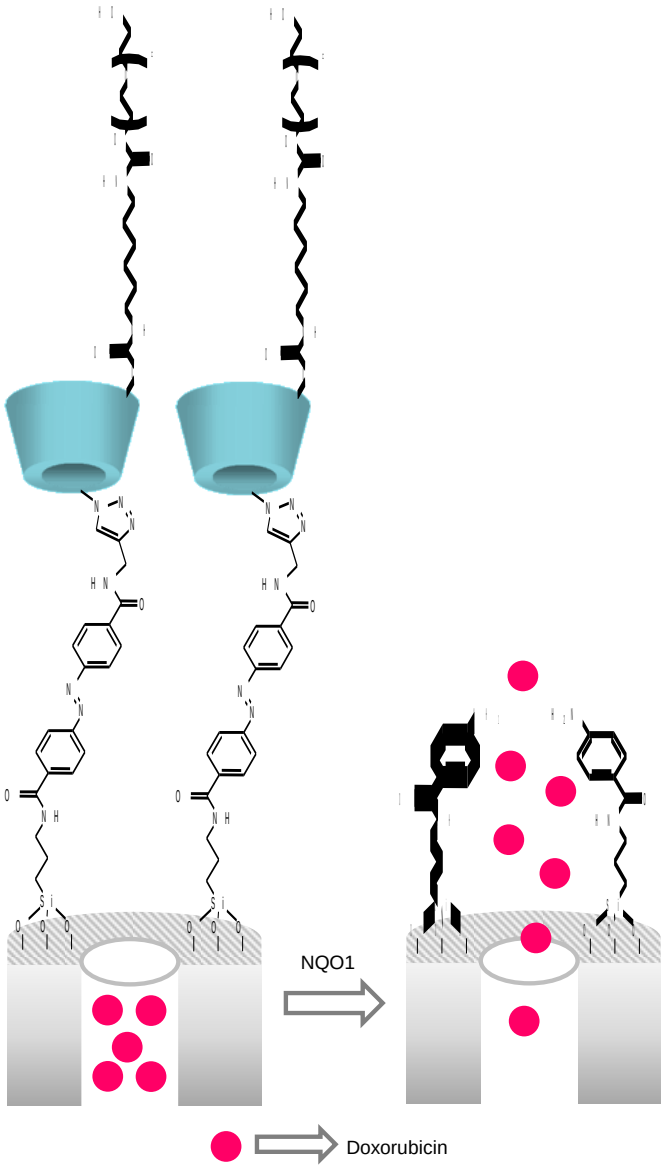

Figure 77. MSNs loaded with Dox and capped with CD derivatives bearing NQO-1-sensitive azo groups. Cargo delivery is due to the cleavage of azo bonds by the NQO1 enzyme.

4.4. Other enzymes

In addition to the examples described above, some other gated nanoparticles able to open in the presence of other enzymes such as glycosidases, transferases, lipases and DNAses have been reported and the nanoparticles used in *in vivo* model applications. Serrano, Martínez-Máñez and co-workers designed a β-galactosidase responsive drug delivery system to target senescent cells.[92] MSNs were loaded with Dox and navitoclax drugs and the external surface was

functionalised with amino groups which were reacted with a galacto-hexasaccharide (galactan) yielded the final materials. Galactan-capped nanoparticles were designed to be uncapped in senescent cells due to the overexpression of β-galactosidase enzyme that induced the hydrolysis of the galacto-hexasaccharide cap (Figure 78). The authors studied the uncapping mechanism of the capped nanoparticles in the absence or presence of β-galactosidase from *Aspergillus oryzae* in water suspensions at pH 4.5. In the absence of the enzyme a negligible release of the drugs was observed, whereas in the presence of β-galactosidase a remarkable cargo delivery was found. The different synthetized nanoparticles were tested *in vitro* and *in vivo* in senescent models. Dox-loaded or navitoclax-loaded nanoparticles administered by tail vein injection to a SK-MEL-103 melanoma tumour-bearing nude mice model of chemotherapy-induced senescence, showed that galactan-functionalised nanodevice reached senescent cells in tumour and improving the inhibition of tumour growth. Moreover, a bleomycin-induced pulmonary fibrosis mouse model in C57BL/6 male mice was used and treated intravenously with the galactan-functionalised nanoparticles loaded with Dox. The solid targeted senescent cells in lungs and had the ability to restore pulmonary functions. In both cases, the galactan-functionalised nanoparticles reduced side effects of the free drugs.

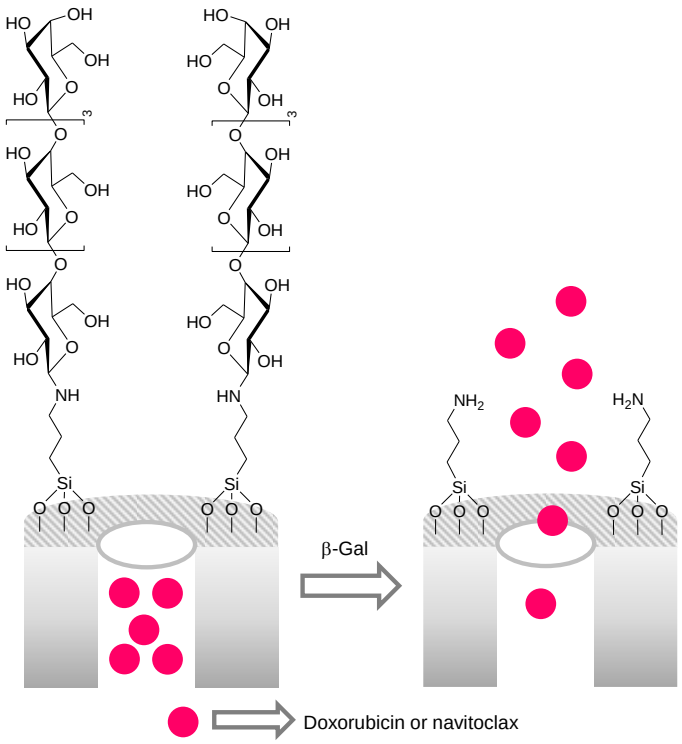

Figure 78. MSNs loaded with Dox or navitoclax and capped with a galacto-hexasaccharide. Cargo delivery is triggered in the presence of β-galactosidase.

Srivastava and co-workers described a DNA wrapped MSNs loaded with Dox to target telomerase positive human and murine cancer cells.[93] Telomerase is a ribonucleoprotein involved in the protection and elongation of telomeres. The telomeres are a region of repetitive nucleotide sequences that protects the end of the chromosome and regulate the cell aging. In normal conditions, telomeres get shorter and telomerase enzyme is at very low levels in cells. In contrast, in cancer cells telomerase is overexpressed. The authors loaded MSNs with Dox, the silica surface functionalised with amino groups, and the oligonucleotide containing the telomeric repeat complementary sequences and telomerase substrate was electrostatically conjugated to the MSNs surface (Figure 79). The authors confirmed the telomerase dependent release disposing suspension of nanoparticles under different telomerase concentrations. A negligible cargo release was registered in the presence of buffer alone, whereas in the presence of telomerase a remarkable Dox delivery was observed. The

telomerase recognized the substrate sequence and elongated the oligonucleotide cap. This resulted in a change in the DNA conformation to hairpin loop conformation and the disassembly of molecular gate. The anti-tumoral activity of the nanoparticles was studied in positive telomerase cells lines (DL, MCF-7 and K-562 cancer cells) and negative cells lines (U-2-OS) as a control. The system showed a significant targeting and thus a high cytotoxic effect in positive cancer cell lines. Finally, the prepared nanodevice was studied in a murine lymphoma model established in a DL tumour-bearing mouse by intraperitoneal administration of free Dox or nanoparticles respectively. The results demonstrated an enhanced effect in the tumour suppression and animals' survival and recovery with the nanoparticles.

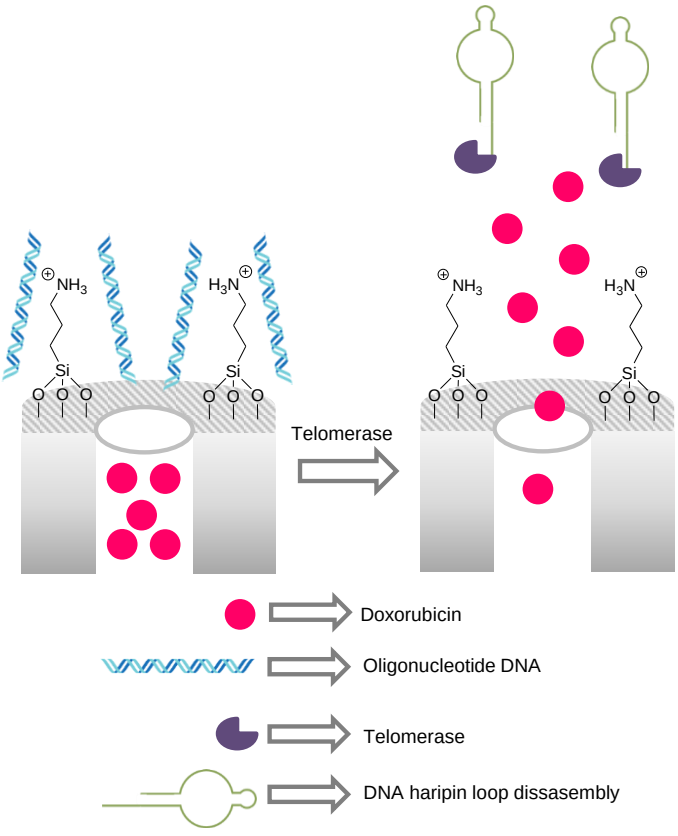

Figure 79. MSNs loaded with Dox and capped, through electrostatic interactions, with a DNA oligonucleotide containing the telomeric repeat complementary sequence and telomerase substrate [5'-(CCCTAA)nAATCCGTCGAGC AGAGTT-3']. Cargo release is observed in the presence of telomerase.

Santos-Oliveira, Martínez-Máñez and co-workers prepared MUC1 aptamer capped MSNs loaded with Dox and radio-labelled with ^{99m}Tc for controlled drug release and tumour detection (Figure 80).[94] MSNs were loaded with Dox and functionalized with amino groups to finally anchor the MUC1 aptamer electrostatically onto the surface of the nanoparticles. The drug release mechanism was based on the degradation of the aptamer in the endocytic compartments after the cell uptake upon MUC1 receptor recognition. Suspensions of the nanoparticles were stirred in the absence and presence of DNAse. A negligible cargo release was observed in the absence of the enzyme, whereas a high cargo release was observed in the presence of DNAse. The nanomaterial was evaluated *in vitro* in MDA-MB-231 cells, showing a remarkable targeting and cytotoxic effect when compared with no tumoral mammary MCF-10 cells that do not overexpress the MUC1 receptor. Moreover, the nanoparticles labelled with ^{99m}Tc were evaluated by systemic administration (retro-orbital injection) in MDA-MB-231 tumour-bearing Balb/c mice. The results demonstrated a high accumulation of the nanoparticles in the tumour site, showing the radiopharmaceutical potential use of the nanomaterial.

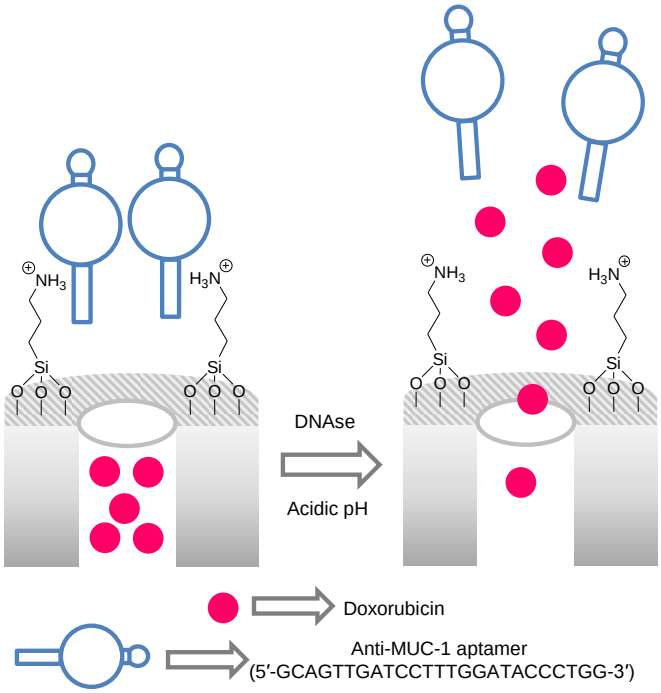

Figure 80. MSNs loaded with Dox, decorated with amino groups and capped electrostatically with an anti-MUC-1 aptamer. Cargo release was observed in the presence of DNAse.

MSNs loaded with antibiotics and capped with lipid bilayers were prepared and used for the intracellular elimination of *Staphylococcus aureus*.[95] MSNs were functionalised with 3-[2-(2-aminoethylamino)ehtylamino]propyltrimethoxysilane and the pores loaded with antibiotic gentamicin. On the other hand, liposomes composed by DOPC, DOPE, cholesterol and DOPE-PEG_{2000}-OMe were prepared and conjugated (using EDC as coupling agent) with UBI_{29-41}, a cationic human antimicrobial peptide fragment which shows high specificity and sensitivity to detect bacterial infection. The final nanodevice was obtained when the gentamicin-loaded nanoparticles were fused with the UBI_{29-41}-conjugated liposomes (Figure 81). Tryptic soy broth suspensions of the liposome-coated nanoparticles showed moderate gentamicin release (ca. 20% after 48 h) in the absence of *S. aureus* or lipase enzyme (excreted by bacteria at sites of infection). However, in the presence of bacteria or lipase an increase in antibiotic release was observed (ca. 38 and 78% respectively). These increases were ascribed to the rupture of the liposome coating induced by *S. aureus* or lipase upon hydrolysis of ester bonds in phospholipids. CLSM measurements carried out with *S. aureus* treated with nanoparticles showed bacteria death as a consequence of membrane disruption and permeation of gentamicin. Besides, confocal microscopy measurements showed a marked reduction in *S. aureus* viability after treatment with the nanoparticles. On the other hand, the prepared nanoparticles were also able to effectively kill bacteria in *S. aureus*-infected MC3T3-E1 and RAW 264.7 cells. Finally, *in vivo* studies were performed to test the efficacy of the nanoparticles, administered by tail vein injection, in male BALB/c mice infected with of *S. aureus* Xen-29 (bioluminescent bacteria) by subcutaneously injection. Bioluminescence imaging showed a marked decrease in fluorescence after 12 h and could not be detected after 48 h indicating a remarkable effectivity in inhibition bacterial growth. On the other hand,

immunohistochemistry staining showed decrease in IL-6 and TNF-α (inflammation-related genes) levels.

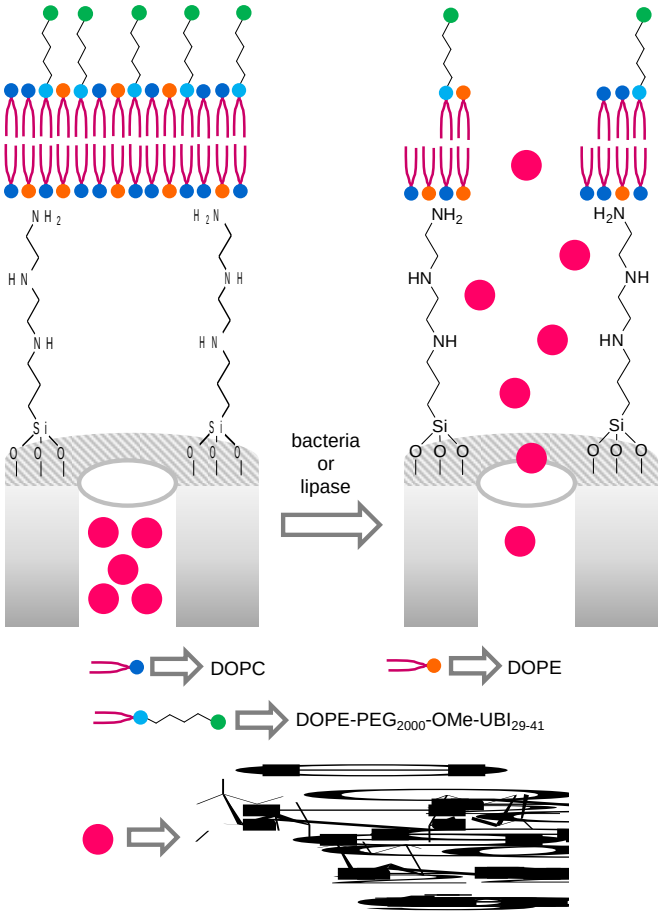

Figure 81. MSNs loaded with gentamicin and capped with a lipid bilayer formed with DOPC, DOPE and DOPE-PEG_{2000}-OMe-UBI_{29-41}. Cargo release is triggered by lipase enzyme.

Martínez-Máñez and co-workers prepared micrometric magnetic MSNs loaded with safranin O and hydrocortisone and capped with a bulky azoderivative for the treatment of inflammatory bowel diseases (IBD).[96] Oleate-coated magnetic iron oxide nanoparticles were prepared and were incorporated into MSNs. Then, the pores of the magnetic mesoporous scaffold were loaded with safranin O or with hydrocortisone (a model drug for inflammation treatment). Finally, the pores of the loaded nanoparticles were capped by grafting a bulk azoderivative containing urea and triethoxysilane moieties (Figure 82). The capping ensemble was prepared by reaction of Congo Red with (3-isocyanatopropyl)triethoxysilane. At neutral

pH both solid presented a negligible cargo release whereas a moderate payload delivery was observed at acidic pH due to partial hydrolysis of urea bonds that linked bulky azoderivative onto the external surface of the support. Besides, a marked release was observed in the presence of a reducing agent such as sodium dithionite, which was ascribed to the reduction of the azo bond in the capping ensemble with subsequent pore opening and payload release. The nanoparticles were tested in an *in vitro* digestion model and the obtained results indicated that these nanodevices could be used for the delivery of the cargo in the reducing colon environment in which azoreductase enzymes are present. The *in vivo* performances of the prepared nanoparticles was tested in Wistar rats treated with 2,4,6-trinitrobenzene sulfonic acid in order to induce an IBD model. Hydrocortisone-loaded capped nanoparticles were orally administered in IBD in rats with a marked decrease in colon inflammation followed by an intensive regeneration of the mucosa structure. Rats treated with only hydrocortisone some tissues started to heal but necrotic zones were still present. The same authors prepared, very recently, a similar material loaded with hydrocortisone and capped with an olsalazine derivative. This material is able to release simultaneously an entrapped cargo and 5-ASA in the presence of azoreductase enzymes. The capped material was also tested in an IBD model in Wistar rats showing a marked decrease in colon inflammation followed by an intensive regeneration of the mucosa structure.[97]

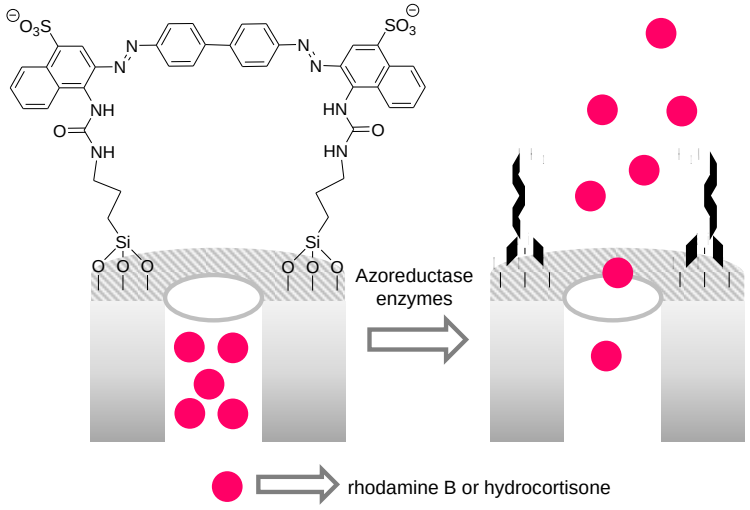

Figure 82. MSNs loaded with rhodamine B or hydrocortisone and capped with a bulky derivative bearing azoreductase-sensitive azo groups. Cargo delivery is due to the presence of azoreductase enzymes.

5. Light-responsive drug delivery systems

Since the first example developed by Fujiwara and coworkers in 2003,[98,99] light has been an appealing external stimulus to trigger cargo release in gated nanoparticles. In biological applications, light can be applied in a noninvasive manner and it is possible to have a fine control in time and in the area when light is applied. However, an important drawback of light as stimulus in biological models is that UV-vis light does not penetrate deep in tissues. A solution to this shortcoming is the use of the more tissue-penetrating NIR irradiation. In fact, most examples of application in living models use NIR light to trigger the release of the entrapped cargo in gated nanoparticles. Examples using gold structures, up-converting nanoparticles (UCNP) to transform a low-energy irradiation in a high energetic irradiation and the use of photosensitizers to generate ROS are described below.

5.1. Gold nanostructures

Zhao, Liu and coworkers developed a thermosensitive system for *in vivo* imaging and controlled release of Dox.[100] In their work, the authors prepared MSNs with a gold nanostar (AuNS) as core. After loading with Dox, the nanoparticles were coated with a mixture of the phospholipids DPPC, DSPC and FA-modified DSPE at a molar ratio of 70:25:5, which has a phase-transition temperature of 42ºC. Release studies in PBS buffer (pH 7.4) showed that cumulative release Dox at 60 h was increased as a function of the temperature due to the permeation of the phospholipid membrane. When temperature is near to the phase-transition temperature (around 40ºC), Dox release was significantly increased. At temperatures above 45ºC, total Dox release was achieved in 60h due to the complete uncapping of the system

(Figure 83). The authors also proved a pulsatile Dox release when nanoparticles were irradiated with a NIR laser (808 nm, 1.0 Wcm^{-2}) in an alternating on (10 min)/off (several minutes) treatment. As imaging tool, the nanoparticles demonstrated excellent contrast performance both, in photoacoustic imaging and X-ray CT due to the presence of AuNS. Authors used these imaging techniques to confirm that the nanoparticles were more easily endocytosed by HeLa cells, which overexpress FR, than in A549 normal cells. TEM images also confirmed this active targeting. In cytotoxicity assays, a survival rate of ca. 73 and 87 % was found for HeLa and A549 cells, respectively when cells were treated with the prepared nanoparticles at 57.8 μgmL^{-1} concentration. However, when HeLa cells were treated with the nanoparticles and irradiated with NIR laser, a more significant decrease in cell viability was found. In contrast, treatments with A549 cells with lower FR content, did not show differences in cell viability. Finally, *in vivo* experiments with HeLa tumor-bearing mice (BALB/c) were performed. Safety evaluation by biochemical analysis of liver enzymes and blood analysis showed no relevant toxicity of the prepared nanoparticles. Further, nanoparticles (36 mg/Kg) were injected through the tail vein for photoacoustic imaging and intratumorally (1.4 mg/mL, 100µL) for CT. In both cases, good contrast features were observed. Finally, mice were treated intratumorally with unloaded nanoparticles and with Dox-loaded nanoparticles and further exposed to 808 nm laser for 10 min. After irradiation, the registered temperature in the tumor was up to 65ºC. Tumor growth reduction was observed in both Dox-loaded and unloaded nanoparticles. However, 8-12 days after treatment, mice treated with non-loaded nanoparticles relapsed and tumor starts growing again. In contrast, mice treated with the combination of Dox-loaded nanoparticles and laser light showed an improved therapeutic efficiency, which was further confirmed by histological analysis.

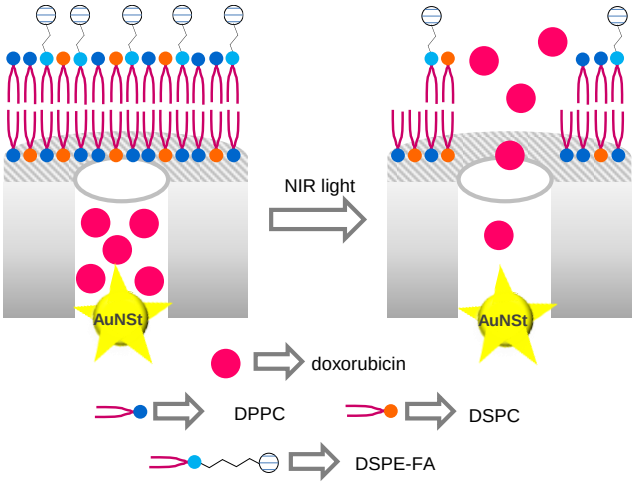

Figure 83. AuNS@MSNs loaded with Dox and capped with FA-functionalized lipid bilayer. Under 808 nm light, temperature increase triggered Dox release.

Zhao, Xu and coworkers developed a triple-combination NIR-triggered nanotherapeutic vehicle that can also be visualized by photoacoustic/CT multimodal imaging.[101] Au nanorods of 40 x 10 nm were coated by a mesoporous silica layer of around 15 nm thick. Moreover, CdTe QDs were functionalized with APTES and then attached to the mesoporous silica nanoparticles surface. In a subsequent step, the surface was aminated using APTES and carboxylate-containing adamantly moieties were anchored using EDC/NHS. In this point, the material was loaded with Dox. Then, β-CDs were modified with a ethanolamine-modified poly(glycidyl methacrylate) cationic polymer using atomic transfer radical polymerization (ATRP) and ring-opening reactions and incorporated to the nanoparticles by supramolecular interaction with adamantyl groups. Finally, the antioncogene p53 was incorporated by electrostatic interaction with the polycationic polymer. Under NIR light, temperature increase weakens the interaction between β-CD and adamantly group and the complex is dethreated, allowing the release of the p53 gene form surface and Dox from pore voids (Figure 84). The authors proved imaging and gene and Dox delivery from the nanoparticles in HEK293 and C6 cells. The authors also evaluated the system in C6 glioma tumor-bearing nude mice. Five different groups were studied: i) non-treated control mice, treated with ii) unloaded

nanoparticles not containing the p53 gene and irradiated with NIR using an 808 nm laser for 5 min , iii) nanoparticles containing p53 gene, iv) nanoparticles loaded with Dox and irradiated with NIR and v) final nanoparticles containing Dox and p53 and irradiated with NIR. In their study, the authors observed continuous tumor growth inhibition only when mice were treated with the complete system containing Dox, p53 gene and irradiated with NIR.

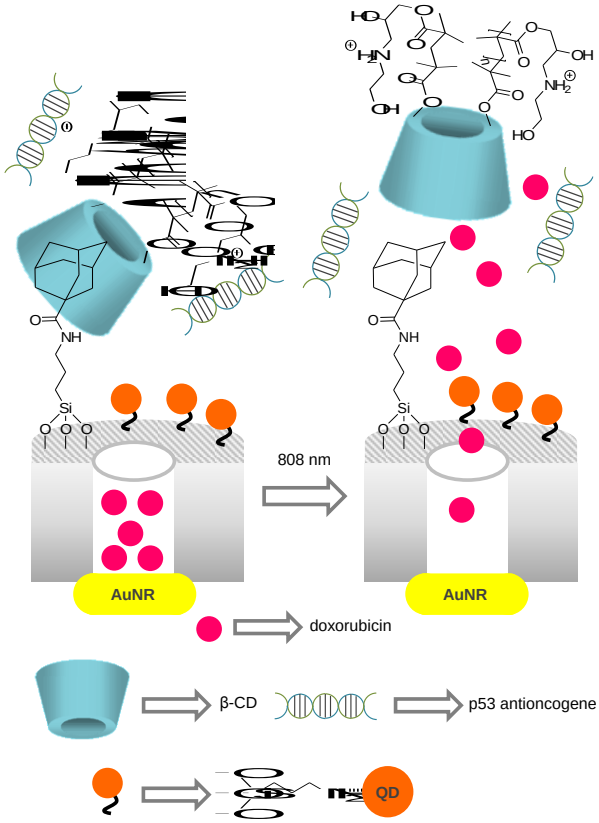

Figure 84. Gold nanorods coated with mesoporous silica, loaded with Dox, capped with a photosensitive inclusion complex and coated with p53 antioncogene. Anchored CdTe QDs acted as photoacoustic imaging enhancers. Cargo release is triggered by NIR irradiation.

Zhao and Xu developed an imaginative gated material able to perform photodynamic therapy, controlled drug release and gene therapy combined with photoacoustic imaging.[102] In their work, the authors used rattle-structured nanoparticles which consisted of hollow mesoporous silica nanoparticles with AuNRs synthesized *in situ* inside the hollow cavity of the

nanoparticle. The nanoparticles were functionalized with amino groups and then adamantanecarboxylic moieties were incorporated to the surface by and amidation reaction. After loading the nanoparticles with the antiproliferative and antiangiogenic drug Sorafenib, pores were capped with a polycation designed with two-armed ethanolamine-functionalized poly(glycidylmethacrylate) units with one β-CD core. Finally, a plasmid corresponding to the antioncogene p53 was condensed by electrostatic interaction with the capping polycation (see Figure 85). Transfection efficiency of unloaded nanoparticles containing luciferase reporter gene in HepG2 and HEK293 was confirmed by fluorescence microscopy. Moreover, transfection efficiency of green fluorescence protein plasmid was higher (39%) than that obtained with PEI (16%). p53 plasmid was similarly introduced in HepG2 cells with an internalization ratio of 85.7%. Besides, when the polycation-capped nanoparticles were irradiated with 808 nm laser light ($2Wcm^{-2}$) for 5 min, temperature rose 20.2ºC for suspension of 200μ/mL or 46.3ºC when a nanoparticles concentration of 800μ/mL was used. Negligible sorafenib release was found in the absence of NIR light (5% at 250 min). In contrast, massive drug release was obtained when the suspension was irradiated due to the detachment of β-CD containing polycation from the solid surface. When HepG2 cells were treated with the complete system including p53 antioncogene and irradiated with NIR laser light a cell viability of 22% was obtained due to the combined effect of gene, chemo- and photothermal therapy. Additionally, thanks to the AuNRs cores, photoacoustic and CT imaging was also verified. In a final step, hepatoma-bearing nude mice were treated with the final nanoparticles. Any control (PBS, bare nanoparticles without irradiation, gated nanoparticles without Sorafenib, gated nanoparticles without p53 plasmid) achieved tumour suppression along the time. In contrast, tumour growth in animals treated with the complete nanoparticles and irradiated was highly suppressed and tumour size was visibly reduced. The authors found that hepatoma-bearing nude mice injected with the capped nanoparticles and irradiated with NIR light (5 min) showed a rise in tumour temperature up to *ca.* 53ºC.

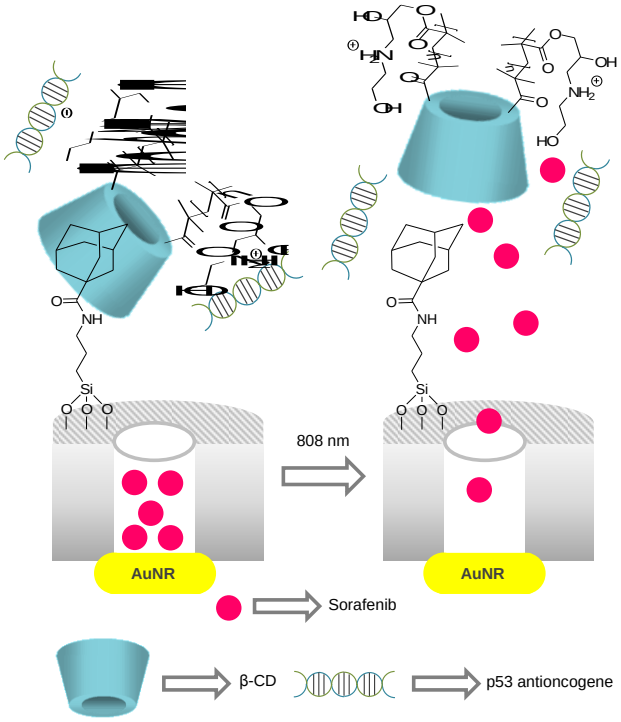

Figure 85. AuNRs coated with mesoporous silica loaded with sorafenib, capped with a photosensitive inclusion complex and with p53 antioncogene. Cargo release is triggered by NIR light.

Wang and co-workers prepared multifunctional yolk-shell MSNs for cancer therapy.[103] In a first step non-porous SiO_2 nanoparticles functionalized with FITC were decorated with aminopropyl moieties and the amino groups reacted with glutaraldehyde. Afterward, the aldehyde moieties were reacted with PEI. Next, $HAuCl_4$ was adsorbed onto the PEI layer and then reduced with ascorbic acid yielding patchy Au/fluorescein-doped SiO_2 nanoparticles. Furthermore, the prepared nanoparticles were coated with a mesoporous silica shell, whose external surface was modified with aminopropyl moieties and the amino groups reacted with carboxylate-terminated PEG using EDC/NHS as coupling agents. The pores of the nanoparticles were loaded with Dox. Suspensions of the prepared nanoparticles at pH 7.4 showed a small Dox release (ca. 10% after 10 h) whereas a marked delivery was observed at

pH 5.0 (ca. 45% after 10 h). The authors ascribed this pH-triggered release to Dox protonation which enhanced its solubility in aqueous environments. Besides, irradiation of suspensions of the nanoparticles with an 808 nm laser also induced a marked Dox release due to the conversion of light into heat by the Au patches. Toxicity of the nanoparticles toward MCF-7 cells was evaluated using the MTT assay. These studies showed a dose-dependent reduction in cell viability due to the release of the entrapped Dox. Reduction in cell viability was enhanced upon 808 nm laser irradiation due to the combination of drug release and photo-thermal effect of Au patches. Besides, unloaded nanoparticles were used for fluorescence imaging using MCF-7 cells. CLSM images showed a marked green fluorescence of the fluorescein in the cell cytoplasm. Finally, a marked reduction in tumour size in MDA-MB-231 breast cancer-bearing mice intratumourally injected with the Dox-loaded nanoparticles and irradiated with a 808 nm laser (once a day for 4 min) was observed. As a marked contrast, the tumour growth was not supressed after mice treatment with free Dox (with the equivalent amount to that present in the administered nanoparticles) and irradiation with a 808 nm laser (once a day for 4 min).

Zink and co-workers prepared octopus-type Janus nanoparticles as inorganic scaffold for synergistic chemo-photothermal therapy.[104] For the preparation of the final nanodevice, Au-poly(acrylic acid) Janus nanoparticles were prepared. Then, silica nanoparticles were prepared onto the external surface of the poly(acrylic acid) phase and further functionalised with aminopropyl moieties. Afterward, Au branches were growth in the Au phase and its surface functionalized with a PEG-SH. The final nanodevice was obtained after loading the poly(acrylic acid) phase with Dox and anchoring LA (for targeting hepatocytes or hepatoma cells which overexpressed asialoglycoprotein receptors) onto the external surface of the silica nanoparticles using EDC/NHS as coupling agents (Figure 86). Aqueous suspensions of the final nanodevice at pH 7.4 showed negligible Dox release (9% after 1 h) whereas a moderate

delivery was observed at pH 5.1 (41% after 1 h). The observed enhanced cargo delivery at acidic pH was ascribed to poly(acrylic acid) protonation with disrupted electrostatic interactions with Dox. Besides, irradiation with an 808 nm laser, increased the amount of drug release (95%) due to photothermal conversion. MTT assays showed a marked reduction in HepG2 cells treated with the nanodevice and irradiated with NIR light. Finally, tail vein injection of the prepared nanodevices combined with NIR irradiation induced marked tumour suppression (ca. 98%) in H-22-tumour-bearing Kunming mice compared to the free drug treatment.

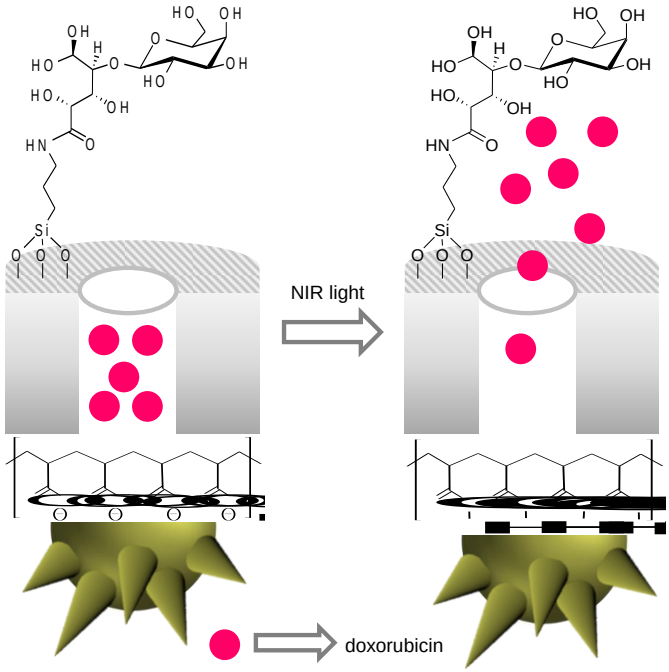

Figure 86. Janus Au-MSNs were loaded with Dox and capped with poly(acrylic acid). Drug release is activated by light. Partial delivery is also observed at acidic pH.

5.2. UCNPs

Wang and coworkers prepared a NIR-triggered system based on the hydrophobic to hydrophilic change of 2-diazo-1,2-naphtoquinone.[105] MSNs containing UCNPs $NaYF_4$:TmYb@$NaYF_4$ nanoparticles in the core were functionalized with APTES. Then, the surface was derivatised with 1,2-naphthoquinone-2-diazo-5-sulfonyl chloride via the

formation of a sulfonamide. The nanoparticles were loaded with Dox and capped using β-CD through the formation of inclusion complexes with 2-diazo-1,2-naphtoquinone moieties. The nanoparticles were unable to release Dox in PBS (less than 6 wt.% after 70 h), while when the suspensions were periodically irradiated with 980 nm laser light a significant Dox release (above 25 wt.%) was observed. UCNP $NaYF_4$:TmYb@$NaYF_4$ nanoparticles efficiently transform NIR into UV light that induced the transformation of 2-diazo-1,2-naphtoquinone to the hydrophilic 3-indenecarboxylic acid, which cannot form the inclusion complex with β-CD, inducing the uncapping of the nanoparticles and cargo release (Figure 87). The authors also found that Dox release was dependent of the intensity of the light (1 or 1.5 Wcm^{-2}) and was turned off when the nanoparticles were not irradiated. When HeLa cells were treated with the capped nanoparticles, cell viability was reduced to 80% and 44% when illuminated for 5 and 15 min, respectively. The authors studied the effectiveness of the nanoparticles in five week old BALB/c mice subcutaneously injected with HeLa cells. Four groups of five mice each treated with i) PBS, ii) capped nanoparticles, iii) NIR light and iv) capped nanoparticles and NIR light were tested. After 14 days, only tumour growth in mice treated with nanoparticles and irradiated with NIR light was partially inhibited. Histopathological studies of major organs such as heart, liver, spleen, lung and kidney confirmed the biocompatibility of the prepared nanoparticles.

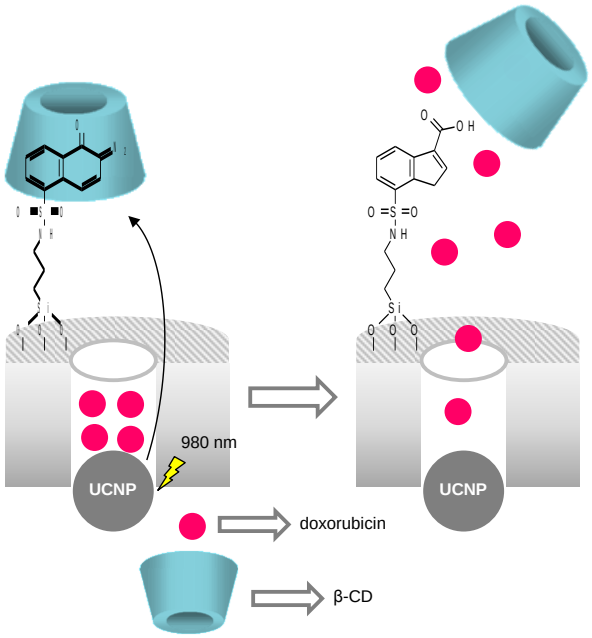

Figure 87. UCNP coated with mesoporous silica loaded with Dox and capped with an inclusion complex with β-CD. Upon irradiation UCNP induced the transformation of 2-diazo-1,2-naphtoquinone to the hydrophilic 3-indenecarboxylic acid inducing cargo release.

Liu and Ju also developed MSNs containing upconverting $NaYF_4$:Tm,Yb nanoparticles and functionalized with amino groups.[106] The photolabile linker 2,5-dioxopyrrolidin-1-yl (2-nitro-5-(prop-2-yn-1-yloxy)benzyl)carbonate was anchored to the support through an acylation reaction with the amine groups in the nanoparticles. The photosensitizer hypocrellin A was loaded in the pore voids and siRNA against polo-like kinase 1 (PLK1) (5´-UGA AGA AGA UCA CCC UCC UUA dTdT-3´) was included in the nanoparticles' surface by electrostatic interaction with the protonated amine groups. Finally, the nanoparticles were capped with PEG chains containing FA through a click reaction with the photolabile linker. siRNA controlled release in PBS was evaluated using 6-carbyfluorescein labelled siRNA. Gated nanoparticles were exposed in an alternate way to 30 min periods of laser light irradiation (980 nm, 2 Wcm^{-2}) and no irradiation. Fluorescence intensity rose up when the

system was irradiated due to the cleavage of the photolabile linker and subsequent siRNA release (Figure 88). In contrast, no fluorescence increase was found in no irradiation periods. Hypocrellin A ROS generation after NIR irradiation was assessed in suspensions of the nanoparticles and in HeLa living cells. NIR light-induced ROS generation causes the rupture of endosome membrane and allowed siRNA scape, which was demonstrated by CSLM. HeLa cells were incubated for 4 h with the functional nanoparticles and irradiated, and expression of polo-like protein kinases and its corresponding messenger RNA was studied by enzyme-linked immunosorbent assays (ELISA). The authors found a down regulation of both mRNA and protein expression confirming the functionality of the system. Moreover, when HeLa cells were treated with the gated nanoparticles and irradiated with NIR light cell proliferation was reduced to 48.3%. Finally, nanoparticles were studied in a HeLa tumor xenograft mouse model. The system was injected intratumorally and then mice were exposed to NIR light (1 Wcm^{-2}) alternating 10 min of irradiation and 10 min of no irradiation for 40 min. *In vivo* experiments demonstrated that the treatment with the capped nanoparticles plus NIR irradiation achieved a pronounced tumor growth reduction after 14 days which was not observed in saline controls neither using unloaded nanoparticles.

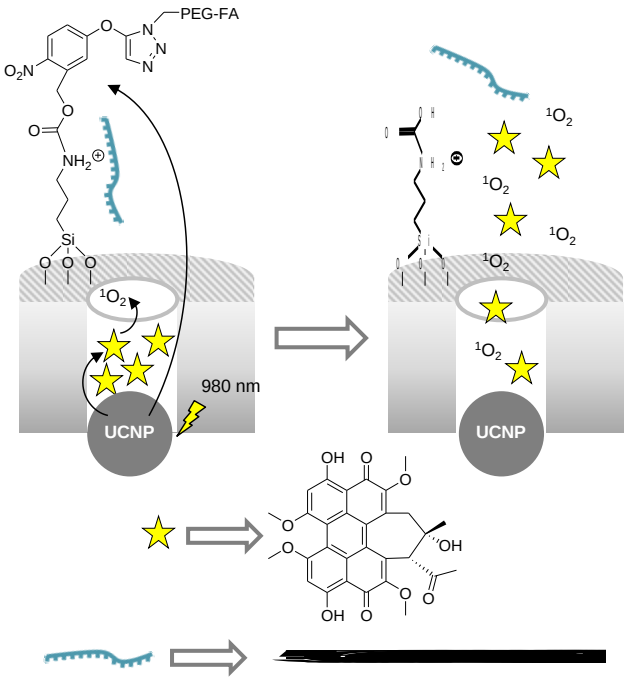

Figure 88. UCNP coated with mesoporous silica, loaded with hypocrellin A and siRNA and capped with a photosensitive FA derivatised PEG (PEG-FA). Upon irradiation at 980 nm, ROS were generated, siRNA and hypocrellin A are released.

5.3. Photosensitizers

Li and coworkers developed a NIR-light triggered nanodevice using red-blood-cell membrane as cap.[107] The system consisted of MSNs with radial pores co-loaded with Dox and the photosensitizer chlorin 6 and capped with red-blood-cell membrane vesicles. The authors confirmed the superior colloidal stability of the prepared nanoparticles in 1640 medium within two weeks. The prevalence in the final nanoparticles of the CD47 receptor from red-blood-cell membrane to avoid macrophage cells was proved. Dox release from the capped nanoparticles was triggered in PBS at pH 5.0, while Dox release at physiological pH (7.4) was negligible over 48h. This pH-dependent behavior was attributed to the decrease of electrostatic interaction between the red-blood-cell membrane and silanol groups in the surface of MSNs at lower pHs (Figure 89). Additionally, the authors found that chlorin 6-

ROS production, when nanoparticles are irradiated with 655 nm laser light, increased membrane permeability also allowing drug release. 4T1 breast cancer cells were treated with the gated nanoparticles. 2´,7´-dichlorofluorescein-diacetate was used as ROS fluorescent reporter. Without irradiation, no signal from the ROS reporter was found. In contrast, after 5 min of laser irradiation at 655 nm a strong fluorescence was observed in CLSM images. Dox diffusion to cytosol was also observed in these experiments. Differences in cytotoxicity of free chlorin 6, free Dox, nanoparticles without the red-blood-cell membrane, gated nanoparticles without chlorin 6 and complete gated nanoparticles with laser irradiation was studied. When cells were treated with the complete gated nanoparticles for 24h and irradiated with laser light (5 min), a cell death of 92.1% was found, while 75.2% cell death was observed without irradiation. The performance of the capped nanoparticles was also evaluated in spontaneous 4T1 mouse breast metastatic cancer model. After an intravenous treatment, blood retention time of the gated nanoparticles was up to 67.2-fold higher than free Dox, chlorin 6 or uncapped nanoparticles and showed lower hemolytic effect. Biodistribution analysis, performed using an IVIS imaging system thanks to the chlorin 6 fluorescence, showed increased accumulation of nanoparticles in tumor sites and decreased accumulation of Dox in heart. Finally, total tumor reduction until 6.1% and no signs of metastasis was found in mice treated with this new theranostic system.

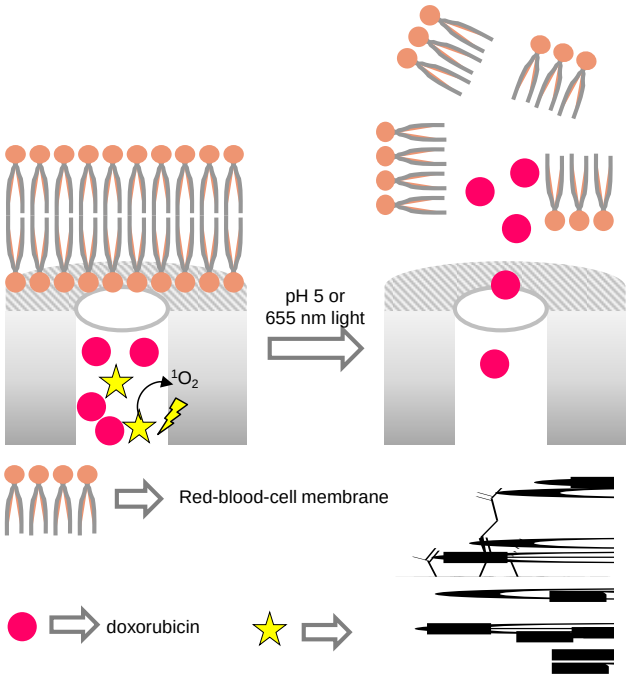

Figure 89. MSNs loaded with Dox and chlorin 6 and capped with a red-blood cell membrane. Dox and chlorin 6 were released at upon irradiation with 655 nm light or at pH 5.

In a following work, the same authors developed a similar system but including magnetic functionality in their design.[108] MSNs were functionalized with APTES and citrate-stabilized iron oxide nanoparticles were incorporated to the mesoporous surface by electrostatic interaction with the protonated amino groups in MSNs. In a further step, the material was loaded with the photosensitizer hypocrellin B and capped with a red-blood cell membrane (Figure 90). The main advantage of the magnetic functionalization is related with the possibility of guiding the nanoparticles to a specific site. After assessing good performance of the nanoparticles in HeLa cells, Balb/c bare mice with tumors created by the injection of 4T1 cancer cells in their right-hind leg were treated intravenously with the nanoparticles. Tumor eradication was achieved when the tumor was covered with a magnet for 1 hour to accumulate the nanoparticles in the tumoral environment, and then irradiated with 560 nm light for 30 min for ROS generation.

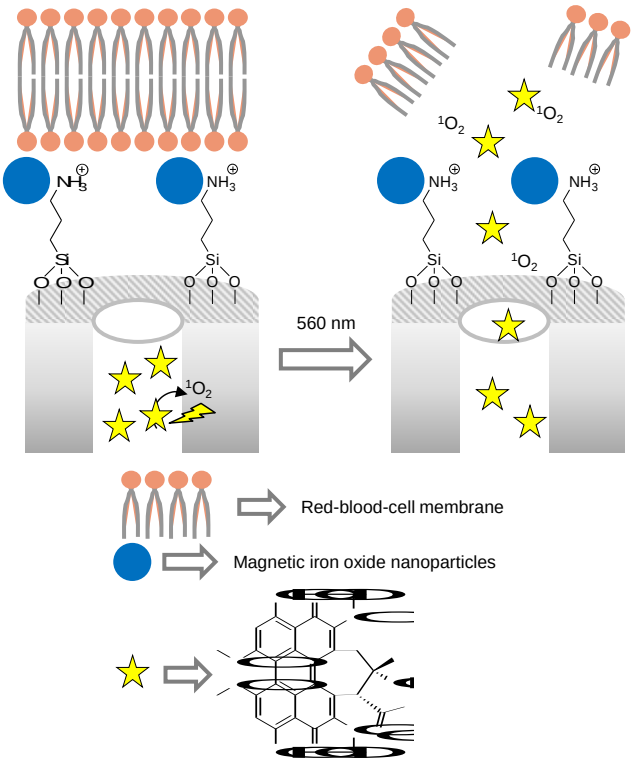

Figure 90. MSNs loaded with hypocrellin A and capped a red-blood cell membrane. Hypocrellin A induced ROS generation upon irradiation with 560 nm light.

Kim and co-workers prepared lipid bilayer-coated MSNs functionalised with cyclosporine A (a hydrophobic binding peptide) for effective chemo-photothermal therapy of pancreatic cancer.[109] For the preparation of the gated nanodevice the pores of the MSNs were loaded with IR-820, a NIR dye that upon irradiation induced photothermal and photodynamic processes causing apoptosis, and the system was capped by the formation of a lipid bilayer composed by DPPC, cholesterol, DSPE-PEG_{2000}-COONH-cyclosporine A and bortezomib, which was included onto the lipid bilayer through electrostatic interactions (Figure 91). Aqueous suspensions of the prepared nanoparticles showed a moderate bortezomib release at pH 7.4 (ca 20% after 35 h), whereas a moderate drug delivery enhancement at pH 5.0 was observed (ca. 50% after 35 h) due to the disruption of the bilayer coating. Besides, irradiation with a 808 nm laser induced a more pronounced bortezomib release at pH 5.0 due to a photothermal effect generated by the entrapped IR-820 dye and bilayer disruption. CLSM

studies, carried out with the prepared nanoparticles loaded with coumarin-6 instead of IR-820, showed internalization of the nanoparticles by PANC-1 and MIA PaCa-2 cells and their localization in the lysosomes. MTT assays conducted with PANC-1 and MIA PaCa-2 cells and the IR-820-loaded nanoparticles showed a reduction in viability due to nanoparticle internalization and release of bortezomib. Besides, a more marked viability reduction was observed upon nanoparticle treatment and NIR irradiation due to the synergic effect of bortezomib and ROS generation which induced apoptosis. *In vivo* studies carried out with a PANC-1 xenograft mouse model showed accumulation of the nanoparticles in tumour through EPR effect and a noticeable inhibition of tumour growth was observed upon nanodevice intravenous administration and NIR irradiation compared to the free drug.

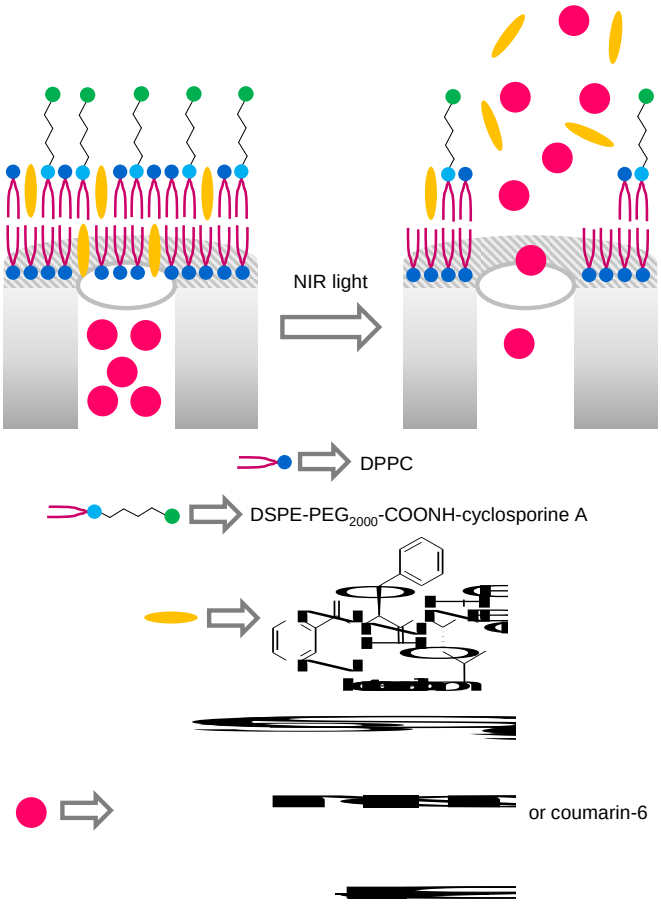

Figure 91. MSNs were loaded with the dye IR-820 and functionalized with a lipid bilayer composed by DPPC, cholesterol, DSPE-PEG_{2000}-COONH-cyclosporine A. Bortezomib was absorbed onto the bilayer by electrostatic interactions.

5.4. Miscellaneous

Ultrathin 2D Ti_3C_2 nanosheets coated with a mesoporous silica shell were used for the development of nanodevices for hepatocellular carcinoma treatment by Yang et al.[110] The surface of the mesoporous layer was functionalised with aminopropyl moieties, which were reacted with *N*-hydroxysulfosuccinimide-PEG_{2000}-maleimide. Finally, the tripeptide Arg-Gly-Asp (RGD) which acts as ligand for targeting integrins overexpressed in hepatocellular carcinoma cells, was anchored onto the grafted PEG, through a Michael reaction (Figure 92). The pores were loaded with Dox. A pH-triggered Dox release from the nanodevice was observed (ca. 17 and 30% at pH 7.4 and 5.0 respectively and after 24 h) which was ascribed to a decrease of the electrostatic interaction between the drug (protonated at acidic pH) and the amino moieties, located inside the pores, which are positively charged at pH 5. Besides, irradiation with an 808 nm laser induced a significant enhancement of Dox release at both tested pHs due to the hyperthermia effect of Ti_3C_2 nanosheets. *In vitro* studies carried out with SMMC-7721 cells and the nanodevices under 808 nm light irradiation showed a marked decrease in cell viability due to the synergic effect of the released Dox and temperature enhancement. Besides, CLSM studies revealed the RGD-mediated endocytosis of the nanodevice in SMMC-7721 cells. SMMC-7721 tumour xenografts in nude mice were used to test the efficacy of the treatment with the nanodevice and 808 nm laser irradiation. The combined treatment induced a total ablation of tumour due to the release of Dox and to a marked increase in temperature (from 30º to 58ºC). Histological evaluation showed significant apoptosis and necrosis of SMMC-7721 cells after the dual therapy.

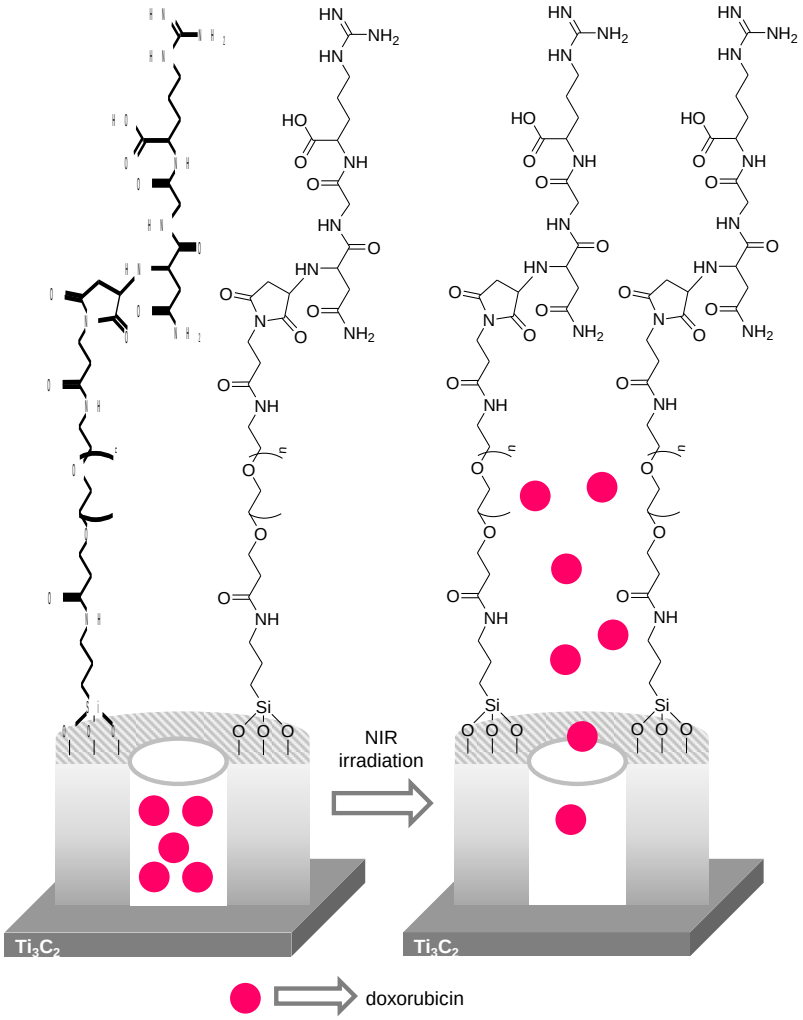

Figure 92. MSNs were loaded with Dox and capped with PEG functionalised with RGD peptide. Drug release is activated by light. Partial delivery is also observed at acidic pH.

A dual therapy was developed by Zhang and co-workers using Dox-loaded MSNs coupled with WS_2 QDs.[111] For the preparation of the nanodevice, the authors functionalized the external surface of MSNs with aminopropyl moieties, which were reacted with 4-adamantane carboxylate benzaldehyde. This procedure yielded MSNs decorated with adamantane moieties linked through acid-labile benzoic-imine bonds. Besides, an adamantine-modified tLyP-1 peptide (with tumour penetrating properties) and WS_2 QDs functionalized with β-CD were also prepared. The final nanodevice was constructed using supramolecular interactions. In a first step, the pores of the MSNs decorated with adamantane were loaded with Dox. Then, the

β-CD-functionalized WS_2 QDs were linked to the adamantine-modified tLyP-1 peptide through host-guest interactions. Finally, these peptide-modified QDs were used to cap the pores of the Dox-loaded and adamantane-coated MSNs using also host-guest interactions (Figure 93). Nanodevices were able to release Dox at acidic pH (65% after 24 h), due to the hydrolysis of benzoic-imine bonds which detached WS_2 QDs containing the tLyP-1 peptide, whereas negligible delivery of drug was observed at neutral pH. *In vitro* CLSM and flow cytometry studies carried out with 4T1 cells showed a marked uptake of the nanodevice, through endocytosis, and its localisation in the cytoplasm. MTT assays showed a dose-dependent reduction in 4T1 cells viability due to nanodevice internalisation and Dox release. Besides, 4T1 cells viability decreased when, after nanodevice internalisation, cells were irradiated with with 808 nm near infrared (NIR) light due to QDs-induced hyperthermia. *In vivo* fluorescent imaging, carried out with 4T1-tumour-bearing mice treated with the nanodevice in this case loaded with indocyanine green instead of Dox, showed preferential accumulation in the tumour due to the targeting abilities of the tLyP-1 peptide. Finally, 4T1-tumour-bearing mice were intravenously injected with the nanodevice loaded with Dox and irradiated with 808 nm NIR light showed a marked tumour growth inhibition, compared to free drug, due to the released Dox and photothermal ablation.

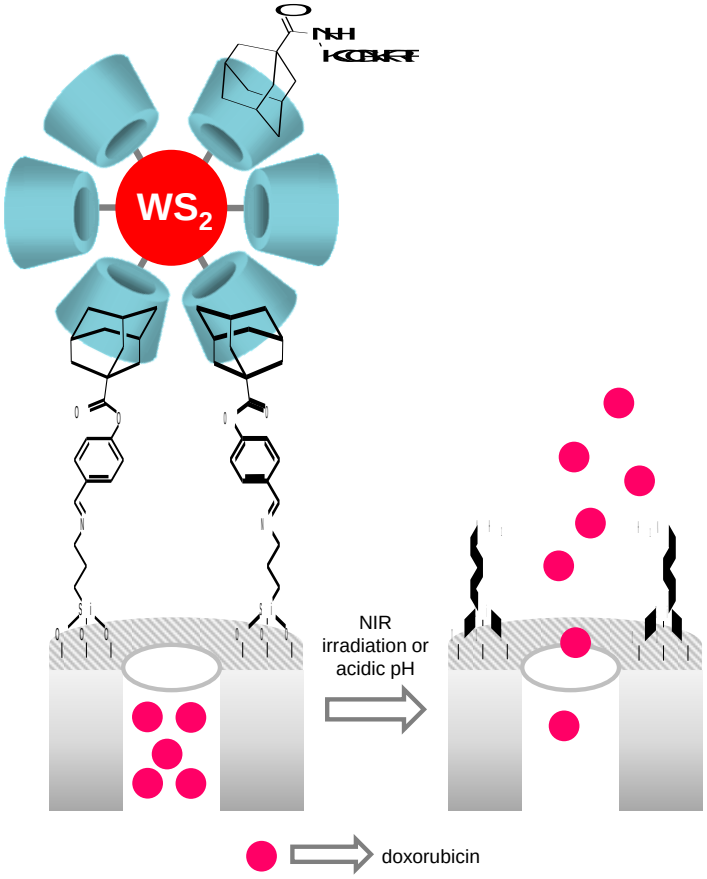

Figure 93. MSNs loaded with Dox and capped with WS_2 QDs functionalized with β-CD containing the adamantine-modified tLyP-1 peptide.

6. Temperature-responsive drug delivery systems

Temperature changes can be significant in the course of a disease. Some processes such as inflammation or infection induce a substantial temperature increase. Also, temperature of tumoral cells is slightly different from normal surrounding cells. This phenomenon can be used to deliver selectively drugs in tissues with higher temperature. In a wider vision, temperature-responsive systems can be used simply to protect by encapsulation a drug until it reaches the body at 37 ºC. As we have seen above, an increase in temperature can be achieved using gold nanoparticles able to transform light in heat (*vide ante*) or superparamagnetic nanoparticles able to generate heat when are exposed to an alternating magnetic fields (AMF) (*vide infra*). Regarding the design of this kind of nanodevices, thermosensitive polymers with

temperature-phase transition, and especially those which contain *N*-isopropylacrylamide units, have been widely used as part of the gating mechanism in temperature-controlled gated nanodevices. These polymers have the ability to exchange its conformation between a hydrated state and a more compact dehydrated state, which makes them ideal as capping moieties.

Yang and Wu took advantage of polymer shrinkage to design nanoparticles for controlled drug delivery.[112] MSNs were functionalized with 3-methacryloxypropyltrimethoxysilane that reacted with *N*-isopropylacrylamide and methacrylic acid through seed precipitation polymerization to form a capping co-polymer with a lower critical solution temperature (LCST) of 39ºC, which indicates a collapsed conformation above this temperature and an hydrated and bulky state below this temperature. Pores were loaded with berberine and evodiamine was adsorbed onto the responsive polymer. Berberine and evodiamine are active components of *Coptidis rhizoma* and *Euodiae Fructus*, respectively, which are used in Traditional Chinese medicine to induce a synergistic antitumoral effect. Finally, a lipid bilayer using DSPE-PEG200 was formed around the nanoparticle. The solid showed no significant release of any of the drugs at neutral pH (7.4) and at 37 ºC. However, drug release increased when pH decreased to 5 or when temperature rose until 41ºC, which represented tumoral microenvironment. Below LCST, the polymer forms a dense layer onto the solid surface that hinders berberine release while the lipid bilayer prevents evodiamine leakage. At high temperature lipid bilayer destabilization and polymer shrinkage allowed the escape of the drugs (Figure 94). Additionally, when pH decreases, lipid bilayer permeation and polymer degradation triggered drug release. In a cellular environment, endocytosis leaded to lipid bilayer and cell membrane fusion, which allowed evodiamine release. In a second step, increased temperature and low pH in lysosomal conditions triggered berberine payload. *In vitro* cytotoxicity of the gated nanoparticles was studied in tumoral HepG2, HCT-8 and HeLa

cells and in non-tumoral HUVEC cells. While treatment with unloaded nanoparticles underwent high viability (>90%), treatment with the drug-loaded system led to an important toxicity most likely due to lipid bilayer permeation and degradation of the polymer in the acidic lysosomes. Moreover, a good inhibition of cell migration and invasion was observed in wound-healing and transwell assays when HepG2 and HCT-8 tumoral cells were treated with the capped nanoparticles. In contrast, the same nanoparticles loaded with berberine and evodiamine were able to inhibit the formation of capillary tubes in normal HUVEC as a model of tumor angiogenesis. Finally, nude mice injected with EMT-6 cells to generate a breast tumor model were treated with the gated nanoparticles via tail vein. Free Taxol was used as control. Taxol showed the strongest tumor inhibition, but animal body weight was importantly decreased due to side effects. Free evodiamine and free berberine showed rapid clearance. In contrast, the prepared nanoparticles showed great tumor inhibition without body weight loss. The effect of the nanoparticles is most likely due to increase in temperature in the tumour microenvironment and by lipid bilayer permeation and polymer degradation at acidic pH. Moreover, TUNEL staining of tissue sections confirmed the capped nanoparticles inhibited tumor growth by inducing apoptosis in tumor cells. The study also showed that the efficacy of the nanoparticles was significantly better than the free drug combination.

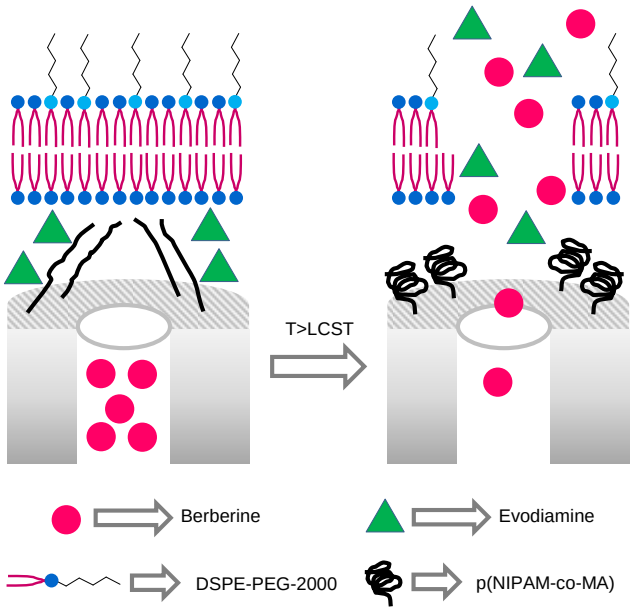

Figure 94. MSNs loaded with berberine and evodiamine and capped with a p(NIPAM-co-MA) polymer and DSPE derivatised with PEG lipid bilayer. In a cellular environment the bilayer was disrupted releasing evodiamine. When temperature was above LCST berberine was released.

Yu, Jin and co-workers studied the ability of gated nanoparticles to target CD133 receptor in laryngeal carcinoma cells.[113] The authors used MSNs functionalized with methacryloxypropyl moieties, loaded with different cargoes (cisplatin, 5-fluorouracil, PTX, fluorescein, an siRNA against the ATP-binding cassette, subfamily G, member 2 (ABCG2)) and capped with the pH- and thermo-sensitive polymer poly[(N-isopropylacrylamide)-*co*-(methacrylic acid)] copolymerized onto the external surface following a seeded precipitation polymerization process.[114] FA was also grafted in the surface thanks to the free carboxylic acid moieties of the polymeric chains (Figure 95). The nanoparticles delivered their cargo at temperature above polymer LCST. This temperature can be also easily tuned as a function of pH. Thus, the amount of cargo released in 24h at pH 7.4 and 45 ºC was around 36%, while only 9.5% of cargo release was obtained at 30ºC. In contrast, when pH is adjusted to 5.5, release reached 35 and 60% at 30 and 45ºC, respectively, which can be explained due to the change of the LCTS with the pH. Cellular uptake of the nanoparticles and subsequent fluorescein release was confirmed by CLSM. The ABCG2 protein expression, which is related with drug multiresistance, was down-regulated when cells were treated with the siRNA-loaded nanoparticles. Likewise, the combination of two nanoparticles, one loaded with the antitumoral drug and the other with siRNA, had a significant cytotoxic effect on $CD133^+$ Hep2 cancer cells, which show ABCG2 up-regulation. Finally, tumor growth of BALB/c-nu/nu mice injected subcutaneously with $CD133^+$ Hep2 cells was inhibited when the mice were treated subsequently with antitumoral-loaded nanoparticles and siRNA-loaded

nanoparticles. Moreover, the apoptosis rate of $CD133^+$ cancer cells in tumor specimen, quantified by terminal deoxynucleotidyl transferase dUTP nick end labeling (TUNEL) staining, was confirmed to be higher in mice treated with combined nanoparticles than in mice treated with only one type of drug-loaded nanoparticles.

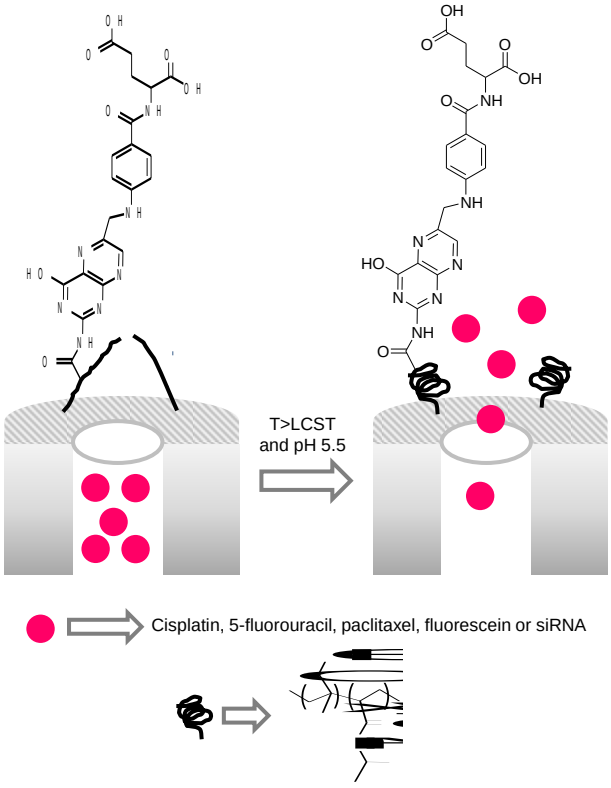

Figure 95. MSNs loaded with different cargoes and capped with FA-functionalized p(NIPAM-*co*-MA) polymer. Cargo release is modulated by changes in temperature and pH.

7. Magnetic hyperthermia-responsive drug delivery systems

It is well-known that the reorientation of superparamagnetic nanoparticles when exposed to AMF generates heat which can be used to kill cancerous cells. This concept, raising of the temperature by AMF also called magnetic hyperthermia, has been used for the design of capped materials for drug delivery. The design of these capped nanoparticles includes superparamagnetic nanoparticles and temperature-responsive capping ensembles such as

certain polymers. Upon application of an AMF the superparamagnetic nanoparticles transform the magnetic field in heat that result in changes in the capping element and cargo release. Due to the technical drawbacks to generate AMFs such as need of high energy, adjustments of external heating and good signal control, this stimulus has not been developed as others. Currently, the obtained heating is not as high as when optical hyperthermia is used, due to the relatively low temperature reached by the superparamagnetic nanoparticles and the rapid heat dissipation in tissues among others. However, magnetic hyperthermia can be considered a promising approach to prepare AMF-driven systems able to exert a synergic effect due to the heating of the tissues plus a controlled release of drugs when using capped materials. In this field, Vallet-Regí et al. validated AMF-sensitive nanoparticles for tumor reduction.[115] The system consisted of superparamagnetic iron oxide nanoparticle embedded in a mesoporous silica matrix and coated with a thermosensitive polymer. Specifically, the external surface of the nanoparticles were first functionalized with both, small PEG chains for colloidal stability and 3-[tris(trimethylsiloxy)silyl]propyl methacrylate. In a further step, radical polymerization was performed using the monomers *N*-isopropylacrylamide, *N*-(hydroxymethyl)acrylamide and *N*'-methylenebis(acrylamide) and ammonium persulfate as radical initiator (Figure 96). The thermosensitive layer had a LCST of 42°C. When the temperature is above this temperature, the polymer chains collapse and a cargo can diffuse from the pore voids to the exterior. The authors validated their nanoparticles in an allograft model using murine melanoma EL4 cells injected subcutaneously in 7-week-old female immunocompetent C57/BL6 mice. First, rhodamine tagged nanoparticles were injected in the tumors and after 96h mice were euthanized. The study revealed that nanoparticles deeply penetrated within all tumor parts. In a subsequent study, six groups of four mice were used to study the performance of Dox-loaded MSNs when an AMF (H x f: 1.89 x 10^9 $Am^{-1}s^{-1}$) was applied for 30 min within three consecutive days. Two groups, i) with and ii) without application of magnetic hyperthermia were used as control. Also, mice treated with Dox-loaded

nanoparticles and iii) with and iv) without application of AMF were studied. Finally, mice treated with v) free Dox and with vi) unloaded nanoparticles and with AMF were included in the study. The researchers only found tumor growth inhibition in mice treated with Dox-loaded nanoparticles and treated with AMF, which can be explained in terms of the synergic effect obtained due to the local heating and Dox release.

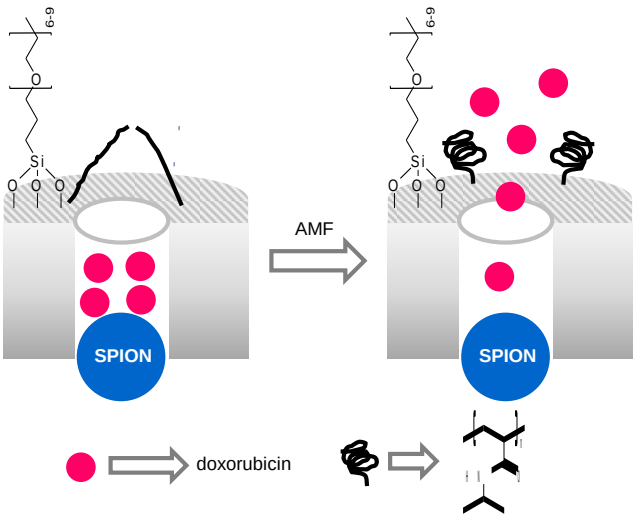

Figure 96. PEG-functionalized magnetic MSNs loaded with Dox and capped with a NIPAM thermosensitive polymer. Upon the application of AMF, the polymer collapsed allowing Dox release.

8. US-responsive drug delivery systems

US are an attractive exogenous stimulus to trigger cargo release from gated particles. This type of irradiation is known to penetrate deep inside tissues by an appropriate selection of the frequency. Additionally, the use of US induces an enhanced particle uptake in cells and a synergic killing effect due to membrane fluidification and ROS generation. US can also be used as a safe, easy and affordable visualization technique. Microbubbles, usually generated by perflorocarbons, give a specific contrast which improves significantly US image. All these features envision that US-driven MSN could be an excellent theranostic system which combines localized drug administration and superior imaging capability. Typical US-induced

cavitation process or the presence of US-sensitive molecules (mechanophores) has been used to design such gated nanosystems in which cargo release in triggered by US.

8.1. Cavitation

Zhang and coworkers developed a multifunctional system including MSNs in a lipidic membrane which can be selectively disrupted by US.[116] MSNs were first functionalized with APTES and then FA was incorporated by coupling FA-NHS with the amino functionalized nanoparticles by means of an amidation reaction. Finally the solid was loaded with coumarin 6 or with the apoptosis inducer diterpenoid Tanshinone IIA (TAN). In a final step, nanoparticles where included in a lipidic membrane formed by mixing DPPC, DPPE and the nanoparticles. Perfluorocarbon octafluoropropane was injected during the shearing process (Figure 97). Right encapsulation of coumarin 6-loaded nanoparticles in the lipidic membrane was confirmed under CLSM. Also, the ultrasound imaging contrast enhancement ability of the final nanoparticles was confirmed. Nanoparticles were injected in a gel mold and in H22 tumor-baring mice. In both cases, image contrast enhancement was significantly higher after administration of nanoparticles in comparison with the models before nanoparticles administration due to the gas in the lipidic membrane and thanks to its specific ultrasonic response. Preferential internalization of TAN-loaded MSNs in cells containing FR was also confirmed using HeLa cells, with high expression of these receptors, and A549 cells, with low levels of this receptors. Finally, TAN-loaded nanoparticles included in the lipidic membranes were injected in Kunming mice with H22 tumors. Authors found remarkable tumor growth suppression when mice were treated with the nanoparticles and subsequently irradiated for 6 min with US using a working intensity of 2 Wcm^{-2} and a frequency of 1MHz. The efficacy of the nanoparticles was associated to US-induced membrane rupture and FA targeting.

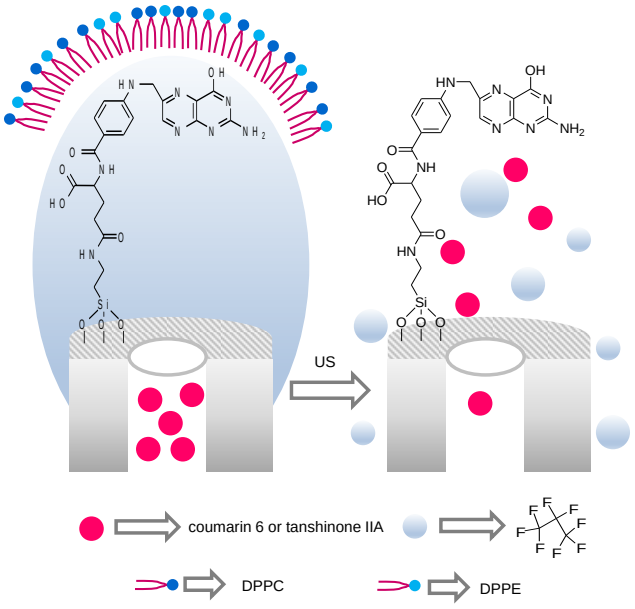

Figure 97. FA-functionalized MSNs loaded with coumarin 6 or TAN and octaperfluoropropane and included in a phospholipid microbubble. Upon the application of US, coumarin 6/TAN were released.

Shao and coworkers developed capped nanoparticles for PTX US-controlled delivery.[117] In their design, hydrophobic hexamethyldisilylamine-functionalized MSNs were loaded with PTX and capped with β-CD functionalized with FA. As the interfacial free energy of a hydrophobic surface is lower against gas than against water, the presence of this hydrophobic barrier between the MSNs surface and β-CD and also in pore voids favors the replacement of water by gas under low energy US and the generation of bubbles, which induces the dethreading of the gated ensemble (Figure 98). Ultrasonic cavitation in the nanoparticles was proved using the conversion of terephthalic acid in the fluorescent hydroxyl terephthalic acid due to the presence of cavitation-generated hydroxyl radicals. PBS suspensions of the gated nanoparticles generated the higher fluorescence when irradiated with 1 MHz US with an intensity of 0.8 W cm^{-2} for 2 min. Also capped MSNs showed controlled PTX release as function of US intensity and exposition time. While PTX release in PBS from gated MSNs reached only 18% after 1h without US irradiation, drug release increased until 90.38% after

1h irradiation with an intensity of 1.0 W cm^{-2}. In a step forward, 4T1 cells were treated with a suspension of FITC-labeled capped MSNs. After 12h incubation, fluorescence images confirmed the presence of the nanoparticles in the cytoplasm and in the perinuclear region. Low toxicity of low energy US alone treatment was assessed. In contrast, cell viability was significantly reduced until 16% when treated with the nanoparticles and irradiated with an intensity of 0.8 W cm^{-2}. Most likely, the accelerated PTX release and increased cell membrane permeability achieved after US irradiation explain the high efficiency of the gated nanodevice. Biocompatibility of the nanoparticles was also studied in Kunming mice. Animals showed no relevant changes in body weight, no significant acute chronic pathological toxicity or adverse effects and no abnormalities in venous blood after intravenous injection of nanoparticles even at high doses (20 mg/kg). Finally, 4T1 tumor-bearing nude mice were intratumorally treated with PBS suspensions of the gated MSNs. After certain time, mice were anesthetized and irradiated with low energy US (0.8 W cm^{-2}, 5 min). Body weight did not suffer relevant changes, whereas tumor growth in mice was inhibited up to 67.58% when treated with a high dose (10 mg/Kg) of nanoparticles and US irradiation.

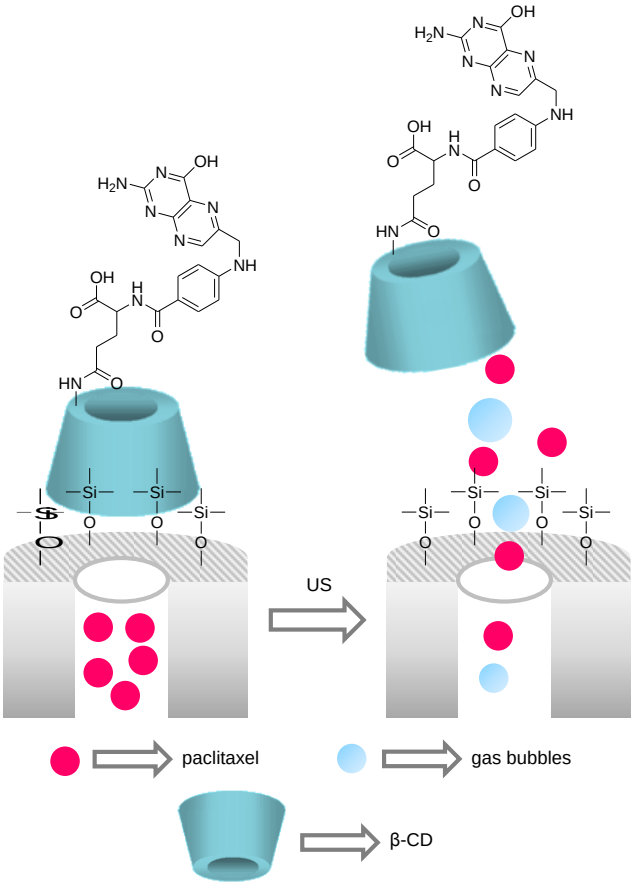

Figure 98. Hydrophobic MSN loaded with PTX and capped with FA-functionalized β-CD. When US are applied, the generated bubbles induced pore uncapping and subsequent PTX release.

8.2. Rupture of chemical bonds (mechanophores)

When US are applied, energy is adsorbed by the irradiated molecules, biomolecules and tissues. This energy can cleave certain sensitive bonds called mechanophores. The rupture of this bond triggers a possible molecular reorganization which could result in a different final specie with different properties. One interesting mechanophore is 2-tetrahydropyranyl methacrylate. Under US irradiation, the rupture of an acetal bond induces a change from hydrophobic to hydrophilic state with release of methacrylic acid. Anirudhan developed US-triggered MSNs applying these principles as gating mechanism.[118] MSNs were functionalized with carboxylates by grafting 3-cyanopropyltrimethoxysilane in the

nanoparticle surface, which was further hydrolyzed with sulphuric acid. A copolymer of tetrahydropyranyl methacrylate (mechanophore) and 2-aminoethyl methacrylate was prepared by free radical polymerization reaction and attached to the carboxylate groups of the MSNs by an amidation reaction with EDC and NHS. When US are applied (100W, 1.3 MHz) the acetal bonds cleaved releasing methacrylic acid (Figure 99). Likewise, the polymer is thermosensitive and exhibits an open conformation at temperatures below 4ºC, while collapses at higher temperatures blocking the pore entrances. Different cargoes were then loaded by diffusion process at low temperature (4ºC). US sensitivity was assessed by measuring the pH of the solution as function of US irradiation time. A LCST near to 36.7 ºC was found for the US irradiated solid suspension, which confirmed their potential application as drug delivery system. 4',6-Diamidino-2-phenylindole (DAPI) labelled and FITC-loaded nanoparticles were studied by CLSM. While untreated material showed uniform images, US-treated samples showed clear polymer degradation and FITC release. Further, histological examination of MSNs-treated rat skin before and after US exposure confirmed that the nanoparticles had no harmful effect on the skin surface. 5-fluorouracil-loaded gated nanoparticles were able to release the drug (69% at 96 hours) across rat skin when US was applied for more than 15 min, while, in the absence of US irradiation less than 10% release was achieved. HeLa cells showed good viability when exposed to US irradiation and low nanoparticles concentration. However, when cells were treated with 5-fluorouracil-loaded nanoparticles at concentration of larger than 25 µg/mL, an enhanced toxicity was achieved after US irradiation. Finally, the system was studied *in vivo* chick chorioallantoic membrane assay. Treatment with the nanoparticles showed non-toxic effect and resulted in an abundant blood vessel growth around the sponge. These data confirmed the drug-retention capability of the system and its subsequent safety. In contrast, US application, induced 5-fluorouracil release and significant anti-angiogenesis activity.

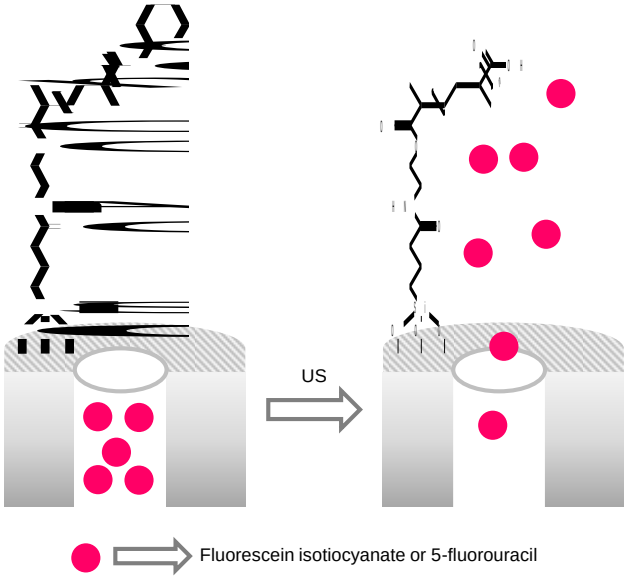

Figure 99. MSN loaded with FITC or 5-fluorouracil and capped with a mecanophore-containing polymer. Upon US application, polymer is degraded and cargo was released.

9. Small molecule-responsive drug delivery systems

Capped mesoporous devices can be also opened using (supra)molecular interactions between the gating ensemble and several chemical species presented in solution (biomolecules, anions, cations and small neutral molecules). One of the main advantages of these systems is that only in scenarios in which the selected triggering (bio)molecule is present the encapsulated cargo is released. However, cargo delivery using specific molecules is difficult to achieve in biological environments due to the presence multiple (bio)molecules and high saline concentration. Due to these facts, only one example of glucose-triggered system with *in vivo* application was described in recent years. Thus, Hou, Zhang and co-workers developed a smart glucose-triggered system.[119] Amino functionalized MSN were reacted with carboxyphenylboronic acid to obtain moieties able to form covalent bonds with 1,2- or 1,3-diols. Insulin was loaded in the pore voids and the polysaccharide sodium alginate was used to block pore entrances by the formation of boroester bonds with the phenylboronic units (Figure 100). PBS suspensions of nanoparticles showed negligible release (less than 8% after 12h), whereas 75% of the

payload was delivered in the same period. Additionally, the material showed cargo release in the presence of glucose. Insulin release could be stopped when the material was transferred to a solution without glucose and re-triggered by changing to a 5 mg/mL glucose solution. Nanoparticles showed no toxicity in HeLa cells and a hemolysis ratio of 0.2%, which demonstrated negligible haemolytic activity. Gated nanoparticles were injected subcutaneously (Insulin dose 10 IU/Kg) in type I diabetic mice. After glucose monitorization, the authors concluded that this novel treatment prolonged the insulin effect up to 12 hours. These data were confirmed by measuring insulin levels, which remained stable within 11 hours indicating high effectivity to maintain stable glucose levels and to avoid hypoglycaemia. Animals maintained their body weight and glycosylated haemoglobin values of around 19.5, which is similar to normal control animals. Treatment with the nanoparticles also alleviated the abnormal lipid metabolism and typical liver injury of diabetic mice. Prolonged circulation up to 96 h and higher insulin levels in the liver were found in mice treated with the nanoparticles in comparison with Novolin treated control ones.

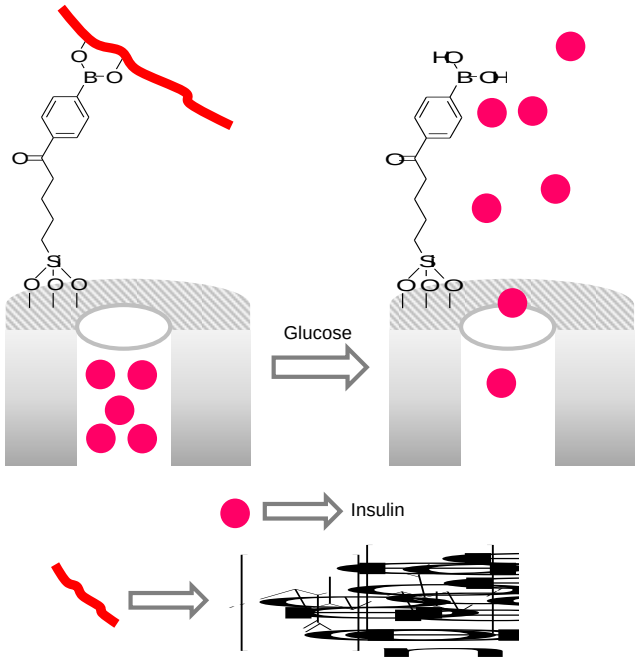

Figure 100. MSN loaded with insulin and capped with alginate. In the presence of glucose, alginate was displaced allowing insulin release.

10. Miscellaneous

MSNs loaded with a collection of histidine kinase autophosphorylation inhibitors (HKAIs) were used for the efficient internalisation and delivery of these hydrophobic drugs into bacteria.[120] For the preparation of the final nanodevices, the pores of MSNs were loaded with selected HKAIs and then the external surface functionalised with *N*-[(3-trimethoxysilyl)propyl]ethylendiamine triacetic acid trisodium salt. Finally, the loaded nanoparticles were coated with the positively charged ε-poly-L-lysine polymer (Figure 101). The antibacterial properties of the prepared nanoparticles were tested against *E. coli* CFT 073, *E. coli* DH5α and *S. marescens* 21,639.[121] The nanoparticles were able to inhibit bacterial growth and had, for all of the solids, MICs more than 10-times lower than that of the free HKAIs. Pore opening was ascribed to the interaction of positively charged capped nanoparticles with the negatively charged bacterial cell wall which induced the displacement of the ε-poly-L-lysine polymer with subsequent HKAIs release. Besides, the HKAIs-loaded nanoparticles did not present any cytotoxic effect in Caco-2 cells and in zebrafish larvae.

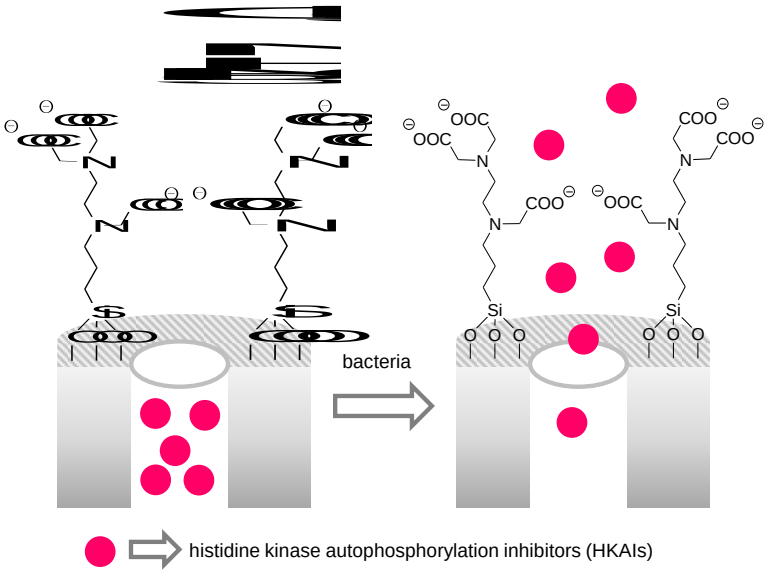

Figure 101. MSNs loaded with HKAIs functionalized with carboxylate groups and capped with ε-poly-L-lysine polymer. Pore opening is due to the interaction of positively charged capped nanoparticles with the negatively charged bacteria.

11. Discussion

Whereas some years ago the vast majority of the studies on gated mesoporous materials were mostly focused on the development of different gating systems and few of them described their use in animal models, today the outlook has changed and most of the reported examples include a specific application *in vivo* for a wide range of diseases. In these studies, gated materials represents a promising opportunity to improve the solubility and bioavailability of drugs and the delivery of an accurate amount of drugs to specific sites, thus reducing side effect and increasing the therapeutic outcome when compared with the administration of free drug.

The use of gated nanomaterials in biomedicine has been mainly focused in the last years on designing nanodevices which take advantage of the microenvironment of diseased cells responding to endogenous cellular stimuli, being applications in cancer therapy the most widely studied. Dealing with endogenous stimuli, changes in pH are the most widely used because the tumour microenvironment is acidic and several gated nanosystems are designed to take advantage of this effect. Moreover pH-responsive gated materials easily open in the acidic environment of the lysosomes. Recently published examples of pH-triggered gated nanosystems include mechanisms related with the hydrolysis of chemical bonds (such as imine, hydrazone, acetal, ketal, amides and esters), protonation processes which induce a disassembly of electrostatically constructed capping ensembles and bilayer disruption. One of the major challenge in designing pH-responsive systems is to achieve a more precise drug release in response to slight pH differences for certain applications (for instance for drug delivery in a tumour microenvironment). Moreover, although less studies, pH responsive

nanosystems are potential candidates for oral drug administration, for instance protecting drugs of the acidic conditions of gastrointestinal tract and thus facilitating their absorption. Further studies in this area will surely been reported in the near future.

Other endogenous stimuli frequently used are redox reactions and enzymes. Typical redox mechanism includes reduction of disulphide linkages and ROS-induced rupture of certain chemical bonds (such as thioketals, ketals, diselenides and disulphides). Most of the reported redox-responsive systems display a marked fast in the presence of the redox stimulus, which has been suggested to be useful in gene delivery applications in which a rapid response is needed to enhance a major gene expression or silencing. Another area of application of such redox-responsive nanodevices is in inflammation or inflammatory disorders in which elevated levels of reactive oxygen species are found. Regarding enzymes, capped nanomaterials have a large potential as the combination of gates and enzymes, capable to opening the gated material, associated to diseased cells or tissues is almost countless. In most of the recently published examples proteases, HAses and NQO1 are the enzymes most commonly used to induce the hydrolysis of capping ensembles and subsequent drug release. Based in the large potential of this approach a number of studies are envisioned to be published in the coming years based in other overexpressed enzymes. However, the preparation of these enzyme-triggered nanodevices is not an easy task. An important issue of these nanodevices is related with the levels of enzyme overexpression in the target cells or tissues. Low levels of enzyme overexpression will induce the release of small amounts of the entrapped cargo which will be reflected in the absence of the required effect. Taking into account the above mentioned facts, several advances are still needed in order to obtain more efficient enzyme-triggered gated nanodevices with application in *in vivo* protocols.

Other endogenous stimuli used to turn-on controlled release processes are temperature changes. From a biological point of view, temperature changes can be significant in the development of certain diseases (such as inflammation) and in tumours taking into account

that temperature in tumour microenvironment is different from the surroundings. An increase in temperature can also be achieved using gold nanoparticles to transform light in heat or superparamagnetic nanoparticles able to generate heat when are exposed to an alternating magnetic fields. Thermoresponsive capped nanodevices are usually coated with organic *co*-polymers (normally containing *N*-isopropylacrylamide units) which changes their conformation upon temperature variation. However, one of the major drawbaks of these thermoresponsive nansosystems for their *in vivo* applications is the need of designing capping poymers which presented specific conformational changes, and subsequent cargo release, in response to small temperaure variations such as 2-3 degrees respect to physiological temperature.

Despite the appealing use of endogenous cellular stimuli, the use of nanodevices responding to external stimuli and the application in realistic *in vivo* settings has also been demonstrated in the last years. The use of external stimuli, such as light, alternating magnetic fields and ultrasounds, as triggers for gated nanodevices is an appealing approach to combine diagnosis and photothermal therapies with drug delivery thus achieving a synergistic cytotoxic effect. Besides, the use of these gated nanodevices triggered by external stimuli in *in vivo* settings presents an interesting advantage such as a major control of cargo release provided by the external activation of the delivery avoiding premature leakages. On the other hand, one of the most noticeable drawbacks of these systems is the need of adequate equipment for the application of the external trigger in the required diseased areas in order to achieve a relevant therapeutic effect.

Among external stimuli employed to development of gated nanomaterials, NIR-triggered and magnetically responsive nanoparticles are gaining increasing attention. Gated nanoparticles triggered by NIR light are a powerful tool to combine chemo- and photothermal therapies with minimal harmful for the non-irradiated tissues. Besides, clinical translation of these nanodevices can be possible due to the deeper tissue penetration of NIR light when compared

with UV and visible radiation. On the other hand, magnetically guided and magnetically responsive nanoparticles can be realistic applied systems to deal with tumours with surgically limited treatments. Moreover, although less studied, ultrasound-responsive gated materials have also a great potential for externally controlled drug release using no harmful radiation. Moreover, it has been also suggested that ultrasound-responsive systems are suitable nanocarriers in gene delivery technologies taking into the account the ability of ultrasounds to change the membrane fluidity and induce pore formation.

As we have show, through the examples in this review, the advantages of using gated nanodevices based on mesoporous silica nanoparticles has been widely demonstrated both *in vitro* and *in vivo* studies with promissing results. However, it is difficult to predict which type of gated nanosystems are more suitable to reach clinical translation. The benefit-to-risk ratio has to be study in detail for each case. At this respect, it has to be taken into account that the synthetic protocol used for the preparation of each different nanomaterial determines their pharmacokinetic profile, mechanical stability, development of protein corona around the particles in bloodstream and possible changes in the particles during their circulation over time and thus the compatibility and safety, being the surface functionalization and particle size the most determining parameters.[122] An in depth comprehension of these issues is essential to optimise the design of new nanoparticles with clinical use perspective. In spite of the advances reported in this field, the reseach in gated materials still have some issues that need to be addressed specially in terms of safety and potential toxicity and more research efforts are needed to finally demonstrate their potential use in clinical applications. To reach this knowledge more *in vivo* studies need to be carried out. Despite these complete studies still have to come, some *in vivo* reseach has advanced in the knowledge of the biodistribution, accumulation, retention and clearance of some gated nanomaterials.[123,124] Although some contradictory results are found in the literature, in most of cases it is demonstrated that gated mesoporous silica nanoparticles circulate and accumulate in tumors and major organs,

(usually in liver, kidney and lungs), with no significant toxicity when exposed to animals. The severity and toxicity of nanoparticles is found to be controlled by several factors in which the dose and administration exposure play a crucial role.[125] On the other hand, the biodegradability of silica based materials is another major concern that migth limit realistic applications. In last years, many studies have evidenced that renal clearance is the main excretion way for mesoporous silica nanoparticles. The silica nanoparticles are constituted by -Si-O- bonds which are susceptible to hydrolytic breakdown, thus generating orthosilicic acid ($Si(OH)_4$), which is well-tolerated by the organism and excreted by urine.[124,126] In fact, some clinical trials have started using silica-based nanoparticles in the last years, being one of them successfully completed and two of them yet in recruiting state.[127] These encouraging results and initiatives suggest that in a near future more mesoporous silica-based nanoparticles could reach clinical trials as more conventional nanomedicines based on liposomes and polymers do. In all these studies the benefit-to-risk ratio has to be carefully analysed for each of the designed nanomaterials and for the specific biomedical application. While cancer therapy has been the most benefited in this field, gated drug delivery nanosystems could also play a crucial role in the treatment of infectious diseases, age-related diseases, inflammatory disorders, etc, which are high cause of mortality and are also attractive therapeutic targets for drug delivery systems. Several new advances in the field of gated nanomaterials are expected in the near future and smart nano-drug delivery technology development based on gated materials for more precise and innovative treatments looks promising.

12. Conclusions

We reviewed herein recent advances in the field of gated materials for controlled delivery applications. This review covers examples in which gated materials have been used in *in vivo* models from 2016 since the first months of 2019. This manuscript is divided into several sections dealing with the different stimuli used to commutate the gating mechanism inducing cargo release. At this respect, in the examples described above, pH, redox reactions, enzyme, light, temperature, magnetic fields, ultrasounds and small molecules have been used as external stimuli. In the early stages of gated materials, published studies were centred on the design of different capping ensembles and were uncommon those in which application in *in vivo* models were described. Today, the scope of the published examples has drastically changed and most of them included specific *in vivo* applications with animal models for a wide range of diseases and several biomedical practical applications. Despite the exponential application of this field in the last years, several drawbacks still need to be overcome (such as toxicity, biodegradability, biodistribution, accumulation, retention, and clearance) after their safe application in clinical trials. New and remarkable advances are anticipated in the near future.

Acknowledgements

The authors thank Spanish Government (project RTI2018-100910-B-C41 (MCUI/AEI/FEDER, UE)) and Generalitat Valenciana (PROMETEO2018/024) for their support.

Received: ((will be filled in by the editorial staff))
Revised: ((will be filled in by the editorial staff))
Published online: ((will be filled in by the editorial staff))

References

[1] (a) Q. Tang, B. Yu, L. Gao, H. Cong, N. Song, C. Lu, *Curr. Med. Chem.* **2018**, *25*, 1837-1866; (b) S. Aftab, A. Shah, A. Nadhman, S. Kurbanoglu, S. O. Aysil, D. D. Dyonisiou, S. S. Shukla, T. M: Aminabhavi, *Int. J. Pharm.* **2018**, *540*, 132-149.

[2] (a) V. Kozlovskaya, B. Xue, E. Kharlampieva, *Macromolecules* **2016**, *49*, 8373-8386; (b) D. K. Mishra, R. Shandilya, P. K. Mishra, *Nanomedicine* **2018**, *14*, 2023-2050; (c) F. Seidi, R. Jenjof, T. Phakkeeree, D. Crespy, *J. Control. Release* **2018**, *284*, 188-212; (d) W. Chen, S. Zhou, L. Ge, W. Wu, X. Jiang, *Biomacromolecules* **2018**, *19*, 1732-1745; (e) M. Vazquez-Gonzalez, I. Willner, *Langmuir* **2018**, *34*, 14692-14710; (f) R. M. Farid, N. A. H. A. Youssef, A. A. Kassem, *Curr. Pharm. Des.* **2017**, *23*, 6613-6629; (g) D. Lombardo, P. Calandra, D. Barreca, S. Magazu, M. A. Kiselev, *Nanomaterials* **2016**, *6*, 125/1-125/26; (h) A. Bansal, Y. Zhang, *Acc. Chem. Res.* **2014**, *47*, 3052-3060.

[3] N. Kamaly, B. Yameen, J. Wu, O. C. Farokhzad, *Chem. Rev.* **2016**, *116*, 2602-2663.

[4] (a) C. Coll, A. Bernardos, R. Martínez-Máñez, F. Sancenón, *Acc. Chem. Res.* **2013**, *46*, 339-349; (b) S. Yi, J. Zheng, P. Lv, D. Zhang, X. Zheng, Y. Zhang, R. Liao, *Bioconjug. Chem.* **2018**, *29*, 2884-2891; (c) N. Song, Y. –W. Yang, *Chem. Soc. Rev.* **2015**, *44*, 3474-3504; (d) C. Argyo, V. Weiss, C. Bräuchle, T. Bein, *Chem. Mater.* **2014**, *26*, 435-451.

[5] (a) C. –H. Lu, I. Willner, *Angew. Chem. Int. Ed.* **2015**, *54*, 12212-12235; (b) Y. Zhang, J. Yu, H. N. Bomba, Y. Zhu, Z. Gu, *Chem. Rev.* **2016**, *116*, 12536-12563; (c) M. Manzano, M. Vallet-Regí, *Chem. Commun.* **2019**, *55*, 2731-2740; (d) T. Zhao, L. Chen, Q. Li, X. Li, *J. Mater. Chem. B* **2018**, *6*, 7112-7121.

[6] P. Yang, S. Gai, J. Lin, *Chem. Soc. Rev.* **2012**, *41*, 3679-3698.

[7] (a) E. Aznar, M. Oroval, Ll. Pascual, J. R. Murguía, R. Martínez-Máñez, F. Sancenón, *Chem. Rev.* **2016**, *116*, 561-718; (b) F. Sancenón, Ll. Pascual, M. Oroval, E. Aznar, R. Martínez-Máñez, *ChemOpen* **2015**, *4*, 418-437; (c) A. Llopis-Lorente, P. Díez, A. Sanchez, M. D. Marcos, F. Sancenón, P. Martínez-Ruíz, R. Villalonga, R. Martínez-Máñez, *Nat. Commun.* **2017**, *8*, 15511.

[8] (a) J. L. Vivero-Escoto, I. I. Slowing, B. G. Trewyn, V. S. –Y. Lin, *Small* **2010**, *6*, 1952-1967; (b) B. Murugan, U. M. Krishnan, *Int. J. Pharm.* **2018**, *553*, 310-326; (c) A. F. Moreira, D. R. Dias, I. J. Correia, *Mesopor. Micropor. Mater.* **2016**, *236*, 141-157; (d) T. L.

Nguyen, Y. Choi, J. Kim, *Adv. Mater.* **2018**, *30*, 1803953; (e) Y. Chen, H. Chen, J. Shi, *Adv. Mater.* **2013**, *25*, 3144-3176.

[9] (a) J. Florek, R. Caillard, F. Kleitz, *Nanoscale* **2017**, *9*, 15252-15277; (b) K. E. Bremmell, C. A. Prestidge, *Drug Dev. Ind. Pharm.* **2019**, *45*, 349-358.

[10] H. Chen, D. Zheng, J. Liu, Y. Kuang, Q. Li, M. Zhang, H. Ye, H. Qin, Y. Xu, C. Li, B. Jiang, *Int. J. Biol. Macromol.* **2016**, *85*, 596-603.

[11] J. Liu, Z. Luo, J. Zhang, T. Luo, J. Zhou, X. Zhao. K. Cai, *Biomaterials* **2016**, *83*, 51-65.

[12] Z. Li, L. Zhang, C. Tang, C. Yin, *Pharm. Res.* **2017**, *34*, 2829-2841.

[13] W. Cheng, C. Liang, X. Wang, H. Tsai, G. Liu, Y. Peng, J. Nie, L. Huang, L. Mei, X. Zeng, *Nanoscale* **2017**, *9*, 17063-17073.

[14] X. Zeng, G. Liu, W. Tao, Y. Ma, X. Zhang, F. He, J. Pan, L. Mei, G. Pan, *Adv. Func. Mater.* **2017**, *27*, 1605985.

[15] X. Xu, C. Wu, A. Bai, X. Liu, H. Lv, Y. Liu, *J. Nanomat.* **2017**, 2069685.

[16] D. Yang, N. Wang, H. Ji, S. Sun, J. Dong, Y. Zhong, C. Qian, H. Xu. *RSC Adv*. **2018**, *8*, 38987-38994.

[17] L. Li, W. Sun, L. Li, Y. Liu, L. Wu, F. Wang, Z. Zhou, Z. Zhang, Y. Huang, *Nanoscale* **2017**, *9*, 314-325.

[18] R. Zhao, T. Li, G. Zheng, K. Jiang, L. Fan, J. Shao, *Biomaterials* **2017**, *143*, 1-16.

[19] J. Liu, X. Guo, Z. Luo, J. Zhang, M. Li, K. Cai, *Nanoscale* **2018**, *10*, 13737-13750.

[20] J. Fang, S. Zhang, X. Xue, X. Zhu, S. Song, B. Wang, L. Jiang, M. Qin, H. Liang, L. Gao, *Int. J. Nanomedicine* **2018**, *13*, 5113-5126.

[21] S. Yang, D. Chen, N. Li, Q. Xu, H. Li, F. Gu, J. Xie, J. Lu, *Small* **2016**, *12*, 360-370.

[22] L. Dai, Q. Zhang, X. Shen, Q. Sun, C. Mu, H. Gu, K. Cai, *J. Mater. Chem. B* **2016**, *4*, 4594-4604.

[23] M. Nejabat, M. Mohammadi, K. Abnous, S. M. Taghdisi, M. Ramezani, M. Alibolandi, *Carbohydr. Polym.* **2018**, *197*, 157-166.

[24] C. Murugan, K. Rayappan, R. Thangam, R. Bhanumathi, K. Shanthi, R. Vivek, R. Thirumurugan, A. Bhattacharyya, S. Sivasubramanian, P. Gunasekaran, S. Kannan, *Sci. Rep.* **2016**, *6*, 34053.

[25] X. Xiao, Y. Liu, M. Guo, W. Fei, H. Zheng, R. Zhang, Y. Zhang, Y. Wei, G. Zheng, F. Li, *J. Biomat. Appl.* **2016**, *31*, 23-35.

[26] L. Shao, R. Zhang, J. Lu, C. Zhao, X. Deng, Y. Wu, *ACS Appl. Mater. Interfaces* **2017**, *9*, 1226-1236.

[27] C. Murugan, S. Venkatesan, S. Kannan, *ACS Omega* **2017**, *2*, 7959-7975.

[28] M. Babaei, K. Abnous, S. M. Taghdisi, S. A. Farzad, M. T. Peivandi, M. Ramezani, M. Alibolandi, *Nanomedicine* **2017**, *12*, 1261-1279.

[29] M. R. Zeiderman, D. E. Morgan, J. D. Christein, W. E. Grizzle, K. M. McMasters, L. R. McNally, *ACS Biomater. Sci. Eng.* **2016**, *2*, 1108-1120.

[30] S. Mu, Y. Liu, T. Wang, J. Zhang, D. Jiang, X. Yu, N. Zhang, *Acta Biomater.* **2017**, *63*, 150-162.

[31] Y. He, Z. Su, L. Xue, H. Xu, C. Zhang, *J. Control. Release* **2016**, *229*, 80-92.

[32] B. Gupta, H. B. Ruttala, B. K. Poudel, S. Pathak, S. Regmi, M. Gautam, K. Poudel, M. H. Sung, W. Ou, S. G. Jin, J. –H. Jeong, S. K. Ku, H. –G. Choi, C. S. Yong, J. O. Kim, *ACS Appl. Mater. Interfaces* **2018**, *10*, 24392-24405.

[33] J. Y. Choi, B. Gupta, T. Ramasamy, J. –H. Jeong, S. G. Jin, H. –G. Choi, C. S. Yong, J. O. Kim, *Colloids Surf. B Biointerfaces* **2018**, *165*, 56-66.

[34] J. G. Croissant, D. Zhang, S. Alsaiari, J. Lu, L. Deng, F. Tamanoi, A. M. Al Malik, J. I. Zink, N. M. Khashab, *J. Control. Release* **2016**, *229*, 183-191.

[35] X. Wang, D. Niu, C. Hu, P. Li., *Curr. Pharm. Des.* **2015,** *21*, 6140-6156.

[36] Y. You, L. Yang, L. He, T. Chen, *J. Mater. Chem. B* **2016**, *4*, 5980-5990.

[37] B. Gupta, H. B. Ruttala, B. K. Poudel, S. Pathak, S. Regmi, M. Gautam, K. Poudel, M. H. Sung, W. Ou, S. G. Jin, J. -H. Jeong, S. K. Ku, H. -G. Choi, C. S. Yong, J. O. Kim, *Acta Biomater.* **2018**, *80*, 364-377.

[38] B. Ma, L. He,Y. You, J. Mo, T. Chen, *Drug Deliv.* **2018**, *25*, 293-306.

[39] P. T. Yin, T. Pongkulapa, H. –Y. Cho, J. Han, N. J. Pasquale, H. Rabie, J. –H. Kim, J. –W. Choi, K. –L. Lee, *ACS Appl. Mater. Interfaces* **2018**, *10*, 26954-26963.

[40] V. Mamaeva, R. Niemi, M. Beck, E. Ozlislei, D. Desai, S. Landor, T. Gronroos, P. Kronqvist, I. K. N. Pettersen, E. McCormack, J. M. Rosenholm, M. Linden, C. Sahlgren, *Mol. Ther*. **2016**, *24*, 926-935.

[41] J. Shen, H. Liu, C. Mu, J. Wolfram, W. Zhang, H. –C. Kim, G. Zhu, Z. Hu, L. –N. Ji, X. Liu, M. Ferrari, Z. –W. Mao, H. Shen, *Nanoscale* **2017**, *9*, 5329-5341.

[42] P. Khosravian, M. S. Ardestani, M. Khoobi, S. N. Ostad, F. A. Dorkoosh, H. A. Javar, M. Amanlou, *Onco Targets Ther.* **2016**, *9*, 7315-7330.

[43] R. Jin, Z. Liu, Y. Bai, Y. Zhou, J.J. Gooding, X. Chen, *Adv. Funct. Mater.* **2018**, *28*, 1801961-1801969.

[44] (a) J. H. Ryu, P. B. Messersmith, H. Lee, *ACS Appl. Mater. Interfaces* **2018**, *10*, 7523-7540; (b) Y. Liu, K. Ai, L. Lu, *Chem. Rev.* **2014**, *114*, 5057-5115.

[45] Y. Li, Y. Duo, J. Bi, X. Zeng, L.Mei, S. Bao, L. He, A. Shan, Y. Zhang and X. Yu, *Int. J. Nanomed.* **2018**, *13*, 1241-1256.

[46] W. Cheng, J. Nie, L. Xu, C. Liang, Y. Peng, G. Liu, T. Wang, L. Mei, L. Huang, X. Zheng, *ACS Appl. Mater. Interfaces* **2017**, *9*, 18462-18473.

[47] W. Cheng, C. Liang, L. Xu, G. Liu, N. Gao, W. Tao, L. Luo, Y. Zuo, X. Wang, X. Zhang, X. Zeng, L. Mei, *Small* **2017**, *13*, 1700623.

[48] Y. Duo, Y. Li, C. Chen, B. Liu, X. Wang, X. Zeng, H. Chen, *RSC Adv.* **2017**, *7*, 39641-39650.

[49] Y. Li, Y. Duo, P. Zhai, L. He, K. Zhon, Y. Zhang, K. Huang, J. Luo, H. Zhang, X. Yu, *Nanomedicine* **2018**, *13*, DOI: 10.2217/nnm-2017-0353.

[50] J. Hu, X. Zhang, Z. Wen, Y. Tan, N. Huang, S. Cheng, H. Zheng, Y. Cheng, *Oncotarget* **2016**, *7*, 73681-73696.

[51] V. Thiyagarajan, S. –X. Lin, C. –H. Lee, C. –F. Weng, *Colloids Surf. B Biointerfaces* **2016**, *141*, 120-131.

[52] P. Srivastava, S. K. Hira, D. N. Srivastava, V. K. Singh, U. Gupta, R. Singh, R. A. Singh, P. P. Manna, *ACS. Appl. Mater. Interfaces* **2018**, *10*, 6917-6929.

[53] J. Wang, D. Xu, T. Deng, Y. Li, L. Xue, T. Yan, D. Huang, D. Deng, *ACS Appl. Nano Mater.* **2018**, *1*, 1976-1984.

[54] V. T. Banala, S. Sharma, P. Barnwal, S. Urandur, R. P. Shukla, N. Ahmad, N. Mittapelly, G. Pandey, M. Dwivedi, N. Kalleti, K. Mitra, S. K. Rath, R. Trivedi, P. R. Mishra, *Adv. Healthcare Mater.* **2018**, *7*, 1800300.

[55] D. Desai, J. Zhang, J. Sandholm, J. Lehtimäki, T. Grönroos, J. Tuomela, J. M. Rosenholm, *Mol. Pharm.* **2017**, *14*, 3218-3227.

[56] H. Xue, Z. Yu, Y. Liu, W. Yuan, T. Yang, J. You, X. He, R. J. Lee, L. Li, C. Xu, *Int. J. Nanomedicine* **2017**, *12*, 5271-5287.

[57] A. E. La Bauve, T. E. Rinker, A. Noureddine, R. E. Serda, J. Y. Howe, M. B. Sherman, A. Rasley, C. J. Brinker, D. Y. Sasaki, O. A. Negrete, *Sci. Rep.* **2018**, *8*, 13990.

[58] Z. Yuan, W. Wu, Z. Zhang, Z. Sun, R. Cheng, G. Pan, X. Wang, W. Cui, *Colloids Surf. B Biointerfaces* **2017**, *158*, 363-369.

[59] A. Sarkar, S. Ghosh, S. Chowdhury, B. Pandey, P. C. Sil, *Biochim. Biophys. Acta* **2016**, *1860*, 2065-2075.

[60] J. Wang, Y. Wang, Q. Liu, L. Yang, R. Zhu, C. Yu, S. Wang, *ACS Appl. Mater. Interfaces* **2016**, *8*, 26511-26523.

[61] C. Y. Lai, B. G. Trewyn, D. M. Jeftinija, K. Jeftinija, S. Xu, S. Jeftinija, V. S. –Y. Lin, *J. Am. Chem. Soc.* **2003**, *125*, 4451-4459.

[62] Y. Tian, R. Guo, Y. Jiao, Y. Sun, S. Shen, Y. Wang, D. Lu, X. Jiang, W. Yang, *Nanoscale Horiz.* **2016**, *1*, 480-487.

[63] H. –J. Liu, X. Luan, H. –Y. Feng, X. Dong, S. –C. Yang, Z. –J. Chen, Q. –Y. Cai, Q. Lu, Y. Zhang, P. Sun, M. Zhao, H. –Z. Chen, J. F. Lovell, C. Fang, *Adv. Func. Mater.* **2018**, *28*, 1801118.

[64] L. Huang, Q. Zhang, L. Dai, X. Shen, W. Chen, K. Cai, *Regen. Biomater.* **2017**, *4*, 111-124.

[65] S. Zhao, M. Xu, C. Cao, Q. Yu, Y. Zhou, J. Liu, *J. Mater. Chem. B*, **2017**, *5*, 6908-6919.

[66] Z. Chen, P. Zhu, Y. Zhang, Y. Liu, Y. He, L. Zhang, Y. Gao, *Mol. Pharm.* **2016**, *13*, 2749-2759.

[67] J. Xie, D. Xiao, J. Zhao, N. Hu, Q. Bao, L. Jiang, L. Yu, *Adv. Healthcare Mater*. **2016**, *5*, 1213-1221.

[68] Y. Lu, Y. Yang, Z. Gu, J. Zhang, H. Song, G. Xiang, C. Yu, *Biomaterials* **2018**, *175*, 82-92.

[69] X. Chen, D. Li, A. Lin, J. Xu, L. Wu, H. Gu, Z. Huang, J. Liu, Y. Zhang, X. Yin, *Int. J. Nanomed.* **2018**, *13*, 3661-3677.

[70] J. Zhou, M. Li, W. Qi Lim, Z. Luo, S. Z. F. Phua, R. Huo, L. Li, K. Li, L. Dai, J. Liu, K. Cai, Y. Zhao, *Theranostics*, **2018**, *8*, 518-532.

[71] Y. Wang, H. -Y. Huang, L. Yang, Z. Zhang, H. Ji, *Sci. Rep.* **2016**, *6*, 25468-25678.

[72] J. -J. Hu, Q. Lei, M. -Y. Peng, D. -W. Zheng, Y. -X. Chen, X. -Z. Zhang, *Biomaterials* **2017**, *128*, 136-146.

[73] D. Shao, M. Li, Z. Wang, X. Zheng, Y. -H. Lao, Z. Chang, F. Zhang, M. Lu, J. Yue, H. Hu, H. Yang, L. Chen, W. -F. Dong, K. W. Leong, *Adv. Mater*. **2018**, *30*, 1801198.

[74] S. Y. Tan, C. Teh, C. Y. Ang, M. Li, P. Li, V. Korzh, Y. Zhao, *Nanoscale* **2017**, *9*, 2253-2261.

[75] S. Ren, J. Yang, L. Ma, X. Li, W. Wu, C. Liu, J. He, L. Miao, *ACS Appl. Mater. Interfaces*, **2018**, *10*, 31947-31958.

[76] X. Li, W. Zhao, X. Liu, K. Chen, S. Zhu, P. Shi, Y. Chen, J. Shi, *Acta Biomater.* **2016**, *30*, 378-387.

[77] L. Yu, Y. Chen, M. Wu, X. Cai, H. Yao, L. Zhang, H. Chen, J. Shi, *J. Am. Chem. Soc*. **2016**, *138*, 9881-9894.

[78] A. Llopis-Lorente, B. Lozano-Torres, A. Bernardos, R. Martínez-Máñez, F. Sancenón, *J. Mater. Chem. B* **2017**, *5*, 3069-3083.

[79] E. Li, Y. Yang, G. Hao, X. Yi, S. Zhang, Y. Pan, B. Xing, M. Gao, *Nanotheranostics* **2018**, *2*, 233-242.

[80] A. García-Fernández, G. García-Laínez, M. L. Ferrándiz, E. Aznar, F. Sancenón, M. J. Alcaraz, J. R. Murguía, M. D. Marcos, R. Martínez-Máñez, A. M. Costero, M. Orzáez, *J. Control. Release* **2017**, *248*, 60-70.

[81] P. Srivastava, S. K. Hira, D. N. Srivastava, U. Gupta, P. Sen, R. A. Singh, P. P. Manna, *ACS Biomater. Sci. Eng*. **2017**, *3*, 3376-3385.

[82] H. Jiang, X. Shi, X. Yu, X. He, Y. An, H. Lu, *Pharm. Res*. **2018**, *35*, 73.

[83] L. Huang, J. Liu, F. Gao, Q. Cheng, B. Lu, H. Zheng, H. Xu, P. Xu, X. Zhang, X. Zeng, *J. Mater. Chem. B* **2018**, *6*, 4618-4629.

[84] J. Ding, T. Liang, Y. Zhou, Z. He, Q. Min, L. Jiang, J. Zhu, *Nano Res.* **2017**, *10*, 690-703.

[85] D. Yang, T. Wang, Z. Su, L. Xue, R. Mo, C. Zhang, *ACS Appl. Mater. Interfaces* **2016**, *8*, 22431-22441.

[86] Y. Ding, Z. Song, Q. Liu, S. Wei, L. Zhou, J. Zhou, J. Shen, *Dalton Trans*. **2017**, *46*, 11875-11883.

[87] J. Zhou, M. Wang, H. Ying, D. Su, H. Zhang, G. Lu, J. Chen, *ACS Biomater. Sci. Eng*. **2018**, *4*, 2404-2411.

[88] (a) Y. –W. Yang, Y. –L. Sun, N. Song, *Acc. Chem. Res.* **2014**, *47*, 1950-1960; (b) M. W. Ambrogio, C. R. Thomas, Y. –L. Zhao, J. I. Zink, J. F. Stoddart, *Acc. Chem. Res.* **2011**, *44*, 903-913.

[89] N. Song, Y. –W. Yang, *Chem. Soc. Rev*. **2015**, *44*, 3474-3504.

[90] S. R. Gayam, P. Venkatesan, Y. -M. Sung, S. -Y. Sung, S. -H. Hu, H. -Y. Hsu, S. -P. Wu, *Nanoscale* **2016**, *8*, 12307-12317.

[91] J. Lee, W. Sun, L. Li, Y. Liu, L. Wu, Fe. Wang, Z. Zhou, Z. Zhang, Y. Huang, *Nanoscale*, **2017**, *9*, 6901-6909.

[92] D. Muñoz-Espín, M. Rovira, I. Galiana, C. Giménez, B. Lozano-Torres, M. Paez-Ribes, S Llanos, S. Chaib, M. Muñoz-Martín, A. C. Ucero, G. Garaulet, F. Mulero, S. G. Dann, T. Van Arsdale, D. J. Shields, A. Bernardos, J. R. Murguía, R. Martínez-Máñez, M. Serrano, *EMBO Mol. Med.* **2018**, *10*, e9355.

[93] P. Srivastava, S. K. Hira, A. Sharma, M. Kashif, P. Srivastava, D. N. Srivastava, R. A. Singh, P. P. Manna, *Bioconjug. Chem*. **2018**, *29*, 2107-2119.

[94] L. Pascual, C. Cerqueira-Countinho, A. García-Fernández, B. de Luís, E. Soares Bernardes, M. Souza Albernaz, S. Missailidis, R. Martínez-Máñez, R. Santos-Oliveira, M. Orzáez, F. Sancenón. *Nanomed. Nanotechnol*. **2017**, *13*, 2495-2505.

[95] S. Yang, X. Han, Y. Yang, H. Qiao, Z. Yu, Y. Liu, J. Wang, T. Tang, *ACS Appl. Mater. Interfaces* **2018**, *10*, 14299-14311.

[96] A. H. Teruel, E. Pérez-Esteve, I. González-Álvarez, M. González-Álvarez, A. M. Costero, D. Ferri, M. Parra, P. Gaviña. V. Merino, R. Martínez-Máñez, F. Sancenón, *J. Control. Release* **2018**, *281*, 58-69.

[97] A. H. Teruel, E. Pérez-Esteve, I. González-Álvarez, M. González-Álvarez, A. M. Costero, D. Ferri, P. Gaviña. V. Merino, R. Martínez-Máñez, F. Sancenón, *Mol. Pharm.* **2019**, *16*, 2418-2429.

[98] N. K. Mal, M. Fujiwara, Y. Tanaka, *Nature* **2003**, *421*, 350−353.

[99] N. K. Mal, M. Fujiwara, Y. Tanaka, T. Taguchi, M. Matsutaka, *Chem. Mater.* **2003**, *15*, 3385−3394.

[100] J. An, X. -Q. Yang, K. Cheng, X. -L. Song, L. Zhang, C. Li, X. -S. Zhang, Y. Xuan, Y. -Y. Song, B. -Y. Fang, X. -L. Hou, Y. -D. Zhao, B. Liu, *ACS Appl. Mater. Interfaces* **2017**, *9*, 41748−41759.

[101] S. Duan, Y. Yang, C. Zhang, N. Zhao, F. -J. Xu, *Small* **2017**, *13*, 1603133.

[102] X. Chen, Q. Zhang, J. Li, M. Yang, N. Zhao, F. -J. Xu, *ACS Nano* **2018**, *12*, 5646−5656.

[103] J. Xu, X. Wang, Z. Teng, G. Lu, N. He, Z. Wang, *ACS Appl. Mater. Interfaces* **2018**, *10*, 24440-24449.

[104] L. Zhang, Y. Chen, Z. Li, L. Li, P. Saint-Cricq, C. Li, J. Lin, C. Wang, Z. Su, J. I. Zink, *Angew. Chem. Int. Ed.* **2016**, *55*, 2118-2121.

[105] R. -L. Han, J. -H. Shi, Z. -J. Liu, Y. -F. Hou, Y. Wang, *ACS Biomater. Sci. Eng.* **2018**, *4*, 3478−3486.

[106] Y. Zhang, K. Ren, X. Zhang, Z. Chao, Y. Yang, D. Ye, Z. Dai, Y. Liu, H. Ju, *Biomaterials* **2018**, *163*, 55−56.

[107] J. Shu, H. Sun, Q. Meng, P. Zhang, Q. Yin, Y. Li, *Theranostics* **2017**, *7*, 523-537.

[108] M. Xuan, J. Shao, J. Zhao, Q. Li, L. Dai, J. Li, *Angew. Chem. Int. Ed.* **2018**, *57*, 6049 –6053.

[109] R. J. Thapa, H. T. Nguyen, M. Gautam, A. Shrestha, E. S. Lee, S. K. Ku, H. –G. Choi, C. S. Yong, J. O. Kim, *Drug Delivery* **2017**, *24*, 1690-1702.

[110] Z. Li, H. Zhang, J. Han, Y. Chen, H. Lin, T. Yang, *Adv. Mater.* **2018**, *30*, 1706981.

[111] Q. Lei, S. –B. Wang, J. –J. Hu, Y. –X. Lin, C. –H. Zhu, L. Rong, X. –Z. Zhang, *ACS Nano* **2017**, *11*, 7201-7214.

[112] Y. Feng, N. Li, H. Yin, T. Chen, Q. Yang, M. Wu, *Mol. Pharm.* **2019**, *16*, 422−436.

[113] X. Qi, D. Yu, B. Jia, C. Jin, X. Liu, X. Zhao, G. Zhang, *Tumor Biol.* **2016**, *37*, 2209–2217.

[114] X. Liu, D. Yu, C.S. Jin, X. W. Song, J. Z. Cheng, X. Zhao, X. M. Qi, G. X. Zhang, *New J. Chem.* **2014**, *38*, 4830−4836.

[115] E. Guisasola, L. Asín, L. Beola, J. M. de la Fuente, A. Baeza, M. Vallet-Regí, *ACS Appl. Mater. Interfaces* **2018**, *10*, 12518−12525.

[116] Y. Lv, Y. Cao, P. Li, J. Liu, H. Chen, W. Hu, L. Zhang, *Adv. Healthcare Mater.* **2017**, *6*, 1700354.

[117] J. Wang, Y. Jiao, Y. Shao, *Materials* **2018**, *11*, 2041-2057.

[118] T. S. Anirudhan, A. S. Nair, *J. Mater. Chem. B* **2018**, *6*, 428—439.

[119] L. Hou, Y. Zheng, Y. Wang, Y. Hu, J. Shi, Q. Liu, H. Zhang, Z. Zhang, *ACS Appl. Mater. Interfaces* **2018**, *10*, 21927−21938.

[120] N. Velikova, N. Mas, L. Miguel-Romero, L. Polo, E. Stolte, E. Zaccaria, R. Cao, N. Taverne, J. R. Murguía, R. Martínez-Máñez, A. Marina, J. Wells, *Nanomedicine* **2017**, *13*, 569-581.

[121] A. Bernardos, E. Piacenza, F. Sancenón, M. Hamidi, A. Maleki, R. J. Turner, R. Martínez-Máñez, *Small* **2019**, *15*, 1900669.

[122] S. Jafari, H. Derakhshankhah, L. Alaei, A. Fattahi, B. S. Varnamkhasti, A. A. Saboury, *Biomed. Pharmacother.* **2019**, *109*, 1100-1111.

[123] Y. Chen, H. Chen, J. Shi, *Adv. Mater.* **2013**, *25*, 3144-3176.

[124] (a) J. G. Croissant, Y. Fatieiev, N. M. Khasab, *Adv. Mater.* **2017**, *29*, 1604634; (b) M. Linden, *The Enzymes*, **2018**, *43*, 155-180.

[125] J. Xie , S. Lee , X. Chen, *Adv. Drug. Deliv. Rev.* **2010,** *62*, 1064-1079.

[126] (a) B. C. Bunker, *J. Non-Cryst. Solids* **1994**, *179*, 300-308; (b) J. F. Popplewell, S. J. King, J. P. Day, P. Ackrill, L. K. Fifield, R. G. Cresswell, M. L. D. Tada, K. Liu, *J. Inorg. Biochem.* **1998**, *69*, 177-180; (c) N. Hao, H. Liu, L. Li, D. Chen, L. Li, F. Tang, *J. Nanosci. Nanotechnol.* **2012**, *12*, 6346-6354.

[127] NIH, U.S. National Library of Medicine, ClinicalTrials.gov, retrieved from https://clinicaltrials.gov/.

Gated materials

Alba García-Fernández, Elena Aznar, Ramón Martínez-Máñez,* and Félix Sancenón

New advances in gating techniques in drug delivery systems

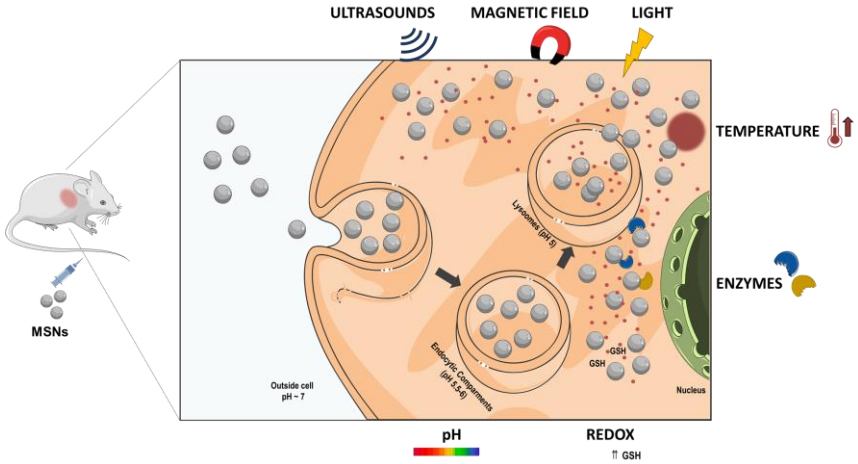

Ramón Martínez-Máñez received his Ph.D. in Chemistry from the University of Valencia in 1986 and was a postdoctoral fellow at Cambridge University, UK. He is a full professor at the Polytechnic University of Valencia. Presently, he is the director of the IDM Research Institute at the Polytechnic University of Valencia. He is the co-author of more than 400 research publications. He received the Jaume I Award from the Generalitat Valenciana in 2018 in the area of New Technologies. His current research interest involves developing new sensing methods for different chemicals of interest, including explosives and chemical warfare agents. He is also involved in designing gated hybrid materials for delivery applications.

Abbreviations

AMF: Alternating magnetic field
APTES: (3-Aminopropyl)triethoxysilane
ATP: Adenosine triphosphate
ATRP: atomic transfer radical polymerization
AuNPs: Gold nanoparticles
BBB: Blood-brain barrier
BSA: Bovine serum albumin
CD: Cyclodextrin
CLSM: Confocal laser scanning microscope
CPT: Camptothecin
CS: Chitosan
CSCs: Cancer stem cells
CT: Computed Tomography
CTAB: Cetyltrimethylammonium bromide
DAPI: 4',6-Diamidino-2-phenylindole
DCC: *N*,*N*'-dicyclohexilcarbodiimide
DNA: Deoxyribonucleic acid
Dox: Doxorubicin
DOPC: 1,2-Dioleoyl-*sn*-glycero-3-phosphocholine
DOPE: 1,2-Dioleoyl-*sn*-glycero-3-phosphoethanolamine
DOPE-PEG_{2000}-OMe: 1,2-Dioleoyl-*sn*-glycero-3-phosphoethanolamine [methoxy-PEG_{2000}]
DOTAP: *N*-[1-(2,3-Dioleoyloxy)propyl]-*N*,*N*,*N*-trimethylammonium chloride
DPPC: 1,2-Dipalmitoyl-*sn*-glycero-3-phosphocholine
DPPE: 1,2-Dipalmitoyl-*sn*-glycero-3-phosphoethanolamine
DSPC: 1,2-Distearoyl-*sn*-glycero-3-phosphocholine
DSPE: 1,2-Distearoyl-*sn*-glycero-3-phosphoethanolamine
DSPE-PEG_{2000}-COOH: 1,2-Distearoyl-*sn*-glycero-3-phosphoethanolamine-*N*-[carboxy-PEG_{2000}]
DSPE-PEG_{2000}-NH_2: 1,2-Distearoyl-*sn*-glycero-3-phosphoethanolamine-*N*-[amino-PEG_{2000}]
DSPE-PEG_{2000}-OMe: 1,2-Distearoyl-*sn*-glycero-3-phosphoethanolamine-[methoxy-PEG_{2000}]
DTT: Dithiothreitol
EDC: 1-Ethyl-3-(3-dimethylaminopropyl) carbodiimide hydrochloride
EGFR: Epidermal growth factor
ELISA: Enzyme-linked immunosorbent assay
EPR: Enhanced permeability and retention
FA: Folic acid
FR: Folate receptor
FITC: Fluorescein isothiocyanate
GSH: Glutathione
HA: Hyaluronic acid
HAses: Hyaluronidases
IBD: Inflammatory bowel disease
ICP: Inductively coupled plasma
LA: Lactobionic acid
MDR: Multidrug-resistant
MIR: Magnetic resonance imaging
miRNA: micro interfering RNA

MMP: Metalloproteinases
MSN: Mesoporous silica nanoparticles
MTT: 3-(4,5-Dimethylthiazol-2-yl)-2,5-diphenyltetrazolium bromide
NHS: *N*-Hydroxysuccinimide
NIR: Near Infrared
PAMAM: Polyamidoamine
PBS: Phosphate-buffered saline
PDA: Polydopamine
PEG: Polyethylene glycol
PEI: Polyethylenimine
P-gp: Glycoprotein-P
PTX: Paclitaxel
QD: Quantum dot
ROS: Reactive oxygen species
shRNA: Short harping RNA
siRNA: Small interfering RNA
TAN: Tanshinone IIA
TAT: Transactivator of transcription
TEM: Transmission electron microscope
TEOS: Tetraethyl orthosilicate
Tf: Transferrin
TNF-α: Tumour necrosis factor alpha
TPT: Topotecan
UCNP: Upconverting nanoparticles
US: Ultrasounds
VEGF: Vascular Endothelial Growth Factor
WST-1: Water-soluble tetrazolium salt